Inflation and Phenomenology in an Extended Two-Higgs-Doublet-Model

Dissertation
zur Erlangung des Doktorgrades
an der Fakultät für Mathematik, Informatik und Naturwissenschaften
Fachbereich Physik
der Universität Hamburg

vorgelegt von

MICHAEL MAXIM MATLIS

Hamburg

2022

Gutachter/in der Dissertation:	Dr. Andreas Ringwald Prof. Dr. Gudrid Moortgat-Pick
Zusammensetzung der Prüfungskommission:	Dr. Andreas Ringwald Prof. Dr. Gudrid Moortgat-Pick Prof. Dr. Roman Schnabel Prof. Dr. Elisabetta Gallo Dr. Bibhushan Shakya
Vorsitzende/r der Prüfungskommission:	Prof. Dr. Roman Schnabel
Datum der Disputation:	19.08.2022
Vorsitzender Fach-Promotionsausschuss PHYSIK:	Prof. Dr. Wolfgang J. Parak
Leiter des Fachbereichs PHYSIK:	Prof. Dr. Günter H. W. Sigl
Dekan des Fachbereichs MIN:	Prof. Dr. Heinrich Graener

Abstract

The Two-Higgs-Doublet-Standard Model-Axion-Seesaw-Higgs-Portal Inflation (2hdSMASH) model containing two Higgs doublets, a Standard Model (SM) singlet complex scalar and three SM singlet right-handed Majorana neutrinos addresses the following shortcomings of the SM: *i)* dark matter by axions, *ii)* strong CP problem by the Peccei-Quinn mechanism, *iii)* neutrino masses and mixing by the seesaw mechanism, *iv)* baryon asymmetry by thermal leptogenesis and *v)* inflation by Higgs portal inflation. In this thesis we investigate the inflationary aspects of 2hdSMASH and its subsequent impact on low energy phenomenology. In particular, we identify four inflationary directions whose parameter values required for successful inflation do not violate perturbative unitarity and vacuum stability conditions. By analyzing the Renormalization-Group (RG) flow of the parameters we identify the constraints from thermal leptogenesis, baryon asymmetry, vacuum stability, perturbative unitarity and Higgs phenomenology. Satisfying all of these constraints ensures a consistent picture of our universe from the electroweak all the way up to the Planck scale. We determine typical benchmark points satisfying theoretical and experimental constraints which can be potentially probed by future colliders.

Zusammenfassung

Das Two-Higgs-Doublet-Standard Model-Axion-Seesaw-Higgs-Portal Inflation (2hd SMASH) Modell, das zwei Higgs-Dubletts, ein komplexes skalares Standard Modell (SM) Singlet und drei rechtshändige SM-Singlett-Majorana-Neutrinos enthält, behebt die folgenden Mängel des SM: *i)* dunkle Materie durch Axionen, *ii)* starkes CP-Problem durch den Peccei-Quinn-Mechanismus, *iii)* Neutrinomassen durch den Seesaw-Mechanismus, *iv)* Baryonen-Asymmetrie durch thermische Leptogenese und *v)* Inflation durch Higgs-Portal-Inflation. In dieser Dissertation untersuchen wir die inflationären Aspekte von 2hdSMASH und ihre daraus resultierenden Auswirkungen auf die niederenergetische Phänomenologie. Insbesondere identifizieren wir vier Inflationsrichtungen, deren für eine erfolgreiche Inflation erforderlichen Parameterwerte, die Bedingungen der perturbativen Unitarität und der Vakuumstabilität nicht verletzen. Durch die Analyse des Renormierungsgruppen (RG)-Flusses der Parameter identifizieren wir die Beschränkungen durch thermische Leptogenese, Baryon-Asymmetrie, Vakuumstabilität, perturbative Unitarität und Higgs Phänomenologie. Die Erfüllung all dieser Beschränkungen gewährleistet ein konsistentes Bild unseres Universums von der elektroschwachen bis hin zur Planck-Skala. Wir bestimmen typische Benchmark-Punkte, die mit theoretischen und experimentellen Beschränkungen vereinbar sind und potenziell mit zukünftigen Teilchenbeschleunigern untersucht werden können.

Contents

Acknowledgments

I would like to thank my supervisors Dr. Andreas Ringwald and Prof. Dr. Gudrid Moortgat-Pick who have dedicated their time and effort to guide me through my PhD and made this work possible. In particular, I would like to express my gratitude to Dr. Andreas Ringwald who introduced me to this topic. I would also like to thank Dr. Yvette Welling for providing insights into inflationary cosmology and Dr. Juhi Dutta for providing the phenomenological insights of section 5.5. Furthermore, I am grateful for fruitful discussions with Dr. Carlos Tamarit, Steven Paasch and Cheng Li.

I would also like to acknowledge the DESY Theory Group and the PIER Helmholtz Graduate School for providing support and a great working environment.

Most importantly, I would like to thank my wife, Mareike Matlis, who supported me every step of the way. Her encouragement, mental support and her love have given me energy to tackle the obstacles I faced during my PhD.

1. Introduction

The Higgs Boson discovery in 2012 by the ATLAS [1] and CMS [2] collaborations brought a lot of excitement into the field of particle physics. Its existence was predicted by P. Higgs, T.W.B. Kibble, G. S. Guralnik, F. Englert and R. Brout in 1964 [3, 4, 5], who were able to explain with the so-called Brout-Englert-Higgs-mechanism (BEH-mechanism) how the masses of elementary particles were generated. Within its theoretical and experimental bounds it is compatible with the Standard Model (SM) of particle physics. However, the Higgs Boson is by no means a completion of the SM and compatible with Beyond the Standard Model (BSM) physics. In fact, the SM is lacking an explanation for the following phenomena:

1) The non-observation of strong CP-violation

2) Non-baryonic dark matter (DM)

3) Neutrino masses and mixing

4) Baryon asymmetry of the universe (BAU)

5) inflation

A minimal extension of the SM which is capable of solving all five of these shortcomings in one smash [6, 7] consists of three SM singlet right-handed neutrinos and a Kim-Shifman-Vainshtein-Zakharov (KSVZ) type axion model [8, 9] involving an exotic quark and a complex SM singlet scalar. This model is dubbed SM-Axion-Seesaw-Higgs Portal inflation (SMASH) and features a solution to *1)* by the Peccei-Quinn (PQ) mechanism [10], *2)* by axion dark matter [11, 12, 13], *3)* by the seesaw mechanism [14, 15, 16, 17], *4)* by thermal leptogenesis [18], and *5)* by Higgs portal inflation [19, 20]. SMASH is remarkably predictive and provides a complete model from particle physics to inflationary cosmology.

A possible variant of SMASH is dubbed Two-Higgs-Doublet-SM-Axion-Seesaw-Higgs-Portal inflation (2hdSMASH) which was superficially introduced in Ref. [21]. The 2hdSMASH model entertains two Higgs doublets, a complex SM singlet PQ scalar and three SM singlet right-handed Majorana neutrinos. This SMASH variant differs

by replacing the KSVZ axion model by a Dine-Fischler-Srednicki-Zhitnitsky (DFSZ) axion model [22, 23] without an additional exotic quark.

There are in general two versions, namely 2hdSMASH(d) and 2hdSMASH(u) which correspond to a Type-I DFSZ and Type-II DFSZ model. Both versions differ by whether leptons couple to the down-type Higgs H_d or to the up-type Higgs H_u. The former is capable of being embedded into familiar Grand-Unified-Theories (GUTs). Henceforth, we describe 2hdSMASH(d) when we talk about the model.

Originally, 2hdSMASH was proposed in Refs. [24, 25] which explained neutrino masses, baryogenesis, the strong CP problem, and dark matter. In Ref. [25] it was therefore dubbed 'Neutrino-DFSZ' (νDFSZ) model to account for the extension with right-handed neutrinos. In this thesis, we add inflation to the νDFSZ model in order to give a complete model for particle physics and cosmology.

Outline and Contribution

After a briew review of SMASH in chapter 2 we introduce 2hdSMASH in chapter 3 by discussing and deriving its features in detail. The field- and particle content of 2hdSMASH is discussed in sections 3.1-3.2 which serve as a review of the field- and particle content of the νDFSZ model discussed in Refs. [24, 25]. In section 3.3 we specify the scalar masses which include three neutral CP-even scalars (the SM-like Higgs h, the heavy Higgs H and the PQ-scalar s), two charged CP-even Higgses $H^{\pm}$, one CP-odd Higgs A and the axion a. All masses, except for the axion, have been stated in Ref. [26] but weren't derived in detail, which we do in appendix B with the help of Refs. [26, 27]. In section 3.4 we discuss the neutrino masses which are in accordance with the seesaw mechanism of Refs. [14, 15, 17, 28]. In section 3.5, we state the theoretical constraints which are specified by the Boundedness-from-Below (BfB) and perturbative unitarity conditons, derived in appendix C. The BfB conditions derived in appendix C.1 are in agreement with Refs. [29, 30, 31]. In appendix C.2 we derive the perturbative unitarity conditions by using a `Mathematica` package of `ScannerS`, cf. Ref. [32], whose procedure follows Ref. [33]. The results obtained for the perturbative unitarity conditions in 2hdSMASH could not be fully compared to any reference so far but were partially verified with Ref. [34]. In section 3.6, we reiterate the naturalness philosophy stated in Refs. [25, 35] and adopt it to our model. In sections 3.7-3.8 we derive the matching of 2hdSMASH to its effective low energy theory and the subsequent alignment limit in order to account for a SM-like Higgs. The former has been superficially discussed in Refs. [26, 34] while the latter has been

discussed in the context of the 2HDM in Ref. [36]. Both in combination have only been superficially shown in Ref. [25] but not worked out in detail as we do. In section 3.9 we discuss the intricacies of the scalar mass spectrum and its dependencies on the parameter space. The discussion has been partially adopted from Ref. [26] and combined with the concepts of Ref. [25] to serve the purpose of acquiring parameter space which is compatible with inflation.

Chapters 4-5 are the main chapters of this thesis and discuss inflation and its connection to particle phenomenology, which has not been discussed in any reference in the context of the νDFSZ model.

Chapter 4 introduces inflationary cosmology in 2hdSMASH and its wide range of realizations. Sections 4.1-4.2 serve as motivation and introduction to inflationary cosmology and are based on the reviews of Refs. [37, 38, 39, 40]. In section 4.3 we specify the various inflationary scenarios, i.e. 2HDM-inflation (THI), PQ-inflation (PQI) and mixed PQ-2HDM inflation (PQTHI). The inflationary quantities, i.e. parameters and observables, are derived in appendix D which contribute to the understanding of effective single field inflation and are attributed to the various inflationary scenarios. THI has been discussed in detail by Refs. [41, 42] and was briefly discussed in Ref. [43] in the context of the DFSZ model. We supplement this discussion by including the inflationary conditions and predictions in detail. Moreover, we explain that THI contradicts our naturalness philosophy with regard to non-minimal inflation for which the non-minimal couplings should be generated radiatively. We adopt this concept of non-minimal inflation from Refs. [7, 6, 21, 44]. Consequently we discuss in section 4.3.2 the four main inflationary scenarios, i.e. PQI and PQTHI. These inflationary realizations in the context of the νDFSZ model do not exist in current literature. In particular we find an inflationary single field direction which is composed by three field space directions. This has not been discussed in any reference to date.

In chapter 5, we connect inflation with particle phenomenology by means of RG-running. Sections 5.1-5.4 discuss the various intricacies of RG-running and RG-analysis in order to satisfy the inflationary constraints at the Planck scale while remaining vacuum stable and perturbative. Within this analysis we include thermal leptogenesis and BAU with regard to neutrino masses and its implications to RG-running. Our RG-analysis considers all constraints and provides analytical understanding and expressions for the RG running parameters. Subsequently, we produce benchmark points of the accumulated analysis which we discuss in section 5.5 with

regard to its phenomenological viability. The RG-analysis with regard to inflation in the νDFSZ model has not been covered by any reference so far. In chapter 6 we conclude and discuss our results.

2. Brief Review of SMASH

This review is based on the review [21] and serves as an introduction to the original model proposed in Refs. [6, 7] from which 2hdSMASH originates. In the following we quote the content of Refs. [6, 7, 21] on SMASH.

The Standard-Model-Axion-Seesaw-Higgs portal inflation (SMASH) model [6, 7] is a minimal extension of the Standard Model (SM). It consists of three right handed SM-singlet neutrinos N_i, with $i = 1, 2, 3$, a vector-like Dirac fermion Q which transforms under the SM-gauge group $SU(3)_C \times SU(2)_L \times U(1)_Y$ as $(3, 1, -1/3)$ or as $(3, 1, 2/3)$ and is based on a KSVZ-type axion model [8, 9] involving a complex SM-singlet scalar σ. SMASH is charged under a global $U(1)_{\rm PQ}$ symmetry given in table 2.1, cf. Ref. [7]. The most general scalar potential of SMASH featuring a global $U(1)_{\rm PQ}$ symmetry is given by

$$V(H,\sigma) = \lambda_H \left(H^\dagger H - \frac{v^2}{2}\right)^2 + \lambda_\sigma \left(|\sigma|^2 - \frac{v_\sigma^2}{2}\right)^2 + 2\lambda_{H\sigma} \left(H^\dagger H - \frac{v^2}{2}\right)\left(|\sigma|^2 - \frac{v_\sigma^2}{2}\right), \tag{2.1}$$

with scalar fields

$$H = \begin{pmatrix} G^+(x) \\ \frac{1}{\sqrt{2}}(h(x) + v + iG^0(x)) \end{pmatrix}, \tag{2.2}$$

$$\sigma(x) = \frac{1}{\sqrt{2}}(\rho(x) + v_\sigma) e^{ia(x)/v_\sigma}, \tag{2.3}$$

where $h(x)$ is the SM-like Higgs, $\rho(x)$ is the PQ-scalar, $a(x)$ is the axion field, $G^\pm(x)$ and $G^0(x)$ are the Goldstone modes which get "eaten" by the $W^\pm$- and Z bosons, respectively. The vacuum expectation values (VEVs) are given by

$$\langle H^\dagger H \rangle = v^2/2 \quad , \quad \langle |\sigma|^2 \rangle = v_\sigma^2/2, \tag{2.4}$$

with $v = 246\,\text{GeV}$ as the electroweak VEV and v_σ as the PQ-breaking scale. The vacuum structure given by the VEVs is protected for $\lambda_{H,\sigma} > 0$ and $\lambda_{H\sigma}^2 < \lambda_H \lambda_\sigma$. Furthermore, the VEVs follow a hierarchy, i.e. $v_\sigma / v \gg 1$, which causes the PQ-scalar

q	u	d	L	N	E	Q	$\tilde{Q}$	σ
$1/2$	$-1/2$	$-1/2$	$1/2$	$-1/2$	$-1/2$	$-1/2$	$-1/2$	1

Table 2.1.: SMASH charge assignments under $U(1)_{\mathrm{PQ}}$ and $U(1)_L$ symmetries. This table is taken from Ref. [7].

(saxion) to acquire a large mass

$$m_\rho = \sqrt{2\lambda_\sigma} v_\sigma + \mathcal{O}\left(\frac{v}{v_\sigma}\right), \tag{2.5}$$

whereas the axion acquires a tiny mass after the QCD phase transition,

$$m_a \equiv \frac{\sqrt{\chi_0}}{f_a} \simeq \frac{m_\pi f_\pi}{f_a} \frac{\sqrt{m_u m_d}}{m_u + m_d}, \tag{2.6}$$

with χ_0 as the QCD topological susceptibility, m_π and f_π as the neutral pion mass and its decay constant and $m_{u,d}$ as the masses of the lightest quarks, cf. Ref. [21]. Here, f_a is the axion decay constant which is related to v_σ via

$$f_a \equiv v_\sigma / N_{\mathrm{DW}} \tag{2.7}$$

with $N_{\mathrm{DW}} = 1$ resulting in $f_a = v_\sigma$.

The fermion sector is represented by the most general Yukawa interaction of SMASH cf. Ref. [7]

$$\begin{aligned} \mathcal{L} \supset -\Bigg[& Y_{uij} q_i \epsilon H u_j + Y_{dij} q_i H^\dagger d_j + G_{ij} L_i H^\dagger E_j + F_{ij} L_i \epsilon H N_j + \frac{1}{2} Y_{ij} \sigma N_i N_j \\ & + y\, \tilde{Q} \sigma Q + y_{Q_d i} \sigma Q d_i + h.c. \Bigg], \end{aligned} \tag{2.8}$$

where SM-like interactions are supplemented by mass terms for the new quark Q and for Dirac- and Majorana neutrinos. The Dirac neutrino masses are generated via the type-I Seesaw mechanism where the smallness is explained by the hierarchy of scales $v_\sigma / v \gg 1$, i.e.

$$m_\nu = -\frac{F\, Y^{-1}\, F^T}{\sqrt{2}} \frac{v^2}{v_\sigma} \tag{2.9}$$

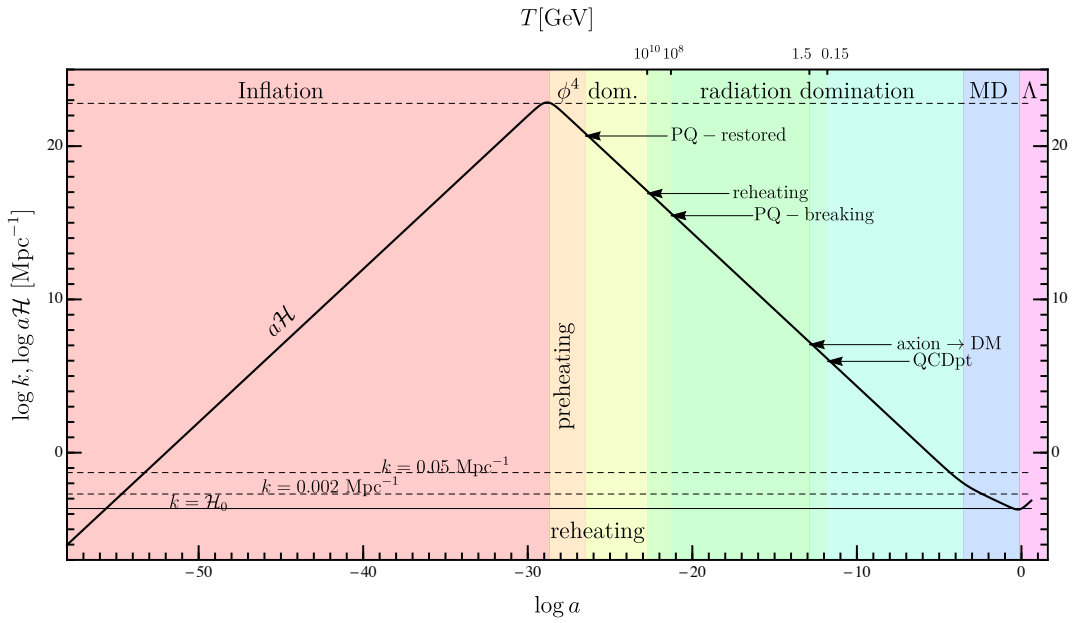

Figure 2.1.: SMASH's complete expansion history of the universe for HHSI. This figure is taken from Ref. [7].

while the Majorana neutrinos and the extra quark acquire very large masses in comparison, cf. Ref. [7]

$$M_{ij} = \frac{Y_{ij}}{\sqrt{2}} v_\sigma + \mathcal{O}\left(\frac{v}{v_\sigma}\right) \quad , \quad m_Q = \frac{y}{\sqrt{2}}\, v_\sigma + \mathcal{O}\left(\frac{v}{v_\sigma}\right) \tag{2.10}$$

In SMASH, the complex scalar singlet σ is non-minimally coupled to gravity, i.e. to the Ricci scalar R via ξ_σ,

$$S \supset -\int d^4x \sqrt{-g}\, \xi_\sigma\, \sigma^* \sigma\, R\,. \tag{2.11}$$

which provides the possibility for inflation, cf. Ref. [6, 7, 21]. Here, the non-minimal coupling ξ_σ can be generated radiatively in a Friedman-Robertson-Walker background. Realizations of inflation in SMASH are based on two inflationary trajectories, where inflation can go along the Hidden-Scalar direction (HSI) or along the mixed Higgs-Hidden-Scalar direction (HHSI) which is featured by $\lambda_{H\sigma} > 0$ or $\lambda_{H\sigma} < 0$, respectively. After inflation ended, SMASH provides an easy expansion history of the universe where the universe expands radiation-like during preheating and reheating, as can be seen in figure 2.1, cf. Ref. [6, 7, 21]. For HHSI, the PQ symmetry is non-thermally restored by the end of preheating. This occurs below the reheating temperature of approximately $T_R \sim 10^{12} - 10^{13}$ GeV, cf. Ref. [45].

3. The 2hdSMASH Model

In this chapter, we introduce the 2hdSMASH model which is a SMASH variant and is based on a νDFSZ-type axion model. First and foremost, we specify its field- and particle content in sections 3.1-3.2 which serves as a review of the νDFSZ proposed in Refs. [24, 25]. In section 3.3 we provide the scalar masses of the 2hdSMASH scalar particle spectrum, which include three neutral CP-even scalars (h, H, s), two charged CP-even scalars ($H^{\pm}$) and two CP-odd scalars (A, a). We identify a as the DFSZ QCD axion which acquires a mass after the QCD phase transition. The other scalar masses are rigorously derived in appendix B where we approximate the mass expressions of the three neutral CP-even scalars by a second order expansion. These mass expressions are numerically verified to an accuracy of more than the digits shown in this thesis. In section 3.4 we state the type-I seesaw formulae providing Dirac- and Majorana neutrino masses. In section 3.5 we discuss theoretical constraints which we derive in appendix C. These involve tree-level Boundedness-from-Below (BfB) and perturbative unitarity conditions which guarantee vacuum stability in a perturbative model. We use these conditions in chapter 4 and particularly in chapter 5 when considering RG running. In section 3.6 we introduce our naturalness philosophy which we adopted from Refs. [25, 35]. Sections 3.7-3.8 serve the purpose of matching 2hdSMASH to its effective low energy theory which is then matched to the SM by means of the alignment limit in order to reproduce SM-like interactions of the 125-GeV neutral Higgs boson. In section 3.9 we discuss the characteristics of the scalar mass spectrum and its interesting features with regard to possible signatures at the High Luminosity Large-Hadron-Collider (HL-LHC) or future colliders.

3.1. Field content and PQ symmetry

The 2hdSMASH model is a SMASH-variant and serves as an extension of the SM where the scalar sector features a complex SM-singlet scalar field S and a type-II 2HDM with two $SU(2)_L$ Higgs doublets Φ_i, $i = 1, 2$. Furthermore, the SM fermion sector is extended by three right handed neutrinos $N_{R,i}$ for which Dirac- and Majorana neutrinos are generated via the type-I Seesaw mechanism. The model is charged under a global $U(1)_{\text{PQ}}$-Symmetry and provides an "invisible" axion which

resembles the νDFSZ axion model (see Ref. [25]). The corresponding PQ-charges of our theory are distributed among the fields as shown in table 3.1. The most general

Field	S	Φ_1	Φ_2	q_L	u_R	d_R	l_L	N_R	e_R
Charge	X_S	X_1	X_2	X_q	X_u	X_d	X_l	X_N	X_e
Value	1	$-\frac{2x}{1+x}$	$\frac{2}{1+x}$	0	$\frac{2}{1+x}$	$\frac{2x}{1+x}$	$\frac{3}{2}-\frac{2}{1+x}$	$-\frac{1}{2}$	$\frac{7}{2}-\frac{4}{1+x}$

Table 3.1.: Charges of fields under the PQ symmetry [25]. Here $x \equiv \tan^2\beta$.

renormalizable scalar potential invariant under $U(1)_{\text{PQ}}$ symmetry transformations is then given by [25]:

$$\begin{aligned} V(\Phi_1,\Phi_2,S) = {} & M_{11}^2\,\Phi_1^\dagger\Phi_1 + M_{22}^2\,\Phi_2^\dagger\Phi_2 + M_{SS}^2\,S^*S \\ & + \frac{\lambda_1}{2}\left(\Phi_1^\dagger\Phi_1\right)^2 + \frac{\lambda_2}{2}\left(\Phi_2^\dagger\Phi_2\right)^2 + \frac{\lambda_S}{2}\left(S^*S\right)^2 \\ & + \lambda_3\left(\Phi_1^\dagger\Phi_1\right)\left(\Phi_2^\dagger\Phi_2\right) + \lambda_4\left(\Phi_1^\dagger\Phi_2\right)\left(\Phi_2^\dagger\Phi_1\right) \\ & + \lambda_{1S}\left(\Phi_1^\dagger\Phi_1\right)\left(S^*S\right) + \lambda_{2S}\left(\Phi_2^\dagger\Phi_2\right)\left(S^*S\right) - \lambda_{12S}\left(\Phi_2^\dagger\Phi_1 S^2 + h.c.\right). \end{aligned} \tag{3.1}$$

Moreover, the most general type-II 2HDM Yukawa Lagrangian extended by Dirac- and Majorana interactions reads[1] [25]:

$$-\mathcal{L}_Y = Y_u\overline{q_L}\tilde{\Phi}_2 u_R + Y_d\overline{q_L}\Phi_1 d_R + Y_e\overline{l_L}\Phi_1 e_R + Y_\nu\overline{l_L}\tilde{\Phi}_1 N_R + \frac{1}{2}y_N\overline{(N_R)^c}SN_R + \text{h.c.}\,, \tag{3.2}$$

where we imply family indices and denote $\tilde{\Phi}_i \equiv i\tau_2\Phi_i^*$.

3.2. Vacuum structure and particle content

The vacuum is determined by the vacuum expectation values (VEVs)

$$\langle\Phi_i\rangle \equiv \left(0, v_i/\sqrt{2}\right)^T \quad , \quad \langle S\rangle \equiv v_S/\sqrt{2} \tag{3.3}$$

for which the scalar potential reaches its minimum, provided that the parameters are adequately chosen[2]. Combining the VEVs of the two-Higgs doublets establishes the electroweak VEV $\sqrt{v_1^2+v_2^2} \equiv v \simeq 246$ GeV with $\tan\beta \equiv v_2/v_2$. By comparison the VEVs respect the hierarchy $v_S/v \gg 1$. This hierarchy is essential to 2hdSMASH since it supports a tiny DFSZ QCD-axion which we will comment on in section 3.3.2.

[1] Choosing another charge assignment to the right handed charged leptons, e_R, one may also realise a Flipped 2HDM in 2hdSMASH [25].

[2] We will discuss the theoretical constraints on these parameters in section 3.5.

After spontaneous symmetry breaking, the two $SU(2)_L$ Higgs doublets Φ_i and the complex singlet S can be expanded around their VEVs and are given by

$$\Phi_i = \begin{pmatrix} h_i^+ \\ \frac{1}{\sqrt{2}}(h_i + v_i + ia_i) \end{pmatrix} \quad , \quad S = \frac{1}{\sqrt{2}} s + v_S + ia_S \, . \tag{3.4}$$

Counting all degrees of freedom amounts to a total of $4 + 4 + 2 = 10$ spin-zero particle excitations around the vacuum. In order to account for physical particle excitations of the two Higgs doublets, a basis transformation into the so-called Higgs-mass basis is required by rotating the fields

$$\begin{pmatrix} h_1 \\ h_2 \end{pmatrix} = \mathcal{O}_\alpha \begin{pmatrix} h \\ H \end{pmatrix} \quad , \quad \begin{pmatrix} a_1 \\ a_2 \end{pmatrix} = \mathcal{O}_\beta \begin{pmatrix} A \\ G_0 \end{pmatrix} \quad , \quad \begin{pmatrix} h_1^+ \\ h_2^+ \end{pmatrix} = \mathcal{O}_\beta \begin{pmatrix} H^\pm \\ G^\pm \end{pmatrix} \tag{3.5}$$

with transformation matrices:

$$\mathcal{O}_X = \begin{pmatrix} \cos(X) & -\sin(X) \\ \sin(X) & \cos(X) \end{pmatrix} \quad , \quad X = \alpha, \beta \tag{3.6}$$

and by rotating the Higgs doublets

$$\begin{pmatrix} \Phi_1' \\ \Phi_2' \end{pmatrix} = \begin{pmatrix} \cos(\beta) & \sin(\beta) \\ -\sin(\beta) & \cos(\beta) \end{pmatrix} \begin{pmatrix} \Phi_1 \\ \Phi_2 \end{pmatrix} = \begin{pmatrix} \Phi_1 \cos(\beta) + \Phi_2 \sin(\beta) \\ -\Phi_1 \sin(\beta) + \Phi_2 \cos(\beta) \end{pmatrix} . \tag{3.7}$$

As a result, we obtain the following expression for Φ_i'

$$\Phi_1' = \begin{pmatrix} H^+ \\ \frac{1}{\sqrt{2}}(v + h\cos(\beta - \alpha) + H\sin(\beta - \alpha) + iA) \end{pmatrix} \tag{3.8}$$

$$\Phi_2' = \begin{pmatrix} G^+ \\ \frac{1}{\sqrt{2}}(h\sin(\beta - \alpha) + H\cos(\beta - \alpha) + iG^0) \end{pmatrix} \tag{3.9}$$

where G^0 corresponds to one neutral and $G^\pm$ to two charged Goldstone bosons which are later "eaten" by the Z- and $W^\pm$-boson after symmetry breaking. The other seven degrees of freedom are associated to seven particle excitations in the spectrum: three neutral CP-even states h, H and s, two charged CP-even states $H^\pm$ and two CP-odd states a and A. We identify h as the SM-like Higgs with a mass of 125 GeV, H as the heavy Higgs, $H^\pm$ as the two charged Higgses, A as the pseudoscalar Higgs and a

as the axion [46, 47]. We note in equations (3.8)-(3.9) the sine- and cosine functions of mixing angles $\beta - \alpha$. These functions determine whether the 2HDM reduces to the SM, i.e. $\beta - \alpha \approx \pi/2$ via the alignment limit which we will comment on in section 3.8 for 2hdSMASH.

3.3. Masses of scalars

In the following, we will give the tree-level scalar and neutrino masses which are calculated in detail in appendix B (see also refs. [24, 26]). Here we just quote the results.

3.3.1. Masses of charged Higgs bosons

The tree-level masses of the charged Higgs bosons are given by

$$m_{H^\pm}^2 = \frac{1}{2}\left(\frac{\left(t_\beta^2+1\right)\lambda_{12S}}{t_\beta} - \frac{\lambda_4 v^2}{v_S^2}\right) v_S^2 \,. \tag{3.10}$$

3.3.2. Masses of CP-odd scalars

One of the two CP-odd scalars is massless at tree level. It is the axion, a, the Nambu-Goldstone boson from the breaking of the $U(1)_{\rm PQ}$ symmetry [46, 47]. It acquires non-perturbatively a small mass through mixing with the neutral pion,

$$m_a \simeq \frac{\sqrt{z}}{1+z}\frac{m_\pi f_\pi}{f_a} \simeq 0.57\ \text{meV}\left(\frac{10^{10}\ \text{GeV}}{f_a}\right), \tag{3.11}$$

where $z = m_u/m_d$ is the ratio of the up- and down quark masses, m_π the pion mass, f_π the neutral pion decay constant and f_a the axion decay constant given by:

$$f_a = \frac{\sqrt{v_S^2 + 4\frac{v_1^2 v_2^2}{v^2}}}{6}\,. \tag{3.12}$$

The axion decay constant f_a and thus the PQ-scale $v_S \simeq 6 f_a$, is constrained by astrophysics and cosmology. From the measured duration of the neutrino signal of the supernova 1987A [48] a lower bound is provided for f_a. An upper bound on f_a is acquired by assuming all cold dark matter consisting of axions. Hence, the PQ-scale

in 2hdSMASH is preferably in the range

$$\begin{aligned} 3.1 \times 10^9\,\text{GeV} \lesssim v_S \lesssim 5.9 \times 10^{10}\,\text{GeV}\,, \text{ for } \tan\beta \lesssim 0.5\,, \\ 5.9 \times 10^9\,\text{GeV} \lesssim v_S \lesssim 5.9 \times 10^{10}\,\text{GeV}\,, \text{ for } \tan\beta \gtrsim 5\,. \end{aligned} \tag{3.13}$$

which we argue in appendix A. Since the hierarchy of scales is so large, i.e. $v_S/v \gg 1$, f_a consists mostly of v_S.

The tree-level mass of the second CP-odd scalar boson, i.e. the pseudoscalar Higgs boson A, is given by

$$m_A^2 = \frac{2\lambda_{12S}}{1+t_\beta^2}\left(\frac{v^2}{v_S^2}t_\beta + \frac{\left(1+t_\beta^2\right)^2}{4t_\beta}\right) v_S^2\,. \tag{3.14}$$

In order to avoid a tachyonic mass for m_A, we require

$$\lambda_{12S} \geq 0\,. \tag{3.15}$$

3.3.3. Masses of CP-even scalars

The masses of the CP-even scalars are given in units of v_S^2 where we expanded the expressions for $v/v_S \ll 1$ in a power series up to second order:

$$\frac{m_h^2}{v_S^2} = \frac{1}{\left(1+t_\beta^2\right)^2}\left[\lambda_1 + t_\beta^4\,\lambda_2 + 2\,t_\beta^2\,\lambda_{34} - \frac{\left(\lambda_{1S} + t_\beta^2\,\lambda_{2S} - 2t_\beta\lambda_{12S}\right)^2}{\lambda_S}\right]\left(\frac{v}{v_S}\right)^2 + \mathcal{O}\left(\left(\frac{v}{v_S}\right)^4\right), \tag{3.16}$$

$$\frac{m_H^2}{v_S^2} = \frac{\left(1+t_\beta^2\right)\lambda_{12S}}{2t_\beta} + \frac{t_\beta}{\left(1+t_\beta^2\right)^2}\left[\frac{2\left(\left(\lambda_{1S}-\lambda_{2S}\right)t_\beta + \lambda_{12S}\left(1-t_\beta^2\right)\right)^2}{\lambda_{12S}\left(1+t_\beta^2\right) - 2t_\beta\lambda_S} + \left(\lambda_1+\lambda_2-2\lambda_{34}\right)t_\beta\right]\left(\frac{v}{v_S}\right)^2 + \mathcal{O}\left(\left(\frac{v}{v_S}\right)^4\right), \tag{3.17}$$

$$\frac{m_s^2}{v_S^2} = \lambda_S + \frac{t_\beta}{\left(1+t_\beta^2\right)^2}\left[\frac{\left(\lambda_{1S}+\lambda_{2S}t_\beta^2 - 2t_\beta\lambda_{12S}\right)^2}{\lambda_S} - \frac{2t_\beta^2\left(\left(\lambda_{1S}-\lambda_{2S}\right)t_\beta + \lambda_{12S}\left(1-t_\beta^2\right)\right)^2}{\lambda_{12S}\left(1+t_\beta^2\right) - 2t_\beta\lambda_S}\right]\left(\frac{v}{v_S}\right)^2 + \mathcal{O}\left(\left(\frac{v}{v_S}\right)^4\right). \tag{3.18}$$

The leading contribution in the series expansion, i.e. $(v/v_S)^0$, vanishes for m_h^2/v_S^2 but remains for m_H^2/v_S^2 and m_s^2/v_S^2. Since m_h is of $\mathcal{O}(v)$, we can associate h as the SM-like Higgs boson which is constrained by collider searches to 125.25 ± 0.17 GeV [49]. The masses of H and s are of order v_S. We checked the accuracy of the masses shown in eqs. (3.16)-(3.18) with numerically determined eigenvalues of the squared mass matrix given in (B.10) of appendix B. The results give an accuracy more than the digits shown in this thesis. The rest of the discussion about the characteristics of the scalar mass spectrum is deferred to sec. 3.9.

3.4. Masses of neutrinos

After symmetry breaking, the last two terms in eq. (3.2) give rise to the aforementioned Majorana- and Dirac neutrino mass terms, realizing the type I seesaw mech-

anism [14, 15, 16, 17]. The neutrino mass matrix reads:

$$M_\nu = \begin{pmatrix} \mathbf{0_{3\times 3}} & M_D \\ M_D^T & M_M \end{pmatrix} = \frac{1}{\sqrt{2}} \begin{pmatrix} \mathbf{0_{3\times 3}} & Y_\nu v_1 \\ Y_\nu^T v_1 & \frac{1}{2} Y_N v_S \end{pmatrix} , \tag{3.19}$$

where M_M represents the Majorana neutrino mass matrix and M_D represents the Dirac neutrino mass matrix. The smallness of the masses of the SM active neutrinos is thus explained by the hierarchy $v_S \gg v_1$:

$$m_\nu = -M_D M_M^{-1} M_D^T = -\frac{Y_\nu Y_N^{-1} Y_\nu^T}{\sqrt{2}} \frac{v_1^2}{v_S} . \tag{3.20}$$

Assuming a diagonal ansatz for the Yukawa coupling matrix Y_N, we obtain the masses for Majorana neutrino masses in a simple way

$$M_N = \frac{1}{\sqrt{2}} Y_N v_S^2 + \mathcal{O}\left(\frac{v}{v_S}\right) . \tag{3.21}$$

3.5. Theoretical constraints

In this section we provide theoretical constraints to ensure vacuum stability and perturbative unitarity in order to have a stable, finite and renormalizable theory. Vacuum stability is determined by the Boundedness-from-Below (BfB) conditions where quartic couplings are constrained by imposing a positive scalar potential in order to avoid tachyonic energy states in all field directions for large and small field values.

The necessary and sufficient BfB conditions are based on copositivity criteria [31, 50, 30] which we derive in appendix C.1. For now, we simply state the results of our analytic derivation. We start with the necessary BfB conditions which are given by:

$$\begin{aligned} &\lambda_1 > 0 \ , \ \lambda_2 > 0 \ , \ \lambda_3 > -\sqrt{\lambda_1 \lambda_2} \ , \ \lambda_{34} > -\sqrt{\lambda_1 \lambda_2} , \\ &\lambda_S > 0 \ , \ \sqrt{\lambda_1 \lambda_S} > \lambda_{1S} > -\sqrt{\lambda_1 \lambda_S} \ , \ \sqrt{\lambda_2 \lambda_S} > \lambda_{2S} > -\sqrt{\lambda_2 \lambda_S} , \\ &\lambda_S \lambda_{34} - \lambda_{1S} \lambda_{2S} + \sqrt{\left(\lambda_1 \lambda_S - \lambda_{1S}^2\right)\left(\lambda_2 \lambda_S - \lambda_{2S}^2\right)} > 0 , \\ &\lambda_{1S} > 0 \ , \ \lambda_{2S} > 0 \ , \ \lambda_{1S} \lambda_{2S} - |\lambda_{12S}|^2 > 0 , \end{aligned} \tag{3.22}$$

where $\lambda_{34} \equiv \lambda_3 + \lambda_4$. The sufficient BfB conditions are acquired by imposing the portal terms of the scalar potential to be positive, i.e.

$$V_4^{\text{Portal}} = \lambda_{1S} h_1^2 s^2 + \lambda_{2S} h_2^2 s^2 - \lambda_{12S} h_1 h_2 s^2 + \text{h.c.} \geq 0 \tag{3.23}$$

which amounts to:

$$\lambda_{1S} \geq 0 \ , \lambda_{2S} \geq 0 \ , \ \ \lambda_{1S}\lambda_{2S} - \lambda_{12S}^2 \geq 0 \, . \tag{3.24}$$

The sufficient BfB conditions of the copositivity criteria are very restrictive. Depending on the values of the parameter set they can be, however, softened. This can be numerically determined by use of the `Mathematica` package `BFB` from Ref. [30] where the BfB conditions are found with the resultants method. If a parameter point is positive (semi-)definite then it's allowed, otherwise it's dismissed. This will be useful when considering inflation in section 4.3.

With the BfB conditions we have ensured a stable vacuum by avoiding tachyonic vacuum states. In order to ensure a finite and renormalizable theory, we impose the perturbative unitarity conditions. These are applied at low- and high energies to prevent large divergencies and thus Landau poles which would make any theory unpredictable. The perturbative unitarity conditions which are derived in appendix C.2 are given by:

$$|\lambda_{1,2,3,1S,2S}| < 8\pi \, , \tag{3.25}$$

$$|\lambda_3 \pm \lambda_4| < 8\pi \, , \tag{3.26}$$

$$\left| \frac{1}{2} \left(\lambda_1 + \lambda_2 \pm \sqrt{(\lambda_1 - \lambda_2)^2 + 4\lambda_4^2} \right) \right| < 8\pi \, , \tag{3.27}$$

$$\left| \frac{1}{2} \left(\lambda_{1S} + \lambda_{2S} \pm \sqrt{16\lambda_{12S}^2 + (\lambda_{1S} - \lambda_{2S})^2} \right) \right| < 8\pi \, , \tag{3.28}$$

$$\left| \frac{1}{2} \left(\lambda_3 + 2\lambda_4 + \lambda_S \pm \sqrt{16\lambda_{12S}^2 + (\lambda_3 + 2\lambda_4 - \lambda_S)^2} \right) \right| < 8\pi \, , \tag{3.29}$$

$$\frac{1}{2} \left| k_{1,2,3} \right| < 8\pi \, . \tag{3.30}$$

Furthermore, we consider the perturbative unitarity constraints for the Yukawa couplings $Y_{u,d,e}$ of the type-I DFSZ model which affect $\tan\beta \equiv v_2/v_1$. The bounds on $\tan\beta$ are thus given by Ref. [51]:

$$0.25 \lesssim \tan\beta \lesssim 170 \, . \tag{3.31}$$

3.6. Naturalness philosophy

According to Refs. [25, 24, 35, 36] there are technically natural limits associated with enhanced Poincaré symmetries for extended Higgs and/or neutrino models. In par-

ticular, the νDFSZ model hosts a variety of parameters which are technically natural to be small, cf. [25, 35]. We adopt these considerations to our naturalness philosophy by applying them to 2hdSMASH. Henceforth, we will consider the portal couplings λ_{1S}, λ_{2S} and λ_{12S}, as well as the Yukawa couplings Y_ν and Y_N to be naturally small, such that $\lambda_{1S,2S,12S}, Y_{N,\nu} \to 0$ follows. This leads to the enhanced Poincaré symmetry $\mathcal{G}_P^\nu \times \mathcal{G}_P^{\text{2HDM}} \times \mathcal{G}_P^S$ effectively decoupling the 2HDM from the neutrino- and PQ-sector below the matching scale determined by the PQ-scalar mass m_s cf. Ref. [25]. This enhanced Poincaré symmetry protects the electroweak scale from large radiative quantum corrections. We can identify two subsystems with the aforementioned natural limits. The limit $Y_{N,\nu}, \lambda_{12S} \to 0$ reinstates the $U(1)_L$-symmetry associated with lepton number, which we can associate with an enhanced Poincaré symmetry $\mathcal{G}_P^\nu \times \mathcal{G}_P^{\text{DFSZ}}$ where ν_R decouples from the DFSZ. Furthermore, the limit $\lambda_{1S,2S,12S} \to 0$ decouples the ν2HDM- from the PQ-sector, leading to the enhanced Poincaré symmetry $\mathcal{G}_P^{\nu\text{2HDM}} \times \mathcal{G}_P^S$. Moreover, we will consider in chapter 4 inflation in 2hdSMASH where the PQ-scalar s will be non-minimally coupled to gravity via the non-minimal coupling ξ_S. We require that ξ_S to be radiatively generated, i.e. $\xi_S \lesssim 1$, which we adopt to our naturalness philosophy from Refs. [44, 52, 7].

3.7. Matching to 2HDM

In this section we show that the full high energy theory of 2hdSMASH reduces to a softly broken $U(1)$-symmetric ν2HDM low-energy theory where the extra $U(1)_L$-symmetry can be associated with lepton number caused by a technically natural limit for $Y_N, Y_\nu, \lambda_{12S} \to 0$, cf. [25]. As discussed in section 3.6, we consider the limit $\lambda_{1S,2S,12S}, Y_{N,\nu} \to 0$ corresponding to the enhanced Poincaré symmetry
$\mathcal{G}_P^\nu \times \mathcal{G}_P^{\text{2HDM}} \times \mathcal{G}_P^S$ which protects the electroweak scale from large radiative corrections, cf. [35, 25]. We will motivate these consideration by matching 2hdSMASH at the matching scale m_s to its low-energy theory where we show that tiny portal couplings will prove to protect the electroweak scale. Therefore, we consider the equation of motion of s at zero momentum at m_s:

$$\frac{\partial V}{\partial s} = 0 \;\Rightarrow\; s^2 = -\frac{h_1^2 \lambda_{1S}}{\lambda_S} + \frac{2 h_1 h_2 \lambda_{12S}}{\lambda_S} - \frac{h_2^2 \lambda_{2S}}{\lambda_S} - \frac{2 M_{SS}^2}{\lambda_S}\,. \tag{3.32}$$

By considering now the scalar potential with s at zero momentum, i.e. integrating s out, we obtain the threshold corrected scalar potential:

$$V = \frac{h_1^2}{2}\left(M_{11}^2 - \frac{\lambda_{1S}M_{SS}^2}{\lambda_S}\right) + \frac{h_2^2}{2}\left(M_{22}^2 - \frac{\lambda_{2S}M_{SS}^2}{\lambda_S}\right) + \frac{\lambda_{12S}M_{SS}^2}{2\lambda_S}h_1h_2\left(\frac{h_1^2\lambda_{1S} + h_2^2\lambda_{2S}}{M_{SS}^2} + 2\right) \tag{3.33}$$
$$+ \frac{h_1^4}{8}\left(\lambda_1 - \frac{\lambda_{1S}^2}{\lambda_S}\right) + \frac{h_2^4}{8}\left(\lambda_2 - \frac{\lambda_{2S}^2}{\lambda_S}\right) + \frac{h_1^2h_2^2}{4}\left(\lambda_{34} - \frac{\lambda_{1S}\lambda_{2S} + 2\lambda_{12S}^2}{\lambda_S}\right) - \frac{M_{SS}^2}{2\lambda_S}\,.$$

The third quadratic term of eq. (3.33) constitutes a non-linear term given by the coupling λ_{12S}. By taking into account that $h_1^2\lambda_{1S} + h_2^2\lambda_{2S} \ll M_{SS}^2 \sim m_s^2$ we can approximate the terms as follows:

$$\frac{\lambda_{12S}M_{SS}^2}{2\lambda_S}h_1h_2\left(\frac{h_1^2\lambda_{1S} + h_2^2\lambda_{2S}}{M_{SS}^2} + 2\right) \approx \frac{\lambda_{12S}M_{SS}^2}{\lambda_S}h_1h_2\,. \tag{3.34}$$

Therefore, the scalar potential can be approximated to:

$$V \simeq \frac{h_1^2}{2}\left(M_{11}^2 - \frac{\lambda_{1S}M_{SS}^2}{\lambda_S}\right) + \frac{h_2^2}{2}\left(M_{22}^2 - \frac{\lambda_{2S}M_{SS}^2}{\lambda_S}\right) + \frac{\lambda_{12S}M_{SS}^2}{\lambda_S}h_1h_2 \tag{3.35}$$
$$+ \frac{h_1^4}{8}\left(\lambda_1 - \frac{\lambda_{1S}^2}{\lambda_S}\right) + \frac{h_2^4}{8}\left(\lambda_2 - \frac{\lambda_{2S}^2}{\lambda_S}\right) + \frac{h_1^2h_2^2}{4}\left(\lambda_{34} - \frac{\lambda_{1S}\lambda_{2S} + 2\lambda_{12S}^2}{\lambda_S}\right) - \frac{M_{SS}^4}{2\lambda_S}\,.$$

The corresponding threshold corrections for the matching of 2hdSMASH to its effective low energy theory can be read off:

$$\bar{M}_{11,22}^2 = \left(M_{11,22}^2 - \frac{\lambda_{1S,2S}M_{SS}^2}{\lambda_S}\right)\,, \tag{3.36}$$

$$\bar{M}_{12}^2 = 2\lambda_{12S}M_{SS}^2\,, \tag{3.37}$$

$$\bar{\lambda}_{1,2} = \left(\lambda_{1,2} - \frac{\lambda_{1S,2S}^2}{\lambda_S}\right)\,, \tag{3.38}$$

$$\bar{\lambda}_{34} = \left(\lambda_{34} - \frac{\lambda_{1s}\lambda_{2s} + 2\epsilon^2}{\lambda_s}\right)\,, \tag{3.39}$$

which represents a softly broken $U(1)$-symmetric 2HDM. The tadpole equation for M_{SS}^2 is calculated by:

$$\frac{\partial V}{\partial s} \stackrel{!}{=} 0 \;\;\Rightarrow\;\; M_{SS}^2 = \frac{1}{2}\left(-\lambda_{1S}v_1^2 + 2v_1v_2\lambda_{12S} - \lambda_{2S}v_2^2 - \lambda_S v_S^2\right)\,. \tag{3.40}$$

The VEVs $v_{1,2,S}$ follow a hierarchy, namely $v_S^2 \gg v_{1,2}^2$. Hence, the tadpole equation M_{SS}^2 can be approximated as follows:

$$M_{SS}^2 = \frac{v_S^2}{2}\left(-\lambda_{1S}\frac{v_1^2}{v_S^2} + 2\frac{v_1 v_2}{v_S^2}\lambda_{12S} - \lambda_{2S}\frac{v_2^2}{v_S^2} - \lambda_S\right) \overset{v_S^2 \gg v_{1,2}^2}{\approx} -\frac{\lambda_S v_S^2}{2}\,. \tag{3.41}$$

Finally, the threshold corrected scalar potential of the effective low-energy theory is acquired and reads:

$$\begin{aligned} V \simeq\ & \frac{h_1^2}{2}\left(M_{11}^2 + \frac{\lambda_{1S}v_S^2}{2}\right) + \frac{h_2^2}{2}\left(M_{22}^2 + \frac{\lambda_{2S}v_S^2}{2}\right) - \frac{h_1 h_2 \lambda_{12S} v_S^2}{2} \\ & + \frac{h_1^4}{8}\left(\lambda_1 - \frac{\lambda_{1S}^2}{\lambda_S}\right) + \frac{h_2^4}{8}\left(\lambda_2 - \frac{\lambda_{2S}^2}{\lambda_S}\right) + \frac{h_1^2 h_2^2}{4}\left(\lambda_{34} - \frac{\lambda_{1S}\lambda_{2S} + 2\lambda_{12S}^2}{\lambda_S}\right), \end{aligned} \tag{3.42}$$

where the effective mass term $m_s \simeq \frac{\lambda_S v_S^4}{8}$ was omitted. The following coupling associations for the effective low-energy theory are thus given by:

$$\begin{aligned} m_{11,22}^2 &= \left(M_{11,22}^2 + \frac{\lambda_{1S,2S}v_S^2}{2}\right) \\ m_{12}^2 &= \lambda_{12S}v_S^2 \\ \bar{\lambda}_{1,2} &= \left(\lambda_{1,2} - \frac{\lambda_{1S,2S}^2}{\lambda_S}\right) \\ \bar{\lambda}_{34} &= \left(\lambda_{34} - \frac{\lambda_{1S}\lambda_{2S} + 2\lambda_{12S}^2}{\lambda_S}\right) \\ M_{SS}^2 &\simeq -\frac{\lambda_S v_S^2}{2} \end{aligned} \tag{3.43}$$

where M_{SS}^2 is related to the aforementioned matching-scale via $m_s \simeq \sqrt{-2M_{SS}^2}$. The threshold corrections are negligible, i.e. $\lambda_{iS}^2/\lambda_S \ll 1$. Therefore, the effective low energy theory of a softly broken $U(1)$-symmetric 2HDM has approximately the following scalar potential $V^{\nu 2\mathrm{HDM}}$:

$$\begin{aligned} V^{\nu 2\mathrm{HDM}} \simeq & m_{11}^2|\Phi_1|^2 + m_{22}^2|\Phi_2|^2 - m_{12}^2\left(\Phi_1^\dagger\Phi_2 + \Phi_2^\dagger\Phi_1\right) \\ & + \frac{\lambda_1}{2}|\Phi_1|^4 + \frac{\lambda_2}{2}|\Phi_2|^4 + \lambda_3\left|\Phi_1\right|^2\left|\Phi_2\right|^2 + \lambda_4\left(\Phi_1^\dagger\Phi_2\right)\left(\Phi_2^\dagger\Phi_1\right). \end{aligned} \tag{3.44}$$

3.8. Alignment limit

From our discussion on the particle content in section 3.2, we arrived at the alignment limit by considering the two Higgs doublets in the Higgs-mass-basis. The alignment limit describes in an extended Higgs sector, such as the 2HDM, the limit to a SM-like Higgs boson which reproduces SM-like couplings. In order to account for SM-like interactions in 2hdSMASH, we need to match the effective low energy theory, i.e. ν2HDM, from section 3.7 to the SM by computing the alignment limit where $\beta - \alpha \approx \pi/2$. We do this in two-steps: a) we express the neutral CP-even squared mass matrix for the case of 2HDM matching; b) we perform the alignment limit in the context of the 2HDM (see Ref.[36]), thus showing that 2hdSMASH reproduces SM-like Higgs boson interactions.

Hence, we start with the most general scalar potential of 2hdSMASH:

$$\begin{aligned} V(\Phi_1,\Phi_2,S) =& M_{11}^2 |\Phi_1|^2 + M_{22}^2 |\Phi_2|^2 + M_{SS}^2 |S|^2 \\ &+ \frac{1}{2}\lambda_1 |\Phi_1|^4 + \frac{1}{2}\lambda_2 |\Phi_2|^4 + \lambda_3 |\Phi_1|^2 |\Phi_2|^2 + \lambda_4 \left(\Phi_1^\dagger \Phi_2\right)\left(\Phi_2^\dagger \Phi_1\right) \\ &+ \frac{1}{2}\lambda_S |S|^4 + \lambda_{1S} |\Phi_1|^2 |S|^2 + \lambda_{2S} |\Phi_2|^2 |S|^2 - \lambda_{12S}\left(\Phi_1^\dagger \Phi_2 S^2 + \Phi_2^\dagger \Phi_1 S^{*2}\right) \end{aligned} \tag{3.45}$$

which leads to the most general neutral CP-even squared scalar mass matrix:

$$\mathcal{M}_{0^+}^2 = \tag{3.46}$$
$$\begin{pmatrix} \frac{1}{2}\left(2M_{11}^2 + 3\lambda_1 v_1^2 + v_2^2(\lambda_3+\lambda_4) + \lambda_{1S} v_S^2\right) & v_1 v_2(\lambda_3+\lambda_4) - \frac{v_S^2 \lambda_{12S}}{2} & \lambda_{1S} v_1 v_S - v_2 v_S \lambda_{12S} \\ v_1 v_2(\lambda_3+\lambda_4) - \frac{v_S^2 \lambda_{12S}}{2} & \frac{1}{2}\left(2M_{22}^2 + v_1^2(\lambda_3+\lambda_4) + 3\lambda_2 v_2^2 + \lambda_{2S} v_S^2\right) & \lambda_{2S} v_2 v_S - v_1 v_S \lambda_{12S} \\ \lambda_{1S} v_1 v_S - v_2 v_S \lambda_{12S} & \lambda_{2S} v_2 v_S - v_1 v_S \lambda_{12S} & \frac{1}{2}\left(2M_{SS}^2 + \lambda_{1S} v_1^2 - 2v_1 v_2 \lambda_{12S} + \lambda_{2S} v_2^2 + 3\lambda_S v_S^2\right) \end{pmatrix}$$

with the tadpole equations:

$$M_{11}^2 = -\frac{-v_2 v_S^2 \lambda_{12S} + v_1^3 \lambda_1 + v_1 v_S^2 \lambda_{1S} + v_1 v_2^2 \lambda_{34}}{2v_1}, \tag{3.47}$$

$$M_{22}^2 = -\frac{-v_1 v_S^2 \lambda_{12S} + v_2^3 \lambda_2 + v_2 v_S^2 \lambda_{2S} + v_2 v_1^2 \lambda_{34}}{2v_2}, \tag{3.48}$$

$$M_{SS}^2 = \frac{1}{2}\left(2v_1 v_2 \lambda_{12S} - v_1^2 \lambda_{1S} - v_2^2 \lambda_{2S} - v_S^2 \lambda_S\right), \tag{3.49}$$

for which we get:

$$\mathcal{M}^2_{0^+} = \begin{pmatrix} \lambda_1 v_1^2 + \frac{v_2 v_S^2 \lambda_{12S}}{2v_1} & v_1 v_2(\lambda_3+\lambda_4) - \frac{v_S^2\lambda_{12S}}{2} & \lambda_{1S} v_1 v_S - v_2 v_S \lambda_{12S} \\ v_1 v_2(\lambda_3+\lambda_4) - \frac{v_S^2\lambda_{12S}}{2} & \frac{v_1 v_S^2 \lambda_{12S}}{2v_2} + \lambda_2 v_2^2 & \lambda_{2S} v_2 v_S - v_1 v_S \lambda_{12S} \\ \lambda_{1S} v_1 v_S - v_2 v_S \lambda_{12S} & \lambda_{2S} v_2 v_S - v_1 v_S \lambda_{12S} & \lambda_S v_S^2 \end{pmatrix}. \tag{3.50}$$

By matching 2hdSMASH with its effective low-energy theory given by the soft $U(1)$-symmetric ν2HDM, we can write down the corresponding scalar potential with threshold corrections:

$$\begin{aligned} \bar{V} \simeq & \frac{h_1^2}{2}\left(m_{11}^2 + \frac{\lambda_{1S} v_S^2}{2}\right) + \frac{h_2^2}{2}\left(m_{22}^2 + \frac{\lambda_{2S} v_S^2}{2}\right) - \frac{h_1 h_2 \lambda_{12S} v_S^2}{2} \\ & + \frac{h_1^4}{8}\left(\lambda_1 - \frac{\lambda_{1S}^2}{\lambda_S}\right) + \frac{h_2^4}{8}\left(\lambda_2 - \frac{\lambda_{2S}^2}{\lambda_S}\right) + \frac{h_1^2 h_2^2}{4}\left(\lambda_{34} - \frac{\lambda_{1S}\lambda_{2S} + 2\lambda_{12S}^2}{\lambda_S}\right), \end{aligned} \tag{3.51}$$

with the following squared mass matrix:

$$\mathcal{M}^2_{0^+} \simeq \begin{pmatrix} \frac{1}{2}\left(2m_{11}^2 + 3v_1^2\left(\lambda_1 - \frac{\lambda_{1S}^2}{\lambda_S}\right) + v_2^2\left(\lambda_{34} - \frac{\lambda_{1S}\lambda_{2S}+2\lambda_{12S}^2}{\lambda_S}\right) + \lambda_{1S} v_S^2\right) & v_1 v_2\left(\lambda_{34} - \frac{\lambda_{1S}\lambda_{2S}+2\lambda_{12S}^2}{\lambda_S}\right) - \frac{v_S^2\lambda_{12S}}{2} \\ v_1 v_2\left(\lambda_{34} - \frac{\lambda_{1S}\lambda_{2S}+2\lambda_{12S}^2}{\lambda_S}\right) - \frac{v_S^2\lambda_{12S}}{2} & \frac{1}{2}\left(2m_{22}^2 + 3v_2^2\left(\lambda_2 - \frac{\lambda_{2S}^2}{\lambda_S}\right) + v_1^2\left(\lambda_{34} - \frac{\lambda_{1S}\lambda_{2S}+2\lambda_{12S}^2}{\lambda_S}\right) + \lambda_{2S} v_S^2\right) \end{pmatrix}. \tag{3.52}$$

For simplicity we make the association $\tilde{\lambda}_{ij} = \lambda_{ij} - \lambda_{ijS}^2/\lambda_S$ as discussed in eq. (3.43). The squared mass matrix is then given by:

$$\tilde{\mathcal{M}}^2_{0^+} = \begin{pmatrix} m_{11}^2 + \frac{1}{2}\left(3\tilde{\lambda}_1 v_1^2 + \tilde{\lambda}_{34} v_2^2\right) & \tilde{\lambda}_{34} v_1 v_2 - m_{12}^2 \\ \tilde{\lambda}_{34} v_1 v_2 - m_{12}^2 & m_{22}^2 + \frac{1}{2}\left(\tilde{\lambda}_{34} v_1^2 + 3\lambda_2 v_2^2\right) \end{pmatrix} \tag{3.53}$$

with $m_{12}^2 = \lambda_{12S} v_S/2$. With a 2×2-rotation matrix R:

$$R = \begin{pmatrix} \cos\alpha & -\sin\alpha \\ \sin\alpha & \cos\alpha \end{pmatrix}, \tag{3.54}$$

we diagonalize the above squared mass matrix of eq. (3.53)

$$D^2_{0^+} \equiv \mathrm{diag}\left(m_H^2, m_h^2\right) = R^\dagger \mathcal{M}^2_{0^+} R\,, \tag{3.55}$$

for which we obtain the following condition to determine $\tan 2\alpha$:

$$\left(D^2_{0^+}\right)_{1,2} \overset{!}{=} 0 \quad \Rightarrow \quad \tan 2\alpha = \frac{2\mathcal{M}_{12}^2}{\sqrt{\mathcal{M}_{11}^2 - \mathcal{M}_{22}^2}}, \tag{3.56}$$

where $\mathcal{M}_{ij} \equiv \left(\mathcal{M}^2_{0^+}\right)_{i,j}$. Hence, we can also determine $\cos 2\alpha$ and $\sin 2\alpha$:

$$\cos 2\alpha = \frac{\mathcal{M}^2_{11} - \mathcal{M}^2_{22}}{\sqrt{\left(\mathcal{M}^2_{11} - \mathcal{M}^2_{22}\right)^2 + 4\mathcal{M}^4_{12}}}\,, \tag{3.57}$$

$$\sin 2\alpha = \frac{2\mathcal{M}^2_{12}}{\sqrt{\left(\mathcal{M}^2_{11} - \mathcal{M}^2_{22}\right)^2 + 4\mathcal{M}^4_{12}}}\,. \tag{3.58}$$

The alignment limit is given by $\cos(\alpha - \beta) \simeq 0$, which we can determine with:

$$\cos^2(\alpha - \beta) = \frac{1}{2}\left(1 + \cos(2\beta)\cos(2\alpha) + \sin(2\beta)\sin(2\alpha)\right)\,. \tag{3.59}$$

The expressions for $\cos 2\beta$ and $\sin 2\beta$ are:

$$\cos 2\beta = \frac{v_1^2 - v_2^2}{v_1^2 + v_2^2}\,, \tag{3.60}$$

$$\sin 2\beta = \frac{2v_1 v_2}{v_1^2 + v_2^2}\,, \tag{3.61}$$

which gives us the following expression for $\cos(\alpha - \beta)$:

$$\cos^2(\alpha - \beta) = \tag{3.62}$$
$$\frac{\left(v_1^2 + v_2^2\right)\sqrt{(\mathcal{M}^2_{11} - \mathcal{M}^2_{22})^2 + 4\mathcal{M}^4_{12}} + (\mathcal{M}^2_{11} - \mathcal{M}^2_{22})(v_1 - v_2)(v_1 + v_2) + 4\mathcal{M}^2_{12}v_1v_2}{2\left(v_1^2 + v_2^2\right)\sqrt{(\mathcal{M}^2_{11} - \mathcal{M}^2_{22})^2 + 4\mathcal{M}^4_{12}}}\,.$$

By inserting the expressions for the matrix elements $\mathcal{M}_{ij}$ into $\cos^2(\alpha - \beta)$ of eq. (3.62), we obtain:

$$\cos^2(\alpha - \beta) = \tag{3.63}$$
$$\frac{\left(v_1^2 + v_2^2\right)\sqrt{\frac{1}{4}\left(2m^2_{11} - 2m^2_{22} + v_1^2(3\tilde{\lambda}_1 - \tilde{\lambda}_{34}) + v_2^2(\tilde{\lambda}_{34} - 3\tilde{\lambda}_2)\right)^2 + 4(m^2_{12} - \tilde{\lambda}_{34}v_1v_2)^2}}{2\left(v_1^2 + v_2^2\right)\sqrt{\frac{1}{4}\left(2m^2_{11} - 2m^2_{22} + v_1^2(3\tilde{\lambda}_1 - \tilde{\lambda}_{34}) + v_2^2(\tilde{\lambda}_{34} - 3\tilde{\lambda}_2)\right)^2 + 4(m^2_{12} - \tilde{\lambda}_{34}v_1v_2)^2}}$$
$$+ \frac{\frac{1}{2}(v_1 - v_2)(v_1 + v_2)\left(2m^2_{11} - 2m^2_{22} + v_1^2(3\tilde{\lambda}_1 - \tilde{\lambda}_{34}) + v_2^2(\tilde{\lambda}_{34} - 3\tilde{\lambda}_2)\right) + 4v_1v_2(\tilde{\lambda}_{34}v_1v_2 - m^2_{12})}{2\left(v_1^2 + v_2^2\right)\sqrt{\frac{1}{4}\left(2m^2_{11} - 2m^2_{22} + v_1^2(3\tilde{\lambda}_1 - \tilde{\lambda}_{34}) + v_2^2(\tilde{\lambda}_{34} - 3\tilde{\lambda}_2)\right)^2 + 4(m^2_{12} - \tilde{\lambda}_{34}v_1v_2)^2}}\,.$$

Since, we are only considering $\tan\beta$ in the range $5 \lesssim \tan\beta \lesssim 170$, we acquire $v_2 \gg v_1$. The 2HDM tadpole equations are given by:

$$m_{11}^2 = \frac{v_1^3\left(\lambda_{1S}^2 - \lambda_1\lambda_S\right) + v_1 v_2^2\left(\lambda_{1S}\lambda_{2S} - \lambda_{34}\lambda_S + 2\lambda_{12S}^2\right) - \lambda_{1S}\lambda_S v_1 v_S^2 + \lambda_S v_2 v_S^2 \lambda_{12S}}{2\lambda_S v_1}, \tag{3.64}$$

$$m_{22}^2 = \frac{v_2^3\left(\lambda_{2S}^2 - \lambda_2\lambda_S\right) + v_2 v_1^2\left(\lambda_{2S}\lambda_{1S} - \lambda_{34}\lambda_S + 2\lambda_{12S}^2\right) - \lambda_{2S}\lambda_S v_2 v_S^2 + \lambda_S v_1 v_S^2 \lambda_{12S}}{2\lambda_S v_2}, \tag{3.65}$$

which we can approximate with $v_S^2 \gg v_2 \gg v_1$ as follows:

$$m_{11}^2 \simeq \frac{m_{12}^2 v_2}{v_1} - \frac{1}{2}v_2^2\tilde{\lambda}_{34} \;\Rightarrow\; v_1 \simeq \frac{m_{12}^2}{m_{11}^2}\frac{v_2}{\left(1 + \frac{\tilde{\lambda}_{34}v_2^2}{2m_{11}^2}\right)}, \tag{3.66}$$

$$m_{22}^2 \simeq -\frac{\tilde{\lambda}_2 v_2^2}{2}, \tag{3.67}$$

where $m_{22}^2 < 0$. Similar as in Ref.[36], we get a naturally small v_1 which also accommodates small Dirac neutrino masses via the type-I seesaw mechanism[3]. Considering that $\lambda_{12S} \to 0$ as discussed in sections 3.6 and 3.7, we utilize the technically natural limit given by $\frac{m_{12}^2}{m_{11}^2} \ll 1$ for $m_{12}^2 \simeq \lambda_{12S}v_S^2$. This limit restores the $U(1)_L$-symmetry. Hence, we get with $x \equiv \frac{m_{12}^2}{m_{11}^2} \ll 1$ the following expression for $\cos^2(\alpha-\beta)$:

$$\cos^2(\alpha-\beta) = \tag{3.68}$$

$$\frac{-\frac{1}{2}\left(\left(\frac{\tilde{\lambda}_{34}v_2^2}{2m_{11}^2}+1\right)^2 - x^2\right)\left(\frac{\tilde{\lambda}_{34}^2 v_2^6(\tilde{\lambda}_{34}-2\tilde{\lambda}_2)}{8m_{11}^6} + \frac{\tilde{\lambda}_{34}v_2^4(3\tilde{\lambda}_{34}-4\tilde{\lambda}_2)}{4m_{11}^4} + \frac{v_2^2(3\tilde{\lambda}_{34}-2\tilde{\lambda}_2)}{2m_{11}^2} + \frac{v_2^2x^2(3\tilde{\lambda}_1-\tilde{\lambda}_{34})}{2m_{11}^2} + 1\right)}{\left(\frac{\tilde{\lambda}_{34}v_2^2}{2m_{11}^2}+1\right)^4\left(\frac{x^2}{\left(\frac{\tilde{\lambda}_{34}v_2^2}{2m_{11}^2}+1\right)^2}+1\right)\sqrt{\left(\frac{v_2^2\left(-2\tilde{\lambda}_2+\tilde{\lambda}_{34}+\frac{x^2(3\tilde{\lambda}_1-\tilde{\lambda}_{34})}{\left(\frac{\tilde{\lambda}_{34}v_2^2}{2m_{11}^2}+1\right)^2}\right)}{2m_{11}^2}+1\right)^2 + \frac{4x^2\left(1-\frac{\tilde{\lambda}_{34}v_2^2}{2m_{11}^2}\right)^2}{\left(\frac{\tilde{\lambda}_{34}v_2^2}{2m_{11}^2}+1\right)^2}}}$$

$$+\frac{\frac{1}{2}\left(\frac{\tilde{\lambda}_{34}v_2^2}{2m_{11}^2}+1\right)^2\left(\left(\frac{\tilde{\lambda}_{34}v_2^2}{2m_{11}^2}+1\right)^2 + x^2\right)\sqrt{\left(\frac{v_2^2\left(-2\tilde{\lambda}_2+\tilde{\lambda}_{34}+\frac{x^2(3\tilde{\lambda}_1-\tilde{\lambda}_{34})}{\left(\frac{\tilde{\lambda}_{34}v_2^2}{2m_{11}^2}+1\right)^2}\right)}{2m_{11}^2}+1\right)^2 + \frac{4x^2\left(1-\frac{\tilde{\lambda}_{34}v_2^2}{2m_{11}^2}\right)^2}{\left(\frac{\tilde{\lambda}_{34}v_2^2}{2m_{11}^2}+1\right)^2}} - 2x^2\left(1-\frac{\tilde{\lambda}_{34}v_2^2}{2m_{11}^2}\right)\left(\frac{\tilde{\lambda}_{34}v_2^2}{2m_{11}^2}+1\right)^2}{\left(\frac{\tilde{\lambda}_{34}v_2^2}{2m_{11}^2}+1\right)^4\left(\frac{x^2}{\left(\frac{\tilde{\lambda}_{34}v_2^2}{2m_{11}^2}+1\right)^2}+1\right)\sqrt{\left(\frac{v_2^2\left(-2\tilde{\lambda}_2+\tilde{\lambda}_{34}+\frac{x^2(3\tilde{\lambda}_1-\tilde{\lambda}_{34})}{\left(\frac{\tilde{\lambda}_{34}v_2^2}{2m_{11}^2}+1\right)^2}\right)}{2m_{11}^2}+1\right)^2 + \frac{4x^2\left(1-\frac{\tilde{\lambda}_{34}v_2^2}{2m_{11}^2}\right)^2}{\left(\frac{\tilde{\lambda}_{34}v_2^2}{2m_{11}^2}+1\right)^2}}},$$

[3]We note that Φ_1 and Φ_2 of Ref. [36] are switched compared to our notation.

which we can expand in a Taylor-series for $x_0 = 0$ up to second order:

$$\cos^2(\alpha-\beta) \approx \frac{m_{12}^4}{m_{11}^4}\frac{v_2^4}{m_{11}^4}\frac{(\tilde{\lambda}_2-\tilde{\lambda}_{34})^2}{\left(1+\frac{v_2^2}{2m_{11}^2}\tilde{\lambda}_{34}\right)^2\left(1-\frac{v_2^2}{2m_{11}^2}(2\tilde{\lambda}_2-\tilde{\lambda}_{34})\right)^2} \tag{3.69}$$

$$\approx \frac{v_1^4}{v_2^4}\frac{4(\tilde{\lambda}_2-\tilde{\lambda}_{34})^2}{\left(\lambda_{12S}\frac{v_S^2}{v_2^2}-\tilde{\lambda}_2\frac{v_1}{v_2}\right)^2}, \tag{3.70}$$

where in the last step we recovered m_{11}^2 and m_{12}^2. We can show that this expression goes to zero with a double suppression given by an approximate $U(1)$-symmetry $\frac{m_{12}^2}{m_{11}^2} \ll 1$ and by the decoupling limit $v_2/v_1 \gg 1$ (cf. Ref.[36])

$$\cos^2(\alpha-\beta) \approx \frac{4(\tilde{\lambda}_2-\tilde{\lambda}_{34})^2 v_1^4}{\lambda_{12S}^2 v_S^4} \longrightarrow 0\,. \tag{3.71}$$

This result reflects that 2hdSMASH accommodates a SM-like Higgs boson with SM-like interactions in the low-energy limit.

3.9. Characteristics of the scalar mass spectrum

In order to satisfy the cosmological and astrophysical constraints, cf. (3.13), we require a hierarchy of scales $v_S/v \gg 1$ which implies the mass spectrum to follow the same hierarchy:

i) a very light axion a which scales like $m_a \propto 1/v_S$;

ii) a light neutral CP-even Higgs h identified as the SM-like Higgs which scales like $m_h \propto v$;

iii) heavy neutral CP-even Higgs H, CP-odd Higgs A and charged Higgses $H^\pm$ which scale like $m_{H,A,H^\pm} \propto v_S$.

The mass of the light Higgs as stated in i) is at the electroweak scale and it has to accommodate the LHC measurements determining its mass to be $m_h = 125.10 \pm 0.14$ GeV [37]. This puts stringent constraints on the quartic couplings as we can see from eq. (3.16). In most parts, the 2HDM couplings λ_i, $i = 1,2,34$, will determine the mass, while the portal couplings λ_{iS}, $i = 1,2,12$, will play a sub-dominant role according to our naturalness philosophy discussed in section 3.6. Hence, the 2HDM couplings have to be chosen to satisfy the measured Higgs mass. The spectrum of the other scalars, on the other hand, strongly depend on the value of $\tan\beta$, λ_{12S}, v_S

and λ_S (see also ref. [26]). This can be seen by considering the following range of parameter values

$$\lambda_{12S}, \lambda_S \gg (v/v_S)^2 \simeq 6 \times 10^{-16} \left(\frac{10^{10}\,\text{GeV}}{v_S} \right)^2 , \tag{3.72}$$

where leading mass terms of eqs. (3.10), (3.14), (3.17) and (3.18) are proportional to v_S^2 and dominate over the next-to-leading terms proportional to v^2. As a consequence we obtain a nearly degenerate mass spectrum of Higgses A, $H^\pm$ and H which are mostly determined by $\tan\beta$, λ_{12S} and v_S,

$$m_A^2 \approx m_{H^\pm}^2 \approx m_H^2 \approx \frac{1}{2} \frac{t_\beta^2 + 1}{t_\beta} \lambda_{12S}\, v_S^2 , \tag{3.73}$$

while the PQ-scalar s differs from the other scalars by the dependence of λ_S and v_S,

$$m_s^2 \approx \lambda_S v_S^2 . \tag{3.74}$$

In order to illustrate this concept, we give four benchmarks points in table 3.2 with different values for λ_{12S} and λ_S. All parameters were chosen such that BfB and perturbative unitarity constraints are obeyed while reproducing a SM-like Higgs with a mass of 125 GeV. Furthermore, the scalar masses were calculated with the full tree-level expression up to order $(v/v_S)^2$. We find good agreement by comparing the results to the approximate mass spectrum of eqs. (3.73)-(3.74), even for $\lambda_{12S} \simeq (v/v_S)^2$.

BP1 illustrates the extreme decoupling limit for $\lambda_{12S}, \lambda_S = \mathcal{O}(1)$, where all extra Higgses are at the PQ-symmetry breaking scale and decoupled from the SM. In this region of parameter space, 2hdSMASH cannot be tested at the LHC or future colliders.

BP2 provides masses of the extra Higgsses in the range of $\sim 10^3 - 10^4$ TeV for $\lambda_{12S} \sim (v/v_S) \sim 10^{-8}$. Only the PQ-scalar s is still decoupled and has a mass around the PQ-symmetry breaking scale for $\lambda_S \sim 1$.

BP3 is phenomenologically more interesting. It illustrates that a portal coupling as low as $\lambda_{12S} \sim (v/v_S)^2 \sim 10^{-16}$ pushes the masses of the extra Higgses all the way down to near the electroweak scale [24, 26]. Observable effects at the HL-LHC and future colliders may be a result of this case [26].

BP4 provides in a addition to $\lambda_{12S} \sim (v/v_S)^2 \sim 10^{-16}$ a tiny PQ self-coupling, i.e.

Parameters	**BP1**	**BP2**	**BP3**	**BP4**
λ_1	0.1	0.1	0.1	0.1
λ_2	0.258	0.258	0.258	0.258
λ_3	0.54	0.54	0.54	0.54
λ_4	-0.14	-0.14	-0.14	-0.14
λ_S	1.0	1.0	1.0	10^{-10}
λ_{1S}	10^{-15}	10^{-15}	10^{-15}	10^{-15}
λ_{2S}	10^{-15}	10^{-15}	10^{-15}	10^{-15}
λ_{12S}	0.1	2.5×10^{-8}	2.5×10^{-16}	2.5×10^{-16}
$\tan\beta$	26	26	26	26
v_S	3.0×10^{10}	3.0×10^{10}	3.0×10^{10}	3.0×10^{10}
m_h (GeV)	125.1	125.1	125.1	125.1
m_H (GeV)	3.4×10^{10}	1.7×10^{7}	1711.5	1711.5
m_s (GeV)	3.0×10^{10}	3.0×10^{10}	3.0×10^{10}	3.0×10^{5}
m_A (GeV)	3.4×10^{10}	1.7×10^{7}	1711.5	1711.5
$m_{H^\pm}$ (GeV)	3.4×10^{10}	1.7×10^{7}	1712.8	1712.8

Table 3.2.: List of benchmarks considering various values of λ_S and λ_{12S} for which BfB- and perturbative unitarity constraints apply while accommodating a 125 GeV Higgs.

$\lambda_S \sim 10^{-10}$, which is required for inflation, as we will discuss in chapter 4. In this case, the mass of the PQ-scalar s is pushed to intermediate scales between the electroweak and the PQ scale, i.e. $\sqrt{\lambda_S} v_S \sim 10^5$ GeV.

By considering the range of portal couplings given in **BP3** and **BP4**, we obtain predictions that could lead to possible signatures at colliders while being favored by theoretical constraints. In fact, tiny values for the portal couplings provide a technically natural limit [24, 35, 25], as we discussed in section 3.6. This technically natural limit helps stabilizing the required hierarchy of scales, i.e. the electroweak- and the PQ-scale $v/v_S \gg 1$ while protecting electroweak masses from large radiative corrections. This can be seen from the following portal terms

$$-\mathcal{L}_{\text{portal}} = \lambda_{1S}\left(\Phi_1^\dagger\Phi_1\right)(S^*S) + \lambda_{2S}\left(\Phi_2^\dagger\Phi_2\right)(S^*S) - \lambda_{12S}\left(\Phi_2^\dagger\Phi_1 S^2 + h.c.\right) . \quad (3.75)$$

where clearly, tiny portal couplings decouple the 2HDM- from the PQ sector. Most importantly, we note that tiny λ_{12S} is mandatory to decouple both sectors while λ_{1S} and λ_{2S} can be slightly larger, but suffciently smaller than 2HDM couplings

$$|\lambda_{12S}| \lesssim \left(\frac{v}{v_S}\right)^2 \simeq 6 \times 10^{-16} \left(\frac{10^{10}\,\text{GeV}}{v_S}\right)^2 \lesssim |\lambda_{1S}|, |\lambda_{2S}| \ll \lambda_{1,2,34}. \quad (3.76)$$

4. Inflationary Cosmology in 2hdSMASH

In this chapter, we will discuss inflationary cosmology in 2hdSMASH which consists of a brief motivation to inflationary cosmology in section 4.1 and a short introduction to single field inflation in section 4.2. In section 4.3 we introduce the general inflationary setup in 2hdSMASH which is described by an effective single field model allowing for seven single field directions. In section 4.3.1 we consider the three single field directions for 2HDM inflation where we comment on the need to describe inflation in the PQ- or mixed PQ-2HDM directions. This will be discussed in section 4.3.2 where the other four field directions are described in the context of PQ- (PQI) and mixed PQ-2HDM inflation (PQTHI).

4.1. Motivation for inflation

In the 1940s, R.A. Alpher, G. Gamow and R.C. Herman proposed the hot big bang model and its subsequent expansion to describe the cosmological origin of elements in the early universe[1] [54, 55]. Not much later, they predicted the cosmic microwave backgound [56, 57] which was detected 16 years later in 1964 by A.A. Penzias and R.W. Wilson [58] and layed the foundation of the widely accepted hot big bang model. Thereinafter, two main problems arose with the hot big bang model, namely the *horizon* and *flatness problem* which we will discuss in the next section. As a consequence, Alan Guth [53] and Alexei A. Starobinsky [59] proposed a solution in the 1980s in which the very early universe experienced a phase of accelerated expansion termed cosmic inflation. During this period of accelerated expansion the universe became flat, homogeneous and isotropic. Ever since, various inflationary models aimed at describing CMB data taken by the Cosmic Background Explorer (COBE), the Wilkinson Microwave Anisotropy Probe (WMAP) and most recently the PLANCK satellite [60, 61].

[1] The information given in this paragraph was extracted from Refs. [37] and [53].

In the following we will formulate the standard big bang model in more detail and discuss the solution of the aforementioned problems in the context of the shrinking Hubble sphere during inflation [38]. In particular, we view all problems associated with the standard big bang model, i.e. horizon problem, flatness problem, entropy and monopole problem, as part of just one problem, namely the *horizon problem* (see Ref. [38] for more details). We therefore follow the general calculations done in Ref. [38].

On large scales, our universe is homogeneous and isotropic and can therefore be described by a 4D space-time metric with maximally symmetric space geometry. This 4D space-time metric is given by the Friedmann-Robertson-Walker (FRW) metric:

$$ds^2 = -dt^2 + a^2(t)\left[\frac{dr^2}{1-kr^2} + r^2 d\Omega^2\right], \tag{4.1}$$

where $d\Omega^2 = d\Theta^2 + sin^2\Theta\, d\varphi^2$ corresponds to the two-dimensional polar metric and k to the curvature parameter with $k = 0, 1, -1$ corresponding to a flat, open and closed universe, respectively. By defining conformal time τ via

$$d\tau = \frac{dt}{a(t)}, \tag{4.2}$$

we can study the causal structure of the FRW metric by studying the propagation of light. Hence, we express the FRW metric in terms of conformal time

$$ds^2 = a^2(\tau)\left[-d\tau^2 + \frac{dr^2}{1-kr^2} + r^2 d\Omega^2\right], \tag{4.3}$$

with a time-dependent scale factor $a(\tau)$. For light traveling radially in an isotropic universe the FRW metric is represented by a static Minkowski metric

$$ds^2 = a^2(\tau)\left[-d\tau^2 + dr^2\right], \tag{4.4}$$

for which we consider null geodesics, i.e. $ds^2 = 0$. This gives us the causal structure of the FRW universe:

$$r(\tau) \simeq \pm\tau, \tag{4.5}$$

where light propagates through space in straight lines by $\pm 45^\circ$ angles and thus represents light cones of spacetime (see fig. 4.1). Any event outside of these light cones is causally disconnected to the particle horizon, since all massive particles travel on

timelike geodesics, i.e. $ds^2 > 0$ within light cones. Massive particles which travel spacelike, i.e. $ds^2 < 0$ are thus causally disconnected.

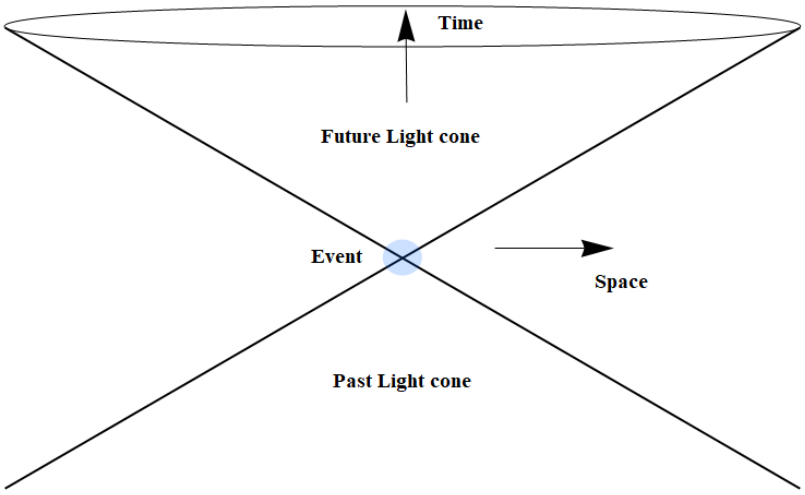

Figure 4.1.: Light cones represented by light traveling on null geodesics, i.e. $ds^2 = 0$, through an event in four dimensional spacetime. Any region outside these light cones is causally disconnected to the event, i.e. $ds^2 < 0$, whereas all causally connected massive particles in relation to the event travel on timelike geodesics, i.e. $ds^2 > 0$.

This can be quantified by defining the comoving particle horizon

$$\Delta r = \tau - \tau_i = \int_{t_i}^{t} \frac{dt'}{a(t')}, \tag{4.6}$$

which is the maximum distance light travels in the interval $\Delta t = t - t_i$. Here, $t_i = 0$ and $a(t_i) = 0$ is at the big bang singularity for which the physical particle horizon

$$d(t) = a(t)r \tag{4.7}$$

is finite. Correspondingly, the big bang started out to be of finite size which restricted causal contact of regions in space. This describes the horizon problem and its important motivation for inflation.

We briefly outline this concept by considering Einstein's field equations in general relativity [62]. The Einstein tensor is given by

$$G_{\mu\nu} \equiv R_{\mu\nu} - \frac{1}{2} g_{\mu\nu} R = \frac{1}{M_p^2} T_{\mu\nu} \tag{4.8}$$

with Ricci-tensor $R_{\mu\nu}$, Ricci-scalar R, FRW metric $g_{\mu\nu}$, reduced Planck mass $M_p^2 =$

$1/8\pi G_N$ and energy momentum tensor $T_{\mu\nu}$. As mentioned above, we assume an isotropic and homogeneous universe with flat FRW metric. Therefore, we can describe the universe as perfect fluid represented by the energy momentum tensor $T_{\mu\nu}$,

$$T^{\mu}{}_{\nu} = g^{\mu\lambda} T_{\lambda\nu} = (\rho + p)\, u^{\mu} u_{\nu} - p\delta^{\mu}_{\nu}\,, \tag{4.9}$$

where ρ is the energy density and p the pressure. Since the universe is at rest in the comoving reference frame, we can take the 4-velocity to be $u^{\mu} = \mathrm{diag}\,(1,0,0,0)$ which gives us the following energy momentum tensor

$$T^{\mu}{}_{\nu} = \mathrm{diag}\,(\rho, -p, -p, -p)\ . \tag{4.10}$$

From the time- and spatial components of the Einstein tensor we acquire the Friedmann equations:

$$\mathcal{H}^2 \equiv \left(\frac{\dot{a}}{a}\right)^2 = \frac{\rho}{3} - \frac{k}{a^2}\,, \tag{4.11}$$

$$\dot{\mathcal{H}} + \mathcal{H}^2 = \frac{\ddot{a}}{a} = -\frac{1}{6}\,(\rho + 3p)\ , \tag{4.12}$$

where $\mathcal{H}$ is the Hubble parameter. The Friedmann equations describe the expansion and acceleration rate of the universe, respectively. By combining both Friedmann equations we obtain the continuity equation

$$\frac{d\rho}{dt} + 3\mathcal{H}\,(\rho + p) = 0\,, \tag{4.13}$$

which we can reformulate into

$$\frac{d\rho}{da} = -\frac{3}{a}\,(\rho + p)\ . \tag{4.14}$$

Integrating both sides gives us the dependence of the energy density w.r.t. the scale factor a

$$\rho \propto a^{-3(1+w)} \tag{4.15}$$

with $w \equiv p/\rho$ as the equation of state parameter. Depending on the energy content

of the universe, the equation of state parameter w is given by

$$w = \begin{cases} \frac{1}{3} & \text{radiation domination} \\ 0 & \text{matter domination} \\ -1 & \text{cosmological constant } \Lambda \end{cases} . \tag{4.16}$$

Since the universe can consist of a collection of energy densities, we introduce the relative energy density

$$\Omega_i \equiv \frac{\rho_{0,i}}{\rho_{\text{cr}}} , \tag{4.17}$$

where $\rho_{0,i}$ are the energy densities measured today and ρ_{cr} is the critical energy density given by

$$\rho_{\text{cr}} = 3\mathcal{H}_0^2 M_p^2 \tag{4.18}$$

with $\mathcal{H}_0$ as the present-day Hubble expansion rate given by $\mathcal{H}_0 = 100\ h$ km s^{-1} Mpc^{-1} and h as the Hubble parameter given by $h = 0.674(5)$ [37]. The total relative energy density is expressed as

$$\Omega_{\text{tot}} = \sum_i \Omega_i + \Omega_k = 1 \tag{4.19}$$

with the relative energy density of curvature $\Omega_k = -k/a_0^2\mathcal{H}_0^2$. We can now define the comoving Hubble radius as

$$(a\mathcal{H})^{-1} = \mathcal{H}_0^{-1} a^{\frac{1}{2}(1+3w)} \propto a^{\frac{1}{2}(1+3w)} , \tag{4.20}$$

which we can use to describe the conformal time and thus the comoving particle horizon

$$\tau \equiv \int_{t_i}^{t} \frac{dt'}{a(t')} = \int_0^a d\log(a)\, (a\mathcal{H})^{-1} . \tag{4.21}$$

Evaluating this integral with comoving Hubble radius $(a\mathcal{H})^{-1} \propto a^{\frac{1}{2}(1+3w)}$ will result in the following comoving particle horizon

$$\tau \propto a^{\frac{1}{3}(1+3w)} . \tag{4.22}$$

For $w \geq 0$ the comoving particle horizon and the comoving Hubble radius grow monotonically with time which indicates that scales at very early times, i.e. at CMB

decoupling, were causally disconnected and outside the comoving Hubble radius. However, these scales which enter the horizon today are near-homogeneous which raises the question whether this picture of the standard big bang cosmology is complete. In fact, the horizon problem is really a problem of the comoving Hubble radius. Furthermore, the flatness problem is also related to the comoving Hubble radius. The time-dependent relative energy density of the universe can be expressed with the Friedmann equation (4.11) as

$$1 - \Omega(a) = -\frac{k}{(a\mathcal{H}(a))^2}\,, \tag{4.23}$$

where $\Omega(a) = \rho(a)/\rho_{\mathrm{cr}}(a)$ and $\rho_{\mathrm{cr}}(a) = 3\mathcal{H}^2(a)$. As expected, the $\Omega(a)$ also depends on the comoving Hubble radius which grows monotonically with time. The right hand side decreases therefore when going back to the big bang, which would make the universe even more flat than today. Thus, a huge amount of fine-tuning would be necessary to salvage this problem while being unnatural.

By solving the problem of the increasing Hubble sphere, i.e. the comoving Hubble radius, the horizon- and flatness problem is simultaneously solved as well. Introducing an epoch where the Hubble sphere decreases, i.e. $(a\mathcal{H})^{-1}$ decreases, at very early times therefore solves the horizon- and flatness problem. This epoch is called cosmic inflation and describes a period of accelerated expansion of the universe, i.e. $\ddot{a} > 0$, at very early times. Before inflation comoving scales where causally connected. During inflation the Hubble sphere shrunk and comoving scales where outside the Hubble radius. These comoving scales which enter our horizon today are thus causally disconnected but nearly homogeneous. The equation of state parameter w, is therefore required to be $w < -1/3$ which describes negative pressure and is determined by the condition of a shrinking comoving Hubble sphere. As a result, conformal time goes to negative infinity when approaching the big bang singularity, i.e.

$$\tau_i \propto \frac{2}{1+3w} a_i^{\frac{1}{2}(1+3w)} = -\infty \tag{4.24}$$

for $a_i = 0$ and $w < -1/3$.

4.2. Physics of single field inflation

We will briefly outline the physics behind single field inflation and follow the calculations done in Ref. [38].

The shrinking of the Hubble sphere is related to the Friedmann equations and sets the following equivalent conditions for inflation

$$\frac{d}{dt}\left(\frac{1}{a\mathcal{H}}\right) < 0 \tag{4.25}$$

$$\Leftrightarrow\ \ddot{a} > 0 \tag{4.26}$$

$$\Leftrightarrow\ p < -\frac{\rho}{3} \tag{4.27}$$

$$\Leftrightarrow\ \epsilon \equiv -\frac{\dot{\mathcal{H}}}{\mathcal{H}^2} < 1 \tag{4.28}$$

where accelerated expansion, negative pressure and a slowly changing Hubble rate are described, respectively. In particular, the latter is regarded as the first slow-roll parameter which we use as one of two main conditions for inflation. As mentioned above, it is equivalent to the previous two descriptions. The second slow-roll parameter is given by

$$|\tilde{\eta}| \equiv \frac{|\dot{\epsilon}|}{\mathcal{H}\epsilon} < 1\,, \tag{4.29}$$

which describes the rate at which ϵ changes per Hubble time. This is taken to be small in order to make inflation last to solve the horizon- and flatness problem. Thus, the conditions for inflation are given by $\epsilon, |\tilde{\eta}| < 1$.

Inflation can be realized by the dynamics of a scalar field ϕ, the so-called inflaton, which is minimally coupled to Einstein gravity described by the total action

$$S = S_{\mathrm{EH}} + S_\phi = \int d^4x\, \sqrt{-g}\left(\frac{1}{2}R + \frac{1}{2}g^{\mu\nu}\partial_\mu\phi\partial_\nu\phi - V(\phi)\right) \tag{4.30}$$

with g as the metric and $V(\phi)$ as the scalar potential. The total action consists of the Einstein-Hilbert action S_{EH} and the action of the inflaton S_ϕ with canonical kinetic term. In scalar field theory, the time-dependent dynamics of ϕ are given by the Klein-Gordon equation

$$\ddot{\phi} + 3\mathcal{H}\dot{\phi} + V_\phi = 0\,, \tag{4.31}$$

where V_ϕ denotes the partial derivative of the scalar potential w.r.t. to ϕ. The second term is called the Hubble friction term and is determined by the Hubble rate

$$\mathcal{H}^2 = \frac{1}{3M_p^2}\left(\frac{1}{2}\dot{\phi}^2 + V\right), \tag{4.32}$$

where we substituted the energy density of the inflaton ρ_ϕ into the Friedmann equation for $k = 0$. The Hubble rate consists of kinetic energy and potential energy. By taking the time derivative of $\mathcal{H}$ and inserting this into ϵ we get

$$\epsilon = \frac{\frac{1}{2}\dot{\phi}^2}{M_p^2\mathcal{H}^2} \ll 1\,, \tag{4.33}$$

which states that potential energy dominates over kinetic energy during inflation. By taking the time derivative of ϵ and inserting it into η we get

$$\tilde{\eta} = 2\,(\epsilon - \eta) = 2\left(\epsilon + \frac{\ddot{\phi}}{\mathcal{H}\dot{\phi}}\right) \ll 1\,, \tag{4.34}$$

where η is given by

$$\eta \equiv -\frac{\ddot{\phi}}{\mathcal{H}\dot{\phi}} \ll 1\,. \tag{4.35}$$

These slow-roll conditions w.r.t. ϕ can be used for the so-called slow-roll approximation. Since $\epsilon \ll 1$, the Hubble rate is approximated by

$$\mathcal{H}^2 = \frac{V}{M_p^2(3-\epsilon)} \approx \frac{V}{3M_p^2}\,. \tag{4.36}$$

Furthermore, $\epsilon \ll 1$ and $\eta \ll 1$ lead to the approximation of the Klein-Gordon equation

$$3\mathcal{H}\dot{\phi} \approx -V_\phi\,. \tag{4.37}$$

These approximations, hence, lead to the slow-roll parameters in the slow-roll approximation given by

$$\epsilon \approx \epsilon_V \equiv \frac{M_p^2}{2}\left(\frac{V_\phi}{V}\right)^2, \tag{4.38}$$

$$\eta \approx \eta_V - \epsilon_V\,, \tag{4.39}$$

$$\eta_V \equiv M_p^2\frac{V_{\phi\phi}}{V}\,, \tag{4.40}$$

where the latter was obtained by the time derivative of the approximated Klein-Gordon equation.

Having explained the dynamics of inflation, we require a measure for the amount of time between the start and the end of inflation. This is quantified by the number of e-folds N defined by

$$N \equiv \log \frac{a_{\text{end}}}{a_i} = \int_{t_i}^{t_{\text{end}}} \mathcal{H} dt \,. \tag{4.41}$$

In the slow-roll approximation we can approximate the number of e-folds by

$$N \simeq \int_{\phi_i}^{\phi_{\text{end}}} \frac{1}{\sqrt{2\epsilon_V}} \frac{d\phi}{M_p} \,, \tag{4.42}$$

where the inflaton field ϕ acts like a clock which measures the time remaining until inflation ends for $\epsilon_V = 1$.

Since ϕ is a quantum mechanical object, i.e. a scalar field, it is subject to quantum fluctuations. These quantum fluctuations around the background field $\phi(t)$ are quantified by

$$\phi(t) \to \phi(\mathbf{x}, t) \equiv \phi(t) + \delta\phi(\mathbf{x}, t) \,. \tag{4.43}$$

In particular, $\delta\phi(\mathbf{x}, t)$ is responsible for local time delays during inflation. These local time delays cause different regions of space to end inflation at different times. As a consequence there are local energy density fluctuations $\delta\rho$ which lead to anisotropies on the homogeneous background. We will briefly outline the concepts of quantum perturbations on the inflaton ϕ and thus on the metric g and derive the scalar- and tensor-perturbation amplitudes, as well as their spectral indices. In the following we adopt the general calculations and concepts of Refs. [38, 39].

We consider the unperturbed FRW metric $g_{\mu\nu}$ of an homogeneous and isotropic spacetime which is given by the following line element

$$ds^2 = g_{\mu\nu} dx^\mu dx^\nu = -dt^2 + a^2(t) d\mathbf{x}^2 \,, \tag{4.44}$$

where $d\mathbf{x}^2 = \delta_{ij}dx^i dx^j$ represents flat spatial slices. Then, the unperturbed action is given by (4.30) and can be written as

$$S = \frac{1}{2}\int d^4x\sqrt{-g}\,\left[R - g^{\mu\nu}\partial_\mu\phi\partial_\nu\phi - 2V\right] \tag{4.45}$$

with $M_p = 1$ for simplicity. Since perturbations of the inflaton ϕ are connected to the metric via Einsteins equations, this metric becomes also perturbed during inflation

$$g_{\mu\nu}(t) \to g_{\mu\nu}(\mathbf{x},t) = g_{\mu\nu}(t) + \delta g_{\mu\nu}(\mathbf{x},t)\,. \tag{4.46}$$

These metric fluctuations are thus not independent and are described with the ADM formalism [63]. The perturbed line element reads

$$ds^2 = -N^2dt^2 + g_{ij}\left(N^i dt + dx^i\right)\left(N^j dt + dx^j\right) \tag{4.47}$$

with $N(\mathbf{x})$ as the lapse function, $N^i(\mathbf{x})$ as the shift vector, and g_{ij} as the three-dimensional metric on hypersurfaces of constant time t [39]. The action of the inflaton ϕ can be written in terms of the perturbed metric of eq. (4.47) as

$$S = \frac{1}{2}\int \sqrt{g}N\left[R^{(3)} - 2V + N^{-2}\left(E^{ij}E_{ij} - E^2\right) + N^{-2}\left(\dot{\phi} - N^i\partial_i\phi\right)^2 - h^{ij}\partial_i\phi\partial_j\phi\right], \tag{4.48}$$

where the 4D Ricci scalar R consists of an intrinsic curvature represented by the 3D Ricci scalar $R^{(3)}$ and an extrinsic curvature represented by K_{ij},

$$K_{ij} \equiv \frac{1}{2N}\left(\dot{g}_{ij} - \nabla_i N_j - \nabla_j N_i\right) \equiv \frac{1}{N}E_{ij}\,, \tag{4.49}$$

$$R = R^{(3)} + N^{-2}\left(E^{ij}E_{ij} - E^2\right) \tag{4.50}$$

with $E \equiv h^{ij}E_{ij}$. Here, $N(\mathbf{x})$ and $N^i(\mathbf{x})$ act as Lagrange multipliers which are non-dynamical and can therefore be fixed by two constraint equations

$$R^{(3)} - 2V - g^{ij}\partial_i\phi\partial_j\phi - N^2\left[E_{ij}E^{ij} - E^2 - \left(\dot{\phi} - N^i\partial_i\phi\right)^2\right] = 0\,, \tag{4.51}$$

$$\nabla_i[N^{-1}(E^i_j - E\delta^i_j)] = 0\,. \tag{4.52}$$

We are now left with ϕ and g_{ij} as dynamical variables and we choose the comoving gauge[2] to derive the quadratic action describing the perturbations from the metric.

[2]It's also possible to choose the spatially flat gauge where all perturbations are treated by the perturbations of the inflaton, $\delta\phi \neq 0$, while the metric perturbations vanish.

Thus, the inflaton fluctuations vanish and remain unperturbed in this gauge, i.e.

$$\delta\phi = 0\,, \tag{4.53}$$

for which we can fix space and time reparametrizations. The perturbations on the metric g, the lapse function N and on the shift vector N_i are given by [39]

$$g_{ij} = a^2\left(1 + 2\zeta(t,\mathbf{x})\right)\delta_{ij}\ ,\ \ N \equiv 1 + \alpha(t,\mathbf{x})\ ,\ \ N_i \equiv \partial_i\beta(t,\mathbf{x})\,, \tag{4.54}$$

where we have used $\zeta(t,\mathbf{x})$ as the comoving curvature perturbation as gauge-invariant quantity [38, 39]. Inserting these perturbations into the constraint equations will give us [39, 64]

$$\alpha = \frac{\dot{\zeta}}{\mathcal{H}}\ ,\ \ \partial^2\beta = -\frac{\partial^2\zeta}{\mathcal{H}} + a^2\epsilon\dot{\zeta}\,, \tag{4.55}$$

where ϵ is the first slow-roll parameter given by

$$\epsilon \equiv -\frac{\dot{\mathcal{H}}}{\mathcal{H}^2} = \frac{\frac{1}{2}\dot{\phi}^2}{\mathcal{H}^2}\,. \tag{4.56}$$

Applying this solution to (4.48), utilizing the equation of motion (eom) of the background and integrating by parts, the action of (4.48) can by expanded to second order [39]

$$S_2 = \int dt\, d^3x\, a^3\epsilon\left(\dot{\zeta}^2 - \frac{1}{a^2}(\partial\zeta)^2\right)\,. \tag{4.57}$$

The absence of a matter term in S_2 leads to the conservation of ζ outside the horizon[3], i.e. on superhorizon scales given by $k \ll a\mathcal{H}$. This can be seen by the eom for the Fourier modes ζ_k [39]

$$\ddot{\zeta}_k + (3+\eta)H\dot{\zeta}_k + \frac{k^2}{a^2}\zeta_k = 0 \tag{4.58}$$

with η as the second slow-roll parameter given by

$$\eta = \frac{\dot{\epsilon}}{\mathcal{H}\epsilon}\,, \tag{4.59}$$

[3]We note that this is only true for single field inflation. In multi field settings this is not true (see Ref. [65] for details).

where on superhorizon scales it simplifies to

$$\ddot{\zeta}_k + (3+\eta)H\dot{\zeta}_k \approx 0\,. \tag{4.60}$$

Thus, the comoving curvature perturbation is frozen for $k \ll aH$ and stays conserved.

By introducing a canonically normalized field $v \equiv a\sqrt{2\epsilon}\zeta \equiv z\zeta$, i.e. the *Mukhanov* variable, we can replace ζ with v/z in the action of eq. (4.57). Varying this action will give us the *Mukhanov-Sasaki* equation which is the eom for v [38, 39],

$$v_k'' + \left(k^2 - \frac{z''}{z}\right) v_k = 0\,, \tag{4.61}$$

where primes denote derivatives w.r.t. the conformal time τ and v_k are the Fourier modes given by [38, 39]

$$v(\tau, \mathbf{x}) = \int \frac{d^3k}{(2\pi)^3} v_k(\tau) e^{i\mathbf{k}\cdot\mathbf{x}}\,. \tag{4.62}$$

In eq. (4.61) we note an effective mass [38, 39]

$$m_{\text{eff}}^2 \equiv \frac{z''}{z} \approx \frac{\tilde{\nu}^2 - 1/4}{\tau^2}\,, \tag{4.63}$$

which is given in the first order slow-roll approximation by [39]

$$\nu \approx \frac{3}{2} + \epsilon + \frac{\eta}{2}\,. \tag{4.64}$$

Thus, the *Mukhanov-Sasaki* equation reads [39]

$$v_k'' + \left(k^2 - \frac{\nu^2 - 1/4}{\tau^2}\right) v_k = 0 \tag{4.65}$$

with exact solution [38, 39]

$$v_k(\tau) = \sqrt{-\tau}\left[\alpha H_\nu^{(1)}(-k\tau) + \alpha H_\nu^{(2)}(-k\tau)\right]\,, \tag{4.66}$$

where $H_\nu^{(1,2)}(-k\tau)$ are Hankel functions of first and second kind. In order to determine α and β we need initial conditions for eq. (4.66). This is obtained by considering the *Mukhanov-Sasaki* equation of (4.65) deep inside the Hubble radius, i.e. on

subhorizon scales $k \gg a\mathcal{H}$ where $\tau \to -\infty$ [38, 39]

$$v_k'' + k^2 v_k = 0\,, \tag{4.67}$$

which resembles an ordinary differential equation of a time-independent harmonic oscillator. Its unique solution is thus given by [38, 39]

$$\lim_{\tau\to-\infty} v_k(\tau) = \frac{e^{-k\tau}}{\sqrt{2k}}\,, \tag{4.68}$$

which implies $\beta = 0$ and $\alpha = \sqrt{\pi/2}$. This initial condition is called the *Bunch-Davies* boundary condition. Hence, we obtain the *Bunch-Davies* mode function [39]

$$|v_k(\tau)| = \frac{\sqrt{\pi}}{2}\sqrt{-\tau}\,\left|H_\nu^{(1)}(-k\tau)\right| \overset{k\tau\to 0}{\longrightarrow} \frac{2^\nu\Gamma(\nu)}{2\sqrt{\pi}}\,\frac{1}{\sqrt{k}}\,(-k\tau)^{-\nu+1/2} \tag{4.69}$$

in the limit to superhorizon scales, i.e. $k \ll aH$ or equivalently $k\tau \to 0$. Hence, the power spectrum for ζ, i.e. $P_\zeta(k)$, is given in this limit by [39]

$$\begin{aligned} P_\zeta(k) &\equiv \lim_{k\tau\to 0}\frac{k^3}{2\pi^2}\,|\zeta_k(\tau)|^2 = \frac{1}{z^2(\tau)}\lim_{k\tau\to 0}\frac{k^3}{2\pi^2}\,|v_k(\tau)|^2 \\ &= \frac{1}{2a^2\epsilon}\,\frac{k^2}{4\pi^2}\,(-k\tau)^{-2\nu+1} = \frac{1}{8\pi^2}\,\frac{\mathcal{H}^2(\tau)}{\epsilon(\tau)}\,(-k\tau)^{-2\nu+3}\,, \end{aligned} \tag{4.70}$$

where time dependencies cancel. At horizon exit the fiducial scale is of Hubble radius, i.e. $k_* = a_*\mathcal{H}_*$, which is when ζ becomes frozen and perturbations are conserved. The comoving time is then given by $\tau_* = -1/k_*$ which results in [39]

$$\boxed{P_\zeta(k) = \frac{1}{8\pi^2}\,\frac{1}{\epsilon_*}\,\frac{\mathcal{H}_*^2}{M_p^2}\,\left(\frac{k}{k_*}\right)^{-2\epsilon_*-\tilde{\eta}_*} = A_s\left(\frac{k}{k_*}\right)^{n_s-1}} \tag{4.71}$$

with the scalar perturbation amplitude A_s and the spectral tilt n_s given by [39]

$$\boxed{A_s = \frac{1}{8\pi^2}\,\frac{1}{\epsilon_*}\,\frac{\mathcal{H}_*^2}{M_p^2}}\,, \tag{4.72}$$

$$\boxed{n_s = 1 - 4\epsilon_* + 2\eta_*}\,, \tag{4.73}$$

where we used the relation $\tilde{\eta} = 2(\epsilon - \eta)$. In slow-roll approximation with ϵ_V, η_V and $\mathcal{H}^2 \approx V/3M_p^2$ we get

$$A_s \simeq \frac{1}{24\pi^2}\frac{V}{\epsilon_V M_p^4}\,, \tag{4.74}$$

$$n_s \simeq 1 - 6\epsilon_V + 2\eta_V\,. \tag{4.75}$$

Determining the power spectrum of tensor perturbations, i.e. primordial gravitational waves, is very similar to scalar perturbations. First, we consider the spatial part of the metric, i.e. the tensor part, which is perturbed [39, 40]

$$g_{ij} = a^2(\tau)\left(\delta_{ij} + 2h_{ij}\right) \tag{4.76}$$

with $\delta g_{ij} = 2h_{ij}$ as transverse $\left(\nabla_i h^{ij} = 0\right)$ and traceless $\left(h^i_i = 0\right)$. The second order Einstein-Hilbert action is thus given by [39]

$$S_2 = \frac{M_p^2}{8}\int d\tau\, d^3x\, a^2\left[h_{ij}'^2 - (\partial h_{ij})^2\right]\,. \tag{4.77}$$

By making a Fourier transformation, we get the Fourier expansion of the transverse and traceless tensor [38, 40]

$$h_{ij} = \int \frac{d^3k}{(2\pi)^3}\sum_{t=+,\times}\varepsilon^s_{ij}(k)h_{\mathbf{k},s}(\tau)e^{i\mathbf{k}\cdot\mathbf{x}} \tag{4.78}$$

with a sum over the two polarizations "+" and "×" describing gravitational waves. The tensor modes are arranged by $\varepsilon^t_{ii} = k^i\varepsilon^t_{ij} = 0$ and $\varepsilon^t_{ij}\varepsilon^{t'}_{ij} = \delta_{tt'}$. By introducing the canonically normalized field [38, 40]

$$v_{\mathbf{k},t} \equiv \frac{a}{2}M_p h_{\mathbf{k},t}\,, \tag{4.79}$$

we can rewrite the second order Einstein-Hilbert action as [38, 40]

$$S_2 = \sum_s \frac{1}{2}\int d\tau d^3\mathbf{k}\left[v'^2_{\mathbf{k},t} - \left(k^2 - \frac{a''}{a}\right)v^2_{\mathbf{k},t}\right] \tag{4.80}$$

with an effective mass [39]

$$m^2_{\text{eff}} = \frac{a''}{a} = \frac{\nu^2 - 1/4}{\tau^2}\,, \tag{4.81}$$

where $\nu \approx 3/2 + \epsilon$. Hence, we get with the *Bunch-Davies* mode function the following power spectrum for primordial gravitational waves [39]

$$\boxed{P_t(k) = \frac{2}{\pi^2}\frac{\mathcal{H}_*^2}{M_p^2}\left(\frac{k}{k_*}\right)^{-2\epsilon_*} = A_t\left(\frac{k}{k_*}\right)^{n_t}}, \tag{4.82}$$

where the factor of "2" represents the two polarization modes. The spectral index and the tensor perturbation amplitude are given by

$$n_t = -2\epsilon\,, \tag{4.83}$$

$$A_t \equiv \frac{2}{\pi^2}\frac{\mathcal{H}_*^2}{M_p^2}\,, \tag{4.84}$$

from which we can define the tensor-to-scalar ratio

$$\boxed{r \equiv \frac{A_t}{A_s} = 16\epsilon}\,. \tag{4.85}$$

4.3. Inflation in 2hdSMASH

Inflation in 2hdSMASH is described by chaotic inflation. Any theory with a plateau-like scalar potential at sufficiently high field values which hosts a slow-roll regime for the fields involved can give rise to chaotic inflation. This idea was first introduced by Andrei Linde in Ref. [66]. In 2hdSMASH chaotic inflation is an automatic feature where the Higgs doublets Φ_1, Φ_2 and the PQ-singlet S are non-minimally coupled to the Ricci scalar R [67, 68, 69, 70, 19]. At operator mass dimension four we show the action of 2hdSMASH in Jordan frame:

$$S_{\text{2hdSMASH}} \supset -\int d^4x\sqrt{-g}\left(\frac{M^2}{2}+\xi_1\left|\Phi_1\right|^2+\xi_2\left|\Phi_2\right|^2+\xi_S\left|S\right|^2\right)R, \tag{4.86}$$

where ξ_i, $i=1,2,S$, are the dimensionless non-minimal couplings and M is the mass which is related to the reduced Planck mass, $M_p \equiv 1/\sqrt{8\pi G}$, given by

$$M^2 = M_p^2+\xi_1 v_1^2+\xi_2 v_2^2+\xi_S v_S^2. \tag{4.87}$$

By means of metric- and scalar field transformation via the so-called Weyl transformation, we transform the action of eq. (4.86) from Jordan to Einstein frame. In Einstein frame the non-minimal couplings cause the quartic potential to be asymptotically flat and convex such that a plateau-like region is created suitable for inflation. This is true for any quartic potential and is preferred by current cosmic microwave background (CMB) measurements [60]. We restrict ourselves to the neutral part of the two $SU(2)_L$ doublets $\Phi_{1,2}$ and define the scalar fields involved in inflation as:

$$\Phi_1^0 = \frac{h_1}{\sqrt{2}}\,e^{i\cdot\theta_1}\ ,\ \Phi_2^0 = \frac{h_2}{\sqrt{2}}\,e^{i\cdot\theta_2}\ ,\ S=\frac{s}{\sqrt{2}}\,e^{i\cdot\theta_S}\,, \tag{4.88}$$

where the angular fields are expressed by $\theta_i \equiv a_i/v_i$. The Weyl-transformation is given by the frame function

$$\Omega^2(x) = 1+\frac{\xi_1 h_1^2(x)+\xi_2 h_2^2(x)+\xi_S s^2(x)}{M_{\text{P}}^2}\,. \tag{4.89}$$

Thus, we transform the metric into Einstein frame via

$$\tilde{g}_{\mu\nu}(x) = \Omega^2(h_1(x),h_2(x),s(x))\,g_{\mu\nu}(x), \tag{4.90}$$

for which we obtain the action in Einstein frame relevant for inflation

$$S^{(\mathrm{E})}_{\mathrm{2hdSMASH}} \supset \int d^4x\sqrt{-\tilde{g}}\left[-\frac{M_P^2}{2}\tilde{R}+\frac{1}{2}\sum_{i,j}\mathcal{G}_{ij}\tilde{g}^{\mu\nu}\partial_\mu\phi_i\partial_\nu\phi_j-\tilde{V}(\phi_i)\right], \tag{4.91}$$

with fields $\phi=(\phi_1,\phi_2,\phi_3,\phi_4,\phi_5,\phi_6)=(h_1,h_2,s,\theta_1,\theta_2,\theta_S)$, Weyl-transformed metric $\tilde{g}^{\mu\nu}(x)=\Omega^2(x)g^{\mu\nu}(x)$, canonical Einstein-Hilbert action given by the graviational term $\frac{M_P^2}{2}\tilde{R}$, induced field space metric $\mathcal{G}_{ij}$ and scalar potential $\tilde{V}(\phi_i)$. The scalar potential is transformed under Weyl-transformation as follows

$$\tilde{V}(\phi_i)=\frac{1}{\Omega^4(\phi_i)}V(\phi_i)\,, \tag{4.92}$$

where a field dependent factor of Ω^{-4} rescales the Jordan frame scalar potential into the Einstein frame and makes it flat for large field values. Therefore, we neglect the quadratic part and only consider the quartic part of the scalar potential at large field values

$$\begin{aligned}&\tilde{V}_{\mathrm{quartic}}(h_1,h_2,s,\tilde{\theta}_1) \\ &=\frac{\lambda_1h_1^4+\lambda_2h_2^4+\lambda_Ss^4+2\left(\lambda_{34}h_1^2h_2^2+\lambda_{1S}h_1^2s^2+\lambda_{2S}h_2^2s^2-2\lambda_{12S}h_1h_2s^2\cos\left(\tilde{\theta}\right)\right)}{8\left(1+\frac{\xi_1h_1^2+\xi_2h_2^2+\xi_Ss^2}{M_P^2}\right)^2},\end{aligned} \tag{4.93}$$

where $\lambda_{34}\equiv\lambda_3+\lambda_4$. We note that we have four dynamical fields, namely h_1, h_2, s and an effective angle $\tilde{\theta}$ which is defined as follows

$$\tilde{\theta}\equiv 2\theta_S+\theta_1-\theta_2\,, \tag{4.94}$$

where orthogonal directions to $\tilde{\theta}$ are omitted since they correspond to flat directions. The cosine of the λ_{12S}-term can take extrema in the interval $[-1,1]$. We make the restriction $\tilde{\theta}\in[0,\pi]$ and determine the extrema by taking the partial derivative of $\tilde{V}_{\mathrm{quartic}}$ w.r.t. $\tilde{\theta}$:

$$\frac{\partial\tilde{V}_{\mathrm{quartic}}}{\partial\tilde{\theta}}\overset{!}{=}0\quad\Rightarrow\quad\tilde{\theta}_0=\{0,\pi\}\,. \tag{4.95}$$

The sufficient conditions for $\tilde{\theta}$ at its extrema are calculated by taking the second partial derivative of $\tilde{V}_{\text{quartic}}$ w.r.t. $\tilde{\theta}$

$$\frac{\partial^2 \tilde{V}_{\text{quartic}}}{\partial \tilde{\theta}^2} = \begin{cases} \dfrac{\lambda_{12S} h_1 h_2 s^2 M_p^4}{8\left(M_p^2 + \xi_1 h_1^2 + \xi_2 h_2^2 + \xi_S s^2\right)^2} \geq 0 \quad , \tilde{\theta}_0 = 0 \\ \\ \dfrac{-\lambda_{12S} h_1 h_2 s^2 M_p^4}{8\left(M_p^2 + \xi_1 h_1^2 + \xi_2 h_2^2 + \xi_S s^2\right)^2} \leq 0 \quad , \tilde{\theta}_0 = \pi \end{cases} . \tag{4.96}$$

Since $\lambda_{12S} \geq 0$ and the product $h_1 h_2 s^2$ is rotation invariant, $\tilde{\theta}$ is stabilized in its minimum at $\tilde{\theta}_0 = 0$. Hence, the potential reads:

$$\tilde{V}_{\text{quartic}}(h_1, h_2, s) = \frac{\lambda_1 h_1^4 + \lambda_2 h_2^4 + \lambda_S s^4 + 2\left(\lambda_{34} h_1^2 h_2^2 + \lambda_{1S} h_1^2 s^2 + \lambda_{2S} h_2^2 s^2 - 2\lambda_{12S} h_1 h_2 s^2\right)}{8\left(1 + \frac{\xi_1 h_1^2(x) + \xi_2 h_2^2(x) + \xi_S s^2(x)}{M_p^2}\right)^2} . \tag{4.97}$$

There is now a three-dimensional induced field space metric in Einstein frame spanned by $\phi = (h_1, h_2, s)$ which is calculated via:

$$\begin{aligned} \mathcal{G}_{ij} &= \frac{\delta_{ij}}{\Omega^2} + \frac{3}{2} M_p^2 \frac{\partial \log \Omega^2}{\partial \phi_i} \frac{\partial \log \Omega^2}{\partial \phi_j} \\ &= \frac{1}{\Omega^2} \begin{pmatrix} 1 + 6\xi_1^2 \frac{h_1^2}{\Omega^2 M_p^2} & 6\xi_1 \xi_2 \frac{h_1 h_2}{\Omega^2 M_p^2} & 6\xi_1 \xi_S \frac{h_1 s}{\Omega^2 M_p^2} \\ 6\xi_1 \xi_2 \frac{h_1 h_2}{\Omega^2 M_p^2} & 1 + 6\xi_2^2 \frac{h_2^2}{\Omega^2 M_p^2} & 6\xi_2 \xi_S \frac{h_2 s}{\Omega^2 M_p^2} \\ 6\xi_1 \xi_S \frac{h_1 s}{\Omega^2 M_p^2} & 6\xi_2 \xi_S \frac{h_2 s}{\Omega^2 M_p^2} & 1 + 6\xi_S^2 \frac{s^2}{\Omega^2 M_p^2} \end{pmatrix} . \end{aligned}$$

The scalar potential is thus symmetric under $h_1 \to -h_1$, $h_2 \to -h_2$, and $s \to -s$. Therefore, we use spherical field space coordinates as parametrisation for h_1, h_2 and s:

$$h_1(x) = \phi(x) \cos\vartheta \sin\gamma, \qquad h_2(x) = \phi(x) \sin\vartheta \sin\gamma, \qquad s(x) = \phi(x) \cos\gamma . \tag{4.98}$$

During inflation the scalar potential given in eq. (4.97) becomes a constant by cancellation since numerator and denominator scale as ϕ^4. Hence, we can make the following approximation

$$\phi^2(x) \gg \frac{M_p^2}{\left(\xi_1 \cos^2\vartheta \sin^2\gamma + \xi_2 \sin^2\vartheta \sin^2\gamma + \xi_S \cos^2\gamma\right)} , \tag{4.99}$$

which allows us to express the scalar potential solely by angles ϑ and γ:

$$\tilde{V}_{\text{quartic}}(\vartheta,\gamma) \simeq \tag{4.100}$$
$$M_p^4 \frac{t_\gamma^4\left(\lambda_1+\lambda_2 t_\vartheta^4+2\lambda_{34}t_\vartheta^2\right)+2t_\gamma^2\left(t_\vartheta^2+1\right)\left(\lambda_{1S}+\lambda_{2S}t_\vartheta^2-2\lambda_{12S}t_\vartheta\right)+\lambda_S\left(t_\vartheta^2+1\right)^2}{8\left(t_\gamma^2(\xi_1+\xi_2 t_\vartheta^2)+\xi_S(1+t_\vartheta^2)\right)^2},$$

where $t_x \equiv \tan x$. Furthermore, we require the portal couplings to be tiny in order to avoid large radiative corrections which is technically natural and associated by an enhanced Poincaré symmetry [4] [25]. Therefore we consider two portal coupling regimes

$$\lambda_{12S} \ll \lambda_{1,2,34,1S,2S,S}\,, \tag{I}$$
$$\lambda_{12S} \lesssim \lambda_{1S} \sim \lambda_{2S} \ll \lambda_{1,2,34,S}\,, \tag{II}$$

where cases with $\lambda_{12S} \gg \lambda_{iS}$ are neglected due to scale-invariance, and cases with $\lambda_{1S,2S} \ll \lambda_{2S,1S}$ are neglected due to the intricacies of RG running[5]. Case (I) is the most general case to consider, whereas case (II) can be understood as the limit $\lambda_{1S,2S} \to 0$ by going from (I) to (II). In (II), all of the portal couplings are tiny, so that the PQ-sector decouples completely from the 2HDM sector. In order to find the most general description, we will focus on (I) and note when (II) can be applied. The scalar potential for case (I) is therefore given by

$$\tilde{V}_{\text{quartic}}(\vartheta,\gamma) \simeq \tag{4.101}$$
$$M_p^4 \frac{t_\gamma^4\left(\lambda_1+\lambda_2 t_\vartheta^4+2\lambda_{34}t_\vartheta^2\right)+2t_\gamma^2\left(t_\vartheta^2+1\right)\left(\lambda_{1S}+\lambda_{2S}t_\vartheta^2\right)+\lambda_S\left(t_\vartheta^2+1\right)^2}{8\left(t_\gamma^2(\xi_1+\xi_2 t_\vartheta^2)+\xi_S(1+t_\vartheta^2)\right)^2}.$$

From this expression we are able to determine the minima and thus the effective single field trajectories. This is done by considering the Jacobian of eq. (4.101) in two-dimensional field space :

$$J(\vartheta,\gamma) = \begin{pmatrix} \frac{\partial \tilde{V}_{\text{quartic}}(\vartheta,\gamma)}{\partial\vartheta} & \frac{\partial \tilde{V}_{\text{quartic}}(\vartheta,\gamma)}{\partial\gamma} \end{pmatrix}^2. \tag{4.102}$$

[4] This was introduced by Ref. [25] in the context of the νDFSZ model which we adopted for 2hdSMASH and discussed in section 3.9.

[5] We comment on the features of RG running with portal couplings in section 5.

With $J_2 \equiv \frac{\partial \tilde{V}_{\text{quartic}}}{\partial \gamma} = 0$ we determine the extrema of γ:

$$\gamma_{0,i} = \begin{cases} \gamma_{\text{THI}} = \dfrac{\pi}{2} \\ \gamma_{\text{PQI}} = 0 \\ \gamma_{\text{PQTHI}} = \gamma_{\text{PQTHI}}(\vartheta) \end{cases} , \tag{4.103}$$

which correspond to the three coarse field space directions for inflation, i.e. 2HDM-inflation denoted by THI, PQ-inflation denoted by PQI and mixed PQ-2HDM-inflation denoted by PQTHI. We have omitted for now the detailed expression of γ_{PQTHI} which will be mentioned in section 4.3.2. There are in principle seven inflationary directions, namely three 2HDM-field directions (h_1, h_2, h_{12}), one PQ-field direction s and three mixed PQ-2HDM directions (sh_1, sh_2, sh_{12}). All of these field directions are effective single field trajectories which omit multi-field effects.

As mentioned above, we will use case (I) as the most general description and take the limit to case (II) for THI and PQI since both sectors decouple from each other and are thus technically natural [25]. In the following, we will start with the discussion on THI, followed by the discussion on PQI and PQTHI. This is done by considering the γ-directions given by γ_{THI}, γ_{PQ} and $\gamma_{\text{PQTHI}}(\vartheta)$, respectively.

4.3.1. 2HDM inflation in 2hdSMASH

In this section we will introduce THI by deriving its field directions, its inflationary conditions and its slow-roll potential. Inflation in the 2HDM model has already been discussed in numerous Refs. [41, 43, 71, 42].

In order to decouple the 2HDM-field directions from the PQ-direction we implement a hierarchy of non-minimal couplings, i.e. $\xi_{1,2} \gg \xi_S$. The effective scalar potential is thus given by

$$\tilde{V}_{\text{quartic}}(\vartheta,\gamma) \simeq \tag{4.104}$$
$$M_p^4 \, \frac{t_\gamma^4 \left(\lambda_1 + \lambda_2 t_\vartheta^4 + 2\lambda_{34} t_\vartheta^2\right) + 2t_\gamma^2 \left(t_\vartheta^2+1\right)\left(\lambda_{1S} + \lambda_{2S} t_\vartheta^2\right) + \lambda_S \left(t_\vartheta^2+1\right)^2}{8 t_\gamma^4 \left(\xi_1 + \xi_2 t_\vartheta^2\right)^2} .$$

The Jacobian from eq. (4.102) for the 2HDM-field directions is determined by γ_{THI}:

$$J\left(\vartheta,\gamma_{\text{THI}}\right) = \left(\frac{\partial \tilde{V}_{\text{quartic}}(\vartheta,\gamma)}{\partial\vartheta} \quad \frac{\partial \tilde{V}_{\text{quartic}}(\vartheta,\gamma)}{\partial\gamma} \right)^T \Bigg|_{\gamma=\gamma_{\text{THI}}} \tag{4.105}$$
$$= \left(0 \quad \frac{t_\vartheta \left(t_\vartheta^2+1\right)\left(-\lambda_1\xi_2 + \lambda_{34}\xi_1 + t_\vartheta^2(\lambda_2\xi_1 - \lambda_{34}\xi_2)\right)}{2\left(\xi_1 + \xi_2 t_\vartheta^2\right)^3} \right)^T ,$$

for which we acquire via $J_2\left(\vartheta,\gamma_{\text{THI}}\right) = 0$ the extrema ϑ_{THI}:

$$\vartheta_{\text{THI}} = \begin{cases} \vartheta_{h_1} = 0 \\ \vartheta_{h_2} = \dfrac{\pi}{2} \\ \vartheta_{h_{12}} = \arctan\left(\sqrt{\dfrac{\lambda_{34}\xi_1 - \lambda_1\xi_2}{\lambda_{34}\xi_2 - \lambda_2\xi_1}}\right) \end{cases} . \tag{4.106}$$

The corresponding inflationary vacuum energies are thus given by [41]

$$\tilde{V}_0^{\text{THI}} = \begin{cases} \tilde{V}_0^{h_1} \simeq \frac{\lambda_1}{8\xi_1^2} \\ \tilde{V}_0^{h_2} \simeq \frac{\lambda_2}{8\xi_2^2} \\ \tilde{V}_0^{h_{12}} \simeq \frac{\lambda_1\lambda_2 - \lambda_{34}^2}{8\left(\lambda_1\xi_2^2 + \lambda_2\xi_1^2 - 2\lambda_{34}\xi_1\xi_2\right)} \end{cases} \tag{4.107}$$

with quartic couplings couplings λ_i^{THI}

$$\text{2HDM-}h_1 :\ \lambda_1 \quad , \quad \text{2HDM-}h_2 :\ \lambda_2 \quad , \quad \text{2HDM-}h_{12} :\ \lambda_{12} \equiv \lambda_1\lambda_2 - \lambda_{34}^2 . \tag{4.108}$$

The critical points $\{\gamma_{\text{THI}}, \vartheta_{\text{THI}}\}$ of eq. (4.106) correspond to the three field space directions, i.e. h_1, h_2 and h_{12}. The hessian matrix in two dimensional space is required

$$H\left(\vartheta_{\text{THI}}, \gamma_{\text{THI}}\right) = \left(\begin{array}{cc} \dfrac{\partial^2 \tilde{V}_{\text{quartic}}(\vartheta,\gamma)}{\partial\gamma^2} & \dfrac{\partial^2 \tilde{V}_{\text{quartic}}(\vartheta,\gamma)}{\partial\gamma\partial\vartheta} \\ \dfrac{\partial^2 \tilde{V}_{\text{quartic}}(\vartheta,\gamma)}{\partial\gamma\partial\vartheta} & \dfrac{\partial^2 \tilde{V}_{\text{quartic}}(\vartheta,\gamma)}{\partial\vartheta^2} \end{array} \right) \Bigg|_{\substack{\gamma=\gamma_{\text{THI}} \\ \vartheta=\vartheta_{\text{THI}}}} \tag{4.109}$$

in order to obtain the sufficient minimum conditions

$$\begin{aligned} &\det H\left(\vartheta_{\text{THI}}, \gamma_{\text{THI}}\right) \geq 0\,, \\ &H_{1,1}\left(\vartheta_{\text{THI}}, \gamma_{\text{THI}}\right) \geq 0 \;\text{ or }\; H_{2,2}\left(\vartheta_{\text{THI}}, \gamma_{\text{THI}}\right) \geq 0\,. \end{aligned} \tag{4.110}$$

These are calculated to be:

2HDM-(h_1):
$\kappa_1 \equiv \lambda_{34}\xi_1 - \lambda_1\xi_2 > 0\,,$
$\kappa_{1s} \equiv \lambda_{1S} > 0\,.$

2HDM-(h_2):
$\kappa_2 \equiv \lambda_{34}\xi_2 - \lambda_2\xi_1 > 0\,,$
$\kappa_{2s} \equiv \lambda_{2S} > 0\,.$

2HDM-(h_{12}):
$-\kappa_1\kappa_2\left(\kappa_1\xi_2 + \kappa_2\xi_1\right) > 0\,,$
$\kappa_1\kappa_2\left(\kappa_1+\kappa_2\right)\left(\kappa_1\xi_2 + \kappa_2\xi_1\right)\left(\kappa_1\lambda_{2s} + \kappa_2\lambda_{1S}\right) > 0\,.$

We note that these conditions simplify drastically for tiny portal couplings and reproduce the known results for pure 2HDM inflation [41] where $\kappa_{1s} = \kappa_{2s} \simeq 0$. As discussed in section 4.3 this is regarded as the limit from case (I) to case (II). For the remainder, we keep the discussion on the minimum conditions for 2HDM-inflation as general as possible and consider case (I) in order to quantify the results in comparison to PQI and PQTHI.

These minimum conditions, however, just describe a part of the inflationary conditions. Since inflation proceeds along a valley (minimum) of a given field space direction it requires that orthogonal field space directions are ridges (maxima). Therefore,

the minimum conditions need to be supplemented by the maximum conditions of the other field space directions in order to fully describe the inflationary conditions. This applies, in particular to the 2HDM-h_1 and 2HDM-h_2 direction. For the 2HDM-h_{12} direction this is already an automatic feature since this field direction is described by a mixture of both field directions and thus requires each individual field direction to be a ridge. However, the minimum conditions for the 2HDM-h_{12} direction needs more refining. Effectively, the first one of the two conditions states

$$\kappa_1 \leq 0 \quad , \quad \kappa_2 \leq 0 \,. \tag{4.111}$$

Therefore, the second condition for $\xi_{1,2} > 0$ reads

$$\kappa_1 \lambda_{2s} + \kappa_2 \lambda_{1S} > 0 \,, \tag{4.112}$$

which is only true for

$$\kappa_{1s} \equiv \lambda_{1S} < 0 \quad , \quad \kappa_{2s} \equiv \lambda_{2S} < 0 \,. \tag{4.113}$$

Moreover, there are kinetic mixing terms for the 2HDM-h_{12} direction. These are quantified by

$$K = \frac{6\xi_1\xi_2}{\Omega^2}\frac{h_1 h_2}{M_p^2} \,, \tag{4.114}$$

which we avoid in the field space metric by assuming a hierarchy for the non-minimal couplings, i.e. $\xi_i \gg \xi_j$. The inflaton field ϕ proceeds along the mixed direction composed by h_1 and h_2 but is parametrically close to either h_1 or h_2. Both options are equivalent since either self-coupling, i.e. λ_1 and λ_2, is of $\mathcal{O}(1)$ and allows for the same predictions. We therefore choose without loss of generality to make the 2HDM-h_{12}-direction parametrically close to the h_2 direction[6]. Hence, we assume a hierarchy for the non-minimal couplings, i.e. $\xi_2 \gg \xi_1$. Given this hierarchy, the inflationary conditions for the 2HDM-h_{12} direction simplify

$$\kappa_{1s,2s,2} \simeq \lambda_{1S,2S,34} \leq 0 \quad \wedge \quad \kappa_1 \simeq \lambda_1 \geq 0 \,. \tag{4.115}$$

The field space metric of (4.98) reduces for all 2HDM-directions to a two dimensional field space and becomes quite simple under the above assumptions for the 2HDM-

[6]The same discussion applies to the 2HDM-h_{12} direction being parametrically close to h_1.

h_{12} direction

$$\mathcal{G}_{ij}^{h_{12}} \simeq \frac{b}{\Omega_{12}^2}\begin{pmatrix} 1 & 0 \\ 0 & \frac{\Omega_{12}^2+6\xi_2^2\frac{\phi^2}{M_p^2}}{\Omega_{12}^2} \end{pmatrix}, \tag{4.116}$$

where b is the mixing parameter given by

$$b \equiv 1 + \left|\frac{\lambda_{34}}{\lambda_1}\right|, \tag{4.117}$$

which is determined via $\cos^2\vartheta_{h_{12}} = 1 - b^{-1}$. The frame function Ω_{12}^2 for the mixed direction becomes

$$\Omega_{12}^2 = b + \xi_2\frac{\phi^2}{M_p^2}, \tag{4.118}$$

which reduces to the frame function for the 2HDM-h_2 direction when $\lambda_{34} \to 0$. This would be the limit where the 2HDM becomes an effective SM. However, we demand $\lambda_{34} \neq 0$ since it will be useful for RG-analysis (see section 5). In order to justify our approach for describing 2HDM-h_{12}-inflation in an effective single field regime, we need to compute the instantaneous masses of h_1 and h_2

$$m_{h_i}^2\Big|_{\substack{\vartheta=\vartheta_{h_{12}}\\ \gamma=\gamma_{\mathrm{THI}}}} \simeq \mathcal{G}^{h_ih_i}\partial_{h_i}^2\tilde{V}_{\mathrm{quartic}}\Big|_{\substack{\vartheta=\vartheta_{h_{12}}\\ \gamma=\gamma_{\mathrm{THI}}}} \simeq \begin{cases} -\frac{\lambda_{34}}{\xi_2} & (h_1) \\ \\ \frac{\lambda_{34}^2}{6\lambda_1\xi_2^2} & (h_2) \end{cases}. \tag{4.119}$$

To estimate whether the orthogonal directions are heavy, i.e. stabilized, or light, i.e. dynamical, we relate those masses to the Hubble rate $\mathcal{H}^2 \approx \tilde{V}/3M_p^2$

$$\frac{m_{h_i}^2}{\mathcal{H}^2} \simeq \begin{cases} -\frac{24\lambda_1\lambda_{34}\xi_2}{\lambda_1\lambda_2-\lambda_{34}^2} \gtrsim 1 & (h_1) \\ \\ \frac{4\lambda_{34}^2}{\lambda_1\lambda_2-\lambda_{34}^2} \lesssim 1 & (h_2) \end{cases}, \tag{4.120}$$

which shows that h_1 is stabilized for $\xi_2 \gg 1$ and h_2 is dynamical for sufficiently small λ_{34}, i.e. $\lambda_1\lambda_2 \geq 5\lambda_{34}^2$.

There are three inflationary trajectories where effective single field inflation proceeds with the inflaton ϕ which can be seen in figure 4.2. Since ϕ is a non-canonical field

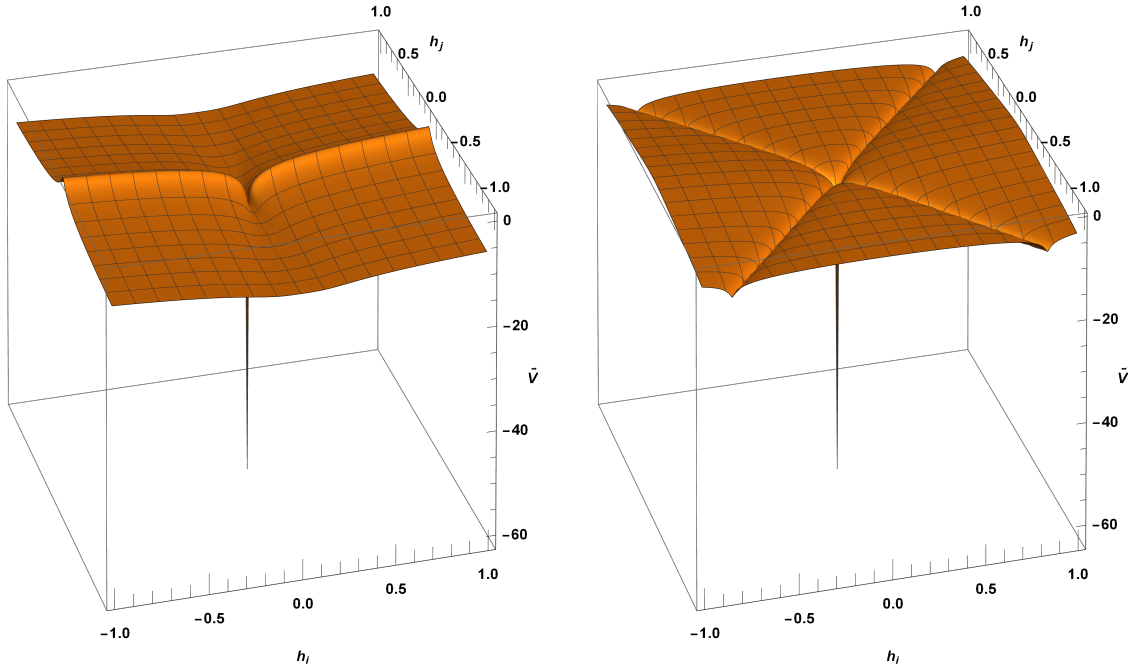

Figure 4.2.: Decadic log Einstein frame scalar potential depicting the 2HDM-field directions in 2hdSMASH shown in units of M_p as a function of the two Higgs fields h_1 and h_2 for pure single field directions (left) and mixed single field direction (right).

we introduce a canonical normalization in the h_1- and h_2-field directions via

$$\Omega^2 \frac{d\chi_i}{d\phi_i} = \sqrt{\Omega^2 + 6\xi_i^2 \frac{\phi^2}{M_p^2}} \quad \text{for } i = 1, 2\,. \tag{4.121}$$

The canonically normalized 2HDM-h_{12}-field direction is determined by a mixture of h_1 and h_2 which is controlled by the mixing parameter b and is given by

$$\Omega_{12}^2 \frac{d\chi_{12}}{d\phi} = \sqrt{b\left(\Omega_{12}^2 + 6\xi_2^2 \frac{\phi^2}{M_{\rm P}^2}\right)}\,. \tag{4.122}$$

This allows us to determine the effective single-field slow-roll potential with canonically normalized inflaton field χ_j, for $j = 1, 2, 12$:

$$\tilde{V}_j^{\rm THI}(\phi) = \frac{\lambda_j^{\rm THI}\, \phi^4(\chi_j)}{8\left(1 + \xi_j \frac{\phi^2(\chi_j)}{M_p^2}\right)^2}\,. \tag{4.123}$$

The conditions on the coupling parameters for inflation in each 2HDM field direction along with the corresponding effective single field slow-roll potential are summarized in Table 4.1

As discussed in section 4.2, inflation occurs when the Hubble radius decreases at

inflation along	Potential (4.104) minimized at	Inflationary conditions	Einstein frame slow roll potential
h_1	$\gamma_0 = \frac{\pi}{2}$ $\vartheta_0 = 0$	$\kappa_1 \geq 0\,,\ \kappa_{1s} \geq 0$ $\kappa_2 \leq 0\,,\ \kappa_{2s} \leq 0$	$\frac{\lambda_1}{8}\phi^4 \left(1 + \xi_1 \frac{\phi^2}{M_P^2}\right)^{-2}$
h_2	$\gamma_0 = \frac{\pi}{2}$ $\vartheta_0 = \frac{\pi}{2}$	$\kappa_2 \geq 0\,,\ \kappa_{2s} \geq 0$ $\kappa_1 \leq 0\,,\ \kappa_{1s} \leq 0$	$\frac{\lambda_2}{8}\phi^4 \left(1 + \xi_2 \frac{\phi^2}{M_P^2}\right)^{-2}$
h_{12}	$\gamma_0 = \frac{\pi}{2}$ $\vartheta_0 = \arctan\left(\sqrt{\frac{\kappa_1}{\kappa_2}}\right)$	$\kappa_1 \leq 0\,,\ \kappa_2 \leq 0$ $\kappa_{1s} \leq 0\,,\ \kappa_{2s} \leq 0$	$\frac{\lambda_{12}}{8}\phi^4 \left(1 + \xi_2 \frac{\phi^2}{M_P^2}\right)^{-2}$

Table 4.1.: Conditions & characteristics for h_1-, h_2- and h_{12}-inflation in 2hdSMASH.

which point the potential energy density dominates the universe. This process is quantified by the slow-roll parameters demanding that the inflaton rolls down the potential well slowly. In slow-roll approximation these parameters are expressed as

$$\epsilon_V = \frac{M_p^2}{2}\left(\frac{\tilde{V}'(\chi)}{\tilde{V}(\chi)}\right)^2 \ , \ \eta_V = M_p^2 \frac{\tilde{V}''(\chi)}{\tilde{V}(\chi)} \tag{4.124}$$

where primes denote derivatives w.r.t. χ and are used to calculate the inflationary observables created during slow-roll inflation. Due to this prolonged stage of slow-roll inflation, the inflaton produces quantum fluctuations along the field trajectory. These quantum fluctuation are transferred to scalar metric perturbations in form of density waves $P_s(k)$ and tensor metric perturbations in form of gravitational waves $P_t(k)$. We give $P_s(k)$ and $P_t(k)$ as (see section 4.2 for details):

$$P_s(k) = A_s \left(\frac{k}{k_*}\right)^{n_s - 1 + \ldots} \ , \ P_t(k) = A_t \left(\frac{k}{k_*}\right)^{n_t + \ldots} \tag{4.125}$$

with n_s as the spectral scalar index and n_t as the tensor spectral index, quantifying the deviation from scale-invariance of the power spectra. The scalar- and tensor metric perturbations are reduced to the scalar perturbation amplitude A_s and to the tensor perturbation amplitude A_t for $k = k_*$ when the modes exit the horizon at the pivot scale k_*. Moreover, the gravitational amplitude A_t is normalized by A_s to acquire the tensor-to-scalar ratio r which relates gravitational waves to CMB measurements. Additionally, the spectral tensor index n_t is related to the tensor-scalar

ratio r for single field inflation via

$$n_t = -\frac{r}{8}\,, \tag{4.126}$$

which leaves us with the relevant inflationary observables A_s, n_s and r in slow-roll approximation for single field inflation:

$$A_s = \frac{1}{24\pi^2 M_{Pl}^4}\frac{\tilde{V}}{\epsilon_V}\ ,\ n_s = 1 - 6\epsilon_V + 2\eta_V\ ,\ r = 16\epsilon_V\,. \tag{4.127}$$

As discussed in Refs. [41, 43, 71, 42], we consider large non-minimal couplings in order to satisfy the scalar density perturbations of the CMB given by PLANCK [61, 60]. We will show that this is required for the 2HDM-field directions by calculating the expression for A_s and constraining the non-minimal couplings $\xi_{1,2}$ with CMB measurements by PLANCK [61, 60]. Moreover, we will calculate n_s and r_s in the large non-minimal coupling limit and relate their expressions to the number of e-folds and make the well-know predictions for Higgs inflation [19].

In the large field limit, i.e. $\xi_{1,2} \gg 1$, we can approximate $\phi(\chi)$ and its inverse $\chi(\phi)$ by solving equations (4.121) and (4.122) [7]

$$\phi_i(\chi_i) \simeq \frac{M_p}{\sqrt{\xi_i}}\sqrt{\exp\left(\sqrt{\frac{2}{3}}\frac{\chi_i}{M_p}\right) - b}\,, \tag{4.128}$$

$$\chi(\phi_i) \simeq \sqrt{\frac{3}{2}} M_p \log\left(b\ M_p^2 + \xi_i \frac{\phi_i^2}{M_p^2}\right)\,, \tag{4.129}$$

from which we acquire with $\phi(\chi)$ the following slow-roll potential

$$\tilde{V}(\chi_i) \simeq \frac{\lambda}{8\xi^2} M_p^4 \left(1 - b\exp\left(-\sqrt{\frac{2}{3}}\frac{\chi}{M_p}\right)\right)^2 \tag{4.130}$$

with mixing parameter b which quantifies whether inflation proceeds in a mixed direction ($b \neq 1$) or in a non-mixed direction ($b = 1$). By taking the first and second partial derivatives of $\tilde{V}$ allows us to compute the slow-roll parameters and thus the

[7] The derivation of the canonically normalized field χ, the slow-roll parameters and the inflationary observables (A_s, n_s, r) in the large ξ limit can be found in appendix D.3.

inflationary observables A_s, n_s and r in the large ξ limit [7]

$$A_s \simeq \frac{\lambda_i}{128\pi^2\xi_i^2\, b}\frac{(1-b\,x_i)^4}{x_i^2}\ ,\ n_s \simeq 1-\frac{8\,b}{3}\frac{b+x_i}{(b-x_i)^2}\ ,\ \simeq \frac{64\,b^2}{3\,(x_i-b)^2} \tag{4.131}$$

with $x_i \equiv \exp\left(\sqrt{2/3}\chi_i/M_p\right)$. This reduces for $b=1$ to

$$A_s \simeq \frac{3\lambda \sinh^4\left(\frac{\chi}{\sqrt{6}M_p}\right)}{2\xi^2}\ ,\ r \simeq \frac{64\,b^2}{3\,(x_i-b)^2}\,, \tag{4.132}$$

$$n_s \simeq \frac{4}{3}\left(\coth\left(\frac{\chi}{\sqrt{6}M_p}\right)-\operatorname{csch}^2\left(\frac{\chi}{\sqrt{6}M_p}\right)-1\right)-\frac{1}{3}\,. \tag{4.133}$$

These quantities can be constrained by CMB measurements. Current constraints on r, A_s and n_s are given by PLANCK 2018 data [61],[60] which were recently updated by Ref. [72]:

$$r_{0.002} < 0.0387985 \quad (95\%\text{C.L., TT,TE,EE+lowE+lensing+BK18+BAO})\,, \tag{4.134}$$

$$A_s = (2.105 \pm 0.030)\times 10^{-9} \quad (68\%\text{C.L., TT,TE,EE+lowE+lensing+BAO})\,, \tag{4.135}$$

$$n_s = 0.9665 \pm 0.0038 \quad (68\%\text{C.L., TT,TE,EE+lowE+lensing+BAO})\,. \tag{4.136}$$

The scalar perturbation amplitude A_s can be used to relate the non-minimal coupling ξ_i to the self-coupling λ_i. From eq. (4.131) we can approximate $A_s \propto \lambda_i/\xi_i^2$ for which we obtain an approximate relation

$$A_s \propto \frac{\lambda_i}{\xi_i^2} \propto 10^{-9} \tag{4.137}$$

$$\Rightarrow\ \xi_i \propto \sqrt{\lambda_i}10^{-5}\,. \tag{4.138}$$

We show this λ-ξ relation in figure 4.3 (left), which we acquired numerically. This relation is furthermore constrained by n_s and r: the non-minimal coupling ξ is constrained by r as shown in figure 4.3 (right) and r is constrained by n_s with PLANCK 2018 [61],[60] and BICEP 2021 [72] data. The blue and red curves correspond to a bluer and redder spectrum of n_s, respectively. The 2HDM quartic couplings are of order $\lambda \sim \mathcal{O}(1)$ at the Planck scale. This is required by RG running and Higgs phenomenology to accommodate a 125 GeV Higgs mass at low energies. Later, we will see that the size of 2HDM quartic couplings cannot be changed by considering different field space directions since the RGEs are strongly coupled. From figure 4.3 (left) and from eq. (4.138) we can see that the non-minimal coupling is of the order $\xi \sim 10^4$.

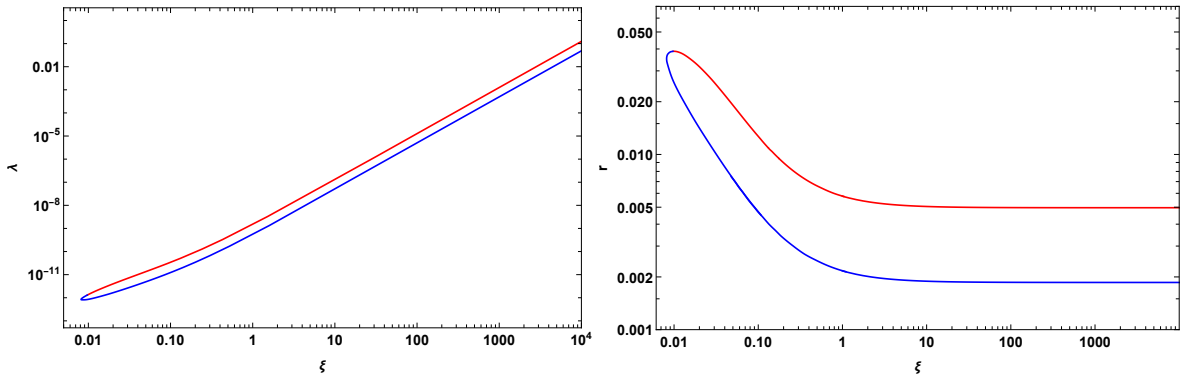

Figure 4.3.: Shown are the 95% C.L. contours of λ vs. ξ (left) and r vs. ξ (right). The red and blue curves indicate the redder and bluer spectrum of n_s.

In order to determine the inflationary observables A_s, n_s and r in the large ξ limit from equation (4.131) properly, we require χ_I and χ_E at horizon crossing and at the end of inflation, respectively. Therefore, we need to compute $\chi(N)$ to determine the number of e-folds required for successful inflation. As defined in eq. (4.41) of section 4.2, the number of e-folds during inflation between some initial time t_I and the time at the end of inflation is given by

$$N = \int_{t_I}^{t_{\text{end}}} \mathcal{H}(t)dt \simeq \int_{\chi_I}^{\chi_{\text{end}}} \frac{d\chi}{\sqrt{2\epsilon}} \tag{4.139}$$

and is approximated to [8]

$$N \simeq \frac{1+6\xi_i}{8M_p^2}\left(\phi_I^2 - \phi_E^2\right) - \frac{3b}{4}\log\left(\frac{b\,M_p^2 + \xi_i\phi_I^2}{b\,M_p^2 + \xi_i\phi_E^2}\right). \tag{4.140}$$

However, the exact number of e-folds can be obtained by solving the Klein-Gordon equation for the canonically normalized field χ. In appendix D.4 we derived the Klein-Gordon equation for χ

$$\frac{d^2\chi}{dN^2} + 3\frac{d\chi}{dN} - \frac{1}{2M_p^2}\left(\frac{d\chi}{dN}\right)^3 + \sqrt{2\epsilon}\left(3M_p - \frac{1}{2M_p}\left(\frac{d\chi}{dN}\right)^2\right) = 0\,, \tag{4.141}$$

which is evaluated until the condition $\epsilon = 1$ marks the end of inflation. This differential equation, however, can only be computed numerically and requires appropriate initial conditions. These initial conditions can be estimated with the covariant formalism described in appendix D.5. We use the expressions $\phi(\Delta N)$ from eq. (D.71)

[8] We give a detailed calculation in appendix D.1.

and $\phi(\chi)$ from eq. (4.129) to determine $\chi(\Delta N)$

$$\chi(\Delta N) \simeq \sqrt{\frac{3}{2}} M_p \log\left(\frac{b^2(1+6\xi)+8\Delta N\xi}{b(1+6\xi)}\right) \approx 5M_p\,, \tag{4.142}$$

$$\chi'(\Delta N) \simeq M_p \frac{4\sqrt{6}M_p}{\Delta N\,(b^2(1+6\xi)+8\Delta N\xi)} \approx 0.02M_p\,. \tag{4.143}$$

Furthermore, we have derived in appendix D.5 the e-fold dependencies of A_s, n_s and r with the covariant formalism. This gives us a better understanding of the parameters scale. In the large ξ limit, these quantities are given by

$$n_s\,(\Delta N) \simeq 1 - \frac{2}{\Delta N}\ ,\ r \simeq \frac{12b}{\Delta N^2}\ ,\ A_s(\Delta N) \simeq \frac{\lambda \Delta N^2}{144\pi^2 b\xi^2}\,, \tag{4.144}$$

where in the non-mixed direction they are given by

$$n_s\,(\Delta N) \simeq 1 - \frac{2}{\Delta N}\ ,\ r \simeq \frac{12}{\Delta N^2}\ ,\ A_s(\Delta N) \simeq \frac{\Delta N^2}{144\pi^2}\frac{\lambda}{\xi^2}\,. \tag{4.145}$$

These inflationary predictions resemble the results of Starobinsky-type inflation [59, 73, 74, 75] and Higgs inflation [19]. As in Higgs inflation and Starobinsky's R^2-inflation, the spectral index n_s and the tensor-to-scalar ratio r are solely dependent on ΔN and independent of ξ. In figure 4.4 we plot the r vs. n_s predictions for 2HDM inflation in the large ξ limit. The general n_s and r predictions are shown as black solid lines which go from low to large ξ where the red dots at $\xi = \infty$ mark our r vs. n_s predictions. Each solid black line corresponds to a given number of e-fold which is in the range of $N \in [50, 70]$. Furthermore, we show the isocontours of constant ξ as gray dashed lines. In fact, the n_s and r predictions are true for any chaotic inflationary model with a single field attractor. The predictions are constrained by the 95% and 68% C.L. contours of PLANCK 2018 data [60, 61] and the BICEP update [72]. Furthermore, we note the remarkable r vs n_s prediction for $N = 60$, which we will also encounter for PQI and PQTHI.

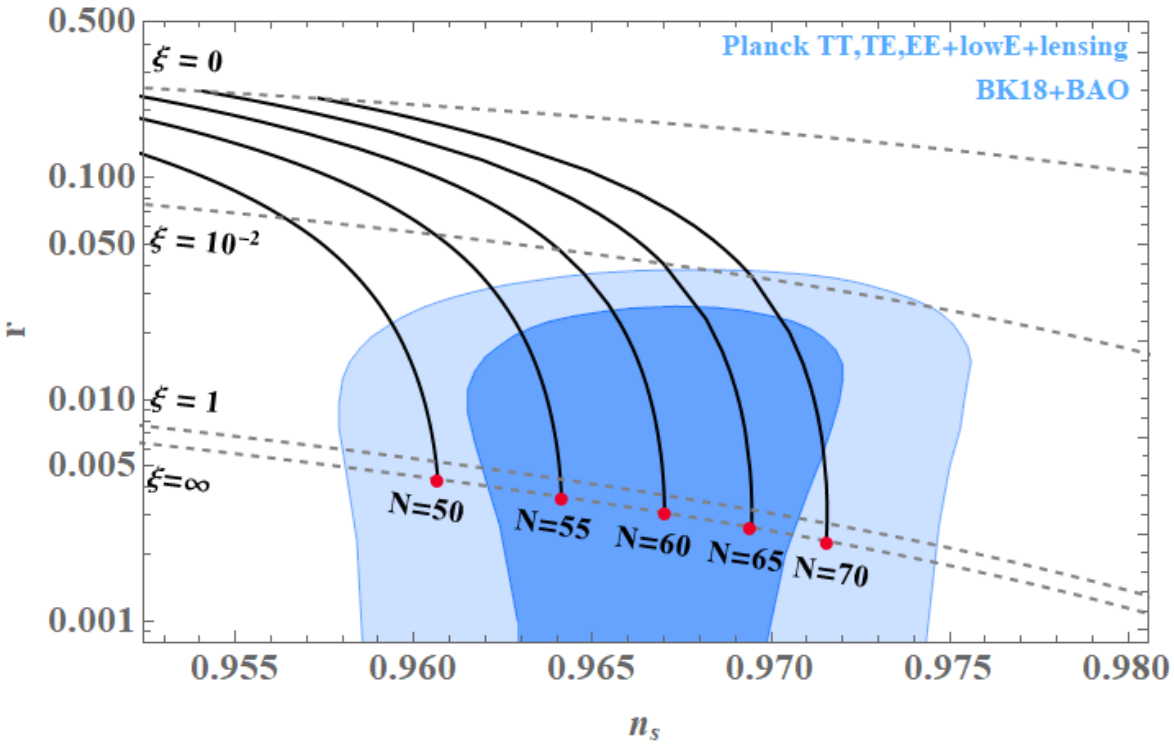

Figure 4.4.: Shown are the 95% and 68% C.L. contours of r vs. n_s (blue) and the inflationary predictions by 2hdSMASH for 2HDM-inflation (solid black). The dashed curves correspond to the isocontours of constant ξ. The main inflationary prediction for the 2HDM are given by $\xi = \infty$ and $N \in [50, 70]$ (red dot).

As mentioned before, we require for THI non-minimal couplings of the order of $\xi \sim 10^4$. Various authors have discussed the negative impact of such a large non-minimal coupling on perturbative unitarity (e.g. Refs. [76, 77]). The claim is that the unitarity scale is below the inflationary scale, i.e. $\Lambda_U = M_P/\xi_{1,2} \lesssim M_P/\sqrt{\xi_{1,2}} = \Lambda_{\text{Inf}}$ for $\xi_{1,2} \gg 1$, which puts predictiveness under scrutiny. Recently, this issue was addressed by Ref. [78] in which they claim that the unitarity scale during inflation is actually higher than previously calculated and thus resolving this issue. However, the results of Ref. [78] are beyond the scope of this work and we leave it to future explorations to investigate whether this applies to Higgs inflation in our model. For our considerations, large non-minimal couplings are unnatural since there isn't an explanation on how these large couplings were generated. The approach by the authors of Refs. [44, 52, 7] alleviate the above concerns on predictive power by non-minimal couplings of the size $\xi_i \lesssim 1$ which implies $\lambda \lesssim 10^{-10}$. We adopt these considerations of Refs. [44, 52, 7] which is according to our philosophy more natural. Non-minimal couplings with the size of $\xi_i \lesssim 1$ can be radiatively generated in the very early universe. Therefore, we require the inflaton's quartic self-coupling to be of order $\lambda \lesssim 10^{-10}$. However, the RGEs for λ_1 and λ_2 are dominated by couplings

which are of $\mathcal{O}(1)$ as can be seen by eqs. (4.146)-(4.147)

$$\begin{aligned}\mathcal{D}\lambda_1 = &\frac{3}{4}g_1^4 + \frac{3}{2}g_1^2 g_2^2 + \frac{9}{4}g_2^4 - \lambda_1\left(3g_1^2 + 9g_2^2\right) + 12\lambda_1^2 \\ &+ 4\lambda_3\lambda_4 + 4\lambda_3^2 + 2\lambda_4^2 + 2\lambda_{1S}^2 + 12\lambda_1 Y_b^2 - 12Y_b^4 \\ &+ 4\lambda_1 Y_\tau^2 - 4Y_\tau^4 + 4\lambda_2 \mathrm{Tr}\left(Y_\nu^\dagger Y_\nu\right) - 4\mathrm{Tr}\left(Y_\nu^\dagger Y_\nu Y_\nu^\dagger Y_\nu\right),\end{aligned} \tag{4.146}$$

$$\begin{aligned}\mathcal{D}\lambda_2 = &\frac{3}{4}g_1^4 + \frac{3}{2}g_1^2 g_2^2 + \frac{9}{4}g_2^4 - \lambda_2\left(3g_1^2 + 9g_2^2\right) + 12\lambda_2^2 \\ &+ 4\lambda_3\lambda_4 + 4\lambda_3^2 + 2\lambda_4^2 + 2\lambda_{2S}^2 + 12\lambda_2 Y_t^2 - 12Y_t^4 .\end{aligned} \tag{4.147}$$

On the other hand, any scenario with $\lambda_{1,2,34} \sim 10^{-10}$ would endanger Higgs phenomenology since these small self-couplings could not reproduce a 125 GeV Higgs. Therefore, we can safely neglect inflationary realizations where only 2HDM-fields are involved. This is the main reason to solely focus on PQI and PQTHI.

4.3.2. PQ- and PQ-2HDM-inflation in 2hdSMASH

In this section, we discuss inflation in the PQ- and PQ-2HDM directions. This corresponds to the field directions determined by γ_{PQI} and γ_{PQTHI} respectively. These types of inflationary field directions have been discussed in the context of a KSVZ-type model, dubbed SMASH [7], where the number of field directions is drastically reduced compared to 2hdSMASH. In the context of the DFSZ-type model, inflation was only discussed in the 2HDM direction where quartic self-couplings where taken to be of order $\mathcal{O}(1)$ (see Ref. [43]). Nevertheless, in the context of the DFSZ model, inflation was not considered in other field space directions nor with a small inflaton self-coupling.

As discussed in the previous section, THI requires $\lambda_i^{\text{THI}} \lesssim 10^{-10}$ for $\xi_{1,2} \lesssim 1$ [44, 52, 7]. According to our naturalness philosophy non-minimal couplings should be radiatively generated and are thus an automatic feature in the very early universe. Accounting for RG running of the 2HDM self-couplings, i.e. β_{λ_1} and β_{λ_2}, this would spoil the picture since either coupling would make the other one large in order to satisfy Higgs phenomenology. Hence, we consider PQI and PQTHI for which we implement a hierarchy of non-minimal couplings, i.e. $\xi_S \gg \xi_{1,2}$, in order to effectively decouple the PQ- from the 2HDM-sector. This makes PQTHI parametrically close to the PQI which results in the suppression of large self-coupling contributions from the 2HDM-sector at the Planck scale. Therefore, we require at the Planck scale $\xi_S \lesssim 1$ and thus $\lambda_{\text{PQI, PQTHI}} \lesssim 10^{-10}$. These small self-couplings can be generated quite naturally for PQI and PQTHI since their RGE's are effectively decoupled from the 2HDM-sector and thus hidden from low energy phenomenology. We discuss these intricacies in section 5 and explain in the following our naturalness philosophy regarding the portal couplings and which role they play for decoupling.

We consider for PQI and PQTHI case (I) but note for PQI the limit to case (II). This consideration can be understood by the decoupling of the 2HDM- from the PQ- sector by going from case (I) to (II). For PQTHI, however, the mixing between these two sectors is allowed to a certain extend. In fact, the mixing is sufficiently suppressed which refines case (I) by

$$\lambda_{12S} \ll \lambda_S \lesssim \lambda_{1S,2S} \ll \lambda_{1,2,34} \quad \text{with} \quad \lambda_{iS}^2/\lambda_S \ll \lambda_{1,2,34} \qquad \text{(I')}$$

and denotes a mild decoupling compared to case (II). Therefore, case (I') decouples the two sectors as well, which corresponds to an enhanced Poincaré symmetry, i.e.

$\mathcal{G}_P^{\text{2HDM}} \times \mathcal{G}_P^{\text{PQ}}$. This is due to the fact, that all 2HDM couplings are much greater than the portal couplings which accounts to a technically natural limit where radiative corrections are negligible to low energy physics.

Hence, we will start with the mixed PQ-2HDM directions before we proceed with the PQ-direction. As mentioned in section 4.3.1, we will keep the discussion on PQI as general as possible, i.e. use case (I), but mention the limiting case by going from (I) to (II).

Thus, we obtain the following scalar potential

$$\tilde{V}(\vartheta,\gamma) \simeq \frac{M_p^4}{8\xi_S^2(1+t_\vartheta^2)^2}\frac{t_\gamma^4\left(\lambda_1+\lambda_2 t_\vartheta^4+2\lambda_{34}t_\vartheta^2\right)+2t_\gamma^2\left(t_\vartheta^2+1\right)\left(\lambda_{1S}+\lambda_{2S}t_\vartheta^2\right)+\lambda_S\left(t_\vartheta^2+1\right)^2}{8\xi_S^2(1+t_\vartheta^2)^2}. \tag{4.148}$$

The Jacobian for the PQTHI is given by

$$\begin{aligned} J(\vartheta,\gamma_{\text{PQTHI}}) &= \begin{pmatrix} \frac{\partial\tilde{V}_{\text{quartic}}}{\partial\vartheta} & \frac{\partial\tilde{V}_{\text{quartic}}}{\partial\gamma}\end{pmatrix}^T \\ &= \begin{pmatrix} \frac{\left(t_\vartheta^3+t_\vartheta\right)\left(\lambda_{1S}+\lambda_{2S}t_\vartheta^2\right)\left(-\lambda_1\lambda_{2S}+\lambda_{1S}\lambda_{34}+t_\vartheta^2(\lambda_{1S}\lambda_2-\lambda_{2S}\lambda_{34})\right)}{2\xi_S^2\left(\lambda_1+\lambda_2 t_\vartheta^4+2\lambda_{34}t_\vartheta^2\right)^2} \\ 0\end{pmatrix}, \end{aligned} \tag{4.149}$$

where we used $\gamma_{\text{PQTHI}}(\vartheta)$ for the PQ-2HDM direction which is given by

$$\gamma_{\text{PQTHI}}(\vartheta) = \arctan\left(\sqrt{\frac{\left(t_\vartheta^2+1\right)\left(-\lambda_{1S}-\lambda_{2S}t_\vartheta^2\right)}{\lambda_1+\lambda_2 t_\vartheta^4+2\lambda_{34}t_\vartheta^2}}\right). \tag{4.150}$$

The extrema for ϑ are thus obtained via $J_1(\vartheta,\gamma_{\text{PQTHI}}) \overset{!}{=} 0$

$$\vartheta_{\text{PQTHI}} = \begin{cases} \vartheta_{sh_1} = 0 \\ \vartheta_{sh_2} = \dfrac{\pi}{2} \\ \vartheta_{sh_{12}} = \arctan\left(\sqrt{\dfrac{\lambda_1\lambda_{2S}-\lambda_{1S}\lambda_{34}}{\lambda_{1S}\lambda_2-\lambda_{2S}\lambda_{34}}}\right)\end{cases}, \tag{4.151}$$

which corresponds to the following γ_{PQTHI}-values

$$\gamma_{\text{PQTHI}} = \begin{cases} \gamma_{sh_1} = \arctan\left(\sqrt{-\frac{\lambda_{1S}}{\lambda_1}}\right) \\ \gamma_{sh_2} = \arctan\left(\sqrt{-\frac{\lambda_{2S}}{\lambda_2}}\right) \\ \gamma_{sh_{12}} = \arctan\left(\sqrt{-\frac{\lambda_{1S}(\lambda_2-\lambda_{34})+\lambda_{2s}(\lambda_1-\lambda_{34})}{\lambda_1\lambda_2-\lambda_{34}^2}}\right) \end{cases} \tag{4.152}$$

for the three possible field directions, i.e. sh_1, sh_2 and sh_{12}. We can now determine the inflationary vacuum energies in the PQ-2HDM direction which need to be positive in order to avoid tachyonic vacuum states

$$V_0^{\text{PQTHI}} \geq 0 \quad \Leftrightarrow \quad \frac{1}{8\xi_S^2} \begin{cases} \lambda_S - \frac{\lambda_{1S}^2}{\lambda_1} \geq 0 \\ \lambda_S - \frac{\lambda_{2S}^2}{\lambda_2} \geq 0 \\ \lambda_S - \frac{\lambda_1\lambda_{2S}^2+\lambda_{1S}^2\lambda_2-2\lambda_{1S}\lambda_{2S}\lambda_{34}}{\lambda_1\lambda_2-\lambda_{34}^2} \geq 0 \end{cases} . \tag{4.153}$$

In the following we give the minimum conditions for the PQ-2HDM direction, i.e. for $sh_{1,2,12}$, in order to determine whether the extrema correspond to inflationary valleys while other directions correspond to inflationary ridges. As in section 4.3.1, the minima conditions are determined via the hessian and obey the conditions given by eq. (4.110) for the PQ-2HDM direction, i.e. $sh_{1,2,12}$.

PQTHI-(sh_1):
$\kappa_{1s} \equiv \lambda_{1S} \leq 0\,,$
$\kappa_{s1} \equiv \lambda_{2S}\lambda_1 - \lambda_{1S}\lambda_{34} \geq 0\,.$

PQTHI-(sh_2):
$\kappa_{2s} \equiv \lambda_{2S} \leq 0\,,$
$\kappa_{s2} \equiv \lambda_{1S}\lambda_2 - \lambda_{2S}\lambda_{34} \geq 0\,.$

PQTHI-(sh_{12}):
$\kappa_{s1}\kappa_{s2}\left(\kappa_{s1}+\kappa_{s2}\right) \leq 0\,,$
$\left(\kappa_{s1}+\kappa_{s2}\right)\left(\lambda_{1S}\kappa_{s2}+\lambda_{2S}\kappa_{s1}\right) \leq 0\,.$

Most importantly, the inflationary conditions are given by the minimum conditions

which are supplemented by the maximum conditions of other field directions in order to classify inflationary valleys and ridges accordingly. Similar to our discussion for 2HDM field space directions of section 4.3.1, the PQTHI-sh_{12} direction already contains this feature automatically since PQTHI-sh_{12} is a mixture of all three fields. However, the conditions of the PQTHI-sh_{12} direction need some refining. The first of the two conditions state

$$\kappa_{s1} \leq 0 \quad , \quad \kappa_{s2} \leq 0 \, . \tag{4.154}$$

This leads to the second condition to become

$$\kappa_{1s} \equiv \lambda_{1S} > 0 \quad , \quad \kappa_{2s} \equiv \lambda_{2S} > 0 \, . \tag{4.155}$$

We list the complete set of inflationary conditions for the 2HDM-h_{12} direction in Table 4.2.

Considering that PQTHI is composed of two or three field directions, i.e. $sh_{1,2,12}$, we need to examine whether orthogonal field directions contribute to inflation. Therefore, we provide the field space metric in these three inflationary directions

$$\mathcal{G}_{ij}^{sh_i} \simeq \frac{b_i}{\Omega_{sh_i}^2} \begin{pmatrix} 1 & 0 & 0 \\ 0 & 1 & 0 \\ 0 & 0 & \frac{\Omega_{sh_i}^2 + 6\xi_S^2 \frac{\phi^2}{M_P^2}}{\Omega_{sh_i}^2} \end{pmatrix} , \tag{4.156}$$

where b_i are the mixing parameters determined via $\sin^2 \gamma_{sh_i} = 1 - b_i^{-1}$,

$$b_1 \equiv 1 + \left| \frac{\lambda_{1S}}{\lambda_1} \right| , \tag{4.157}$$

$$b_2 \equiv 1 + \left| \frac{\lambda_{2S}}{\lambda_2} \right| , \tag{4.158}$$

$$b_{12} \equiv 1 + \left| \frac{\lambda_{2S}(\lambda_1 - \lambda_{34}) + \lambda_{1S}(\lambda_2 - \lambda_{34})}{\lambda_1 \lambda_2 - \lambda_{34}^2} \right| \tag{4.159}$$

and $\Omega_{sh_i}^2$ are the frame functions given by

$$\Omega_{sh_i}^2 = b_i + 6\xi_S \frac{s^2}{M_P^2} \, . \tag{4.160}$$

We can see from the field space metric and its corresponding frame functions that the mixing parameter determine whether inflation occurs in the PQ-2HDM ($b_i \neq 1$) or in the PQ direction ($b_i = 1$) resembling case (II). In order to examine whether the orthogonal field space directions contribute to PQTHI, we compute the instantaneous masses

$$m^2_{\phi_i}\Big|_{\substack{\vartheta=\vartheta_{sh_i}\\ \gamma=\gamma_{sh_i}}} \simeq \begin{cases} -\frac{\lambda_{1S}}{\xi_S} \ , \ \frac{\kappa_{s2}}{2\lambda_2\xi_S} \ , \ -\frac{\kappa_{s2}\lambda_1}{\xi_S\left(\lambda_1\lambda_2-\lambda_{34}^2\right)} & (h_1) \\ -\frac{\lambda_{2S}}{\xi_S} \ , \ \frac{\kappa_{s1}}{2\lambda_1\xi_S} \ , \ -\frac{\kappa_{s1}\lambda_2}{\xi_S\left(\lambda_1\lambda_2-\lambda_{34}^2\right)} & (h_2) \\ \frac{\lambda_{1S}^2}{\lambda_1\xi_S(1+6\xi_S)} \ , \ \frac{\lambda_{2S}^2}{\lambda_2\xi_S(1+6\xi_S)} \ , \ \frac{\kappa_{s1}\lambda_{2S}+\kappa_{s2}\lambda_{1S}}{\xi_S(6\xi_S+1)\left(\lambda_1\lambda_2-\lambda_{34}^2\right)} & (s) \end{cases} , \tag{4.161}$$

where the masses are given for sh_1, sh_2 and sh_{12} directions from left to right. These results are now related to the Hubble rate $\mathcal{H}^2 \approx \tilde{V}/3M_p^2$

$$\frac{m_s^2}{\mathcal{H}^2}\Big|_{\substack{\vartheta=\vartheta_{sh_i}\\ \gamma=\gamma_{sh_i}}} \simeq \frac{24\xi_S}{1+6\xi_S}\frac{\delta\lambda_S}{\tilde{\lambda}} \lesssim 1 \, , \tag{4.162}$$

$$\frac{m_{h_i}^2}{\mathcal{H}^2}\Big|_{\substack{\vartheta=\vartheta_{sh_i}\\ \gamma=\gamma_{sh_i}}} \simeq \frac{12\xi_S}{\tilde{\lambda}} \begin{cases} 2\left|\lambda_{iS}\right| \gtrsim 1 & (sh_i) \\ \left(\lambda_{iS}+(b_j-1)\lambda_{34}\right) \gtrsim 1 & (sh_j) \\ \frac{2\lambda_1\lambda_2(\lambda_{iS}+(b_j-1)\lambda_{34})}{\lambda_1\lambda_2-\lambda_{34}^2} \gtrsim 1 & (sh_{12}) \end{cases} , \tag{4.163}$$

with $\xi_S \sim 2\times 10^4\sqrt{\tilde{\lambda}}$ and $\tilde{\lambda} = \lambda_S - \delta\lambda_S \gtrsim 0$. This shows that all masses of orthogonal directions are stabilized while the inflaton remains dynamical at the inflationary valley.

For the PQ-direction, i.e. $\gamma_{\rm PQ} = 0$, we acquire the following minimum condition given by the single component hessian

$$\frac{\xi_S\left(\lambda_{1S}+\lambda_{2S}t_\vartheta^2-2\lambda_{12S}t_\vartheta\right)-\lambda_S\left(\xi_1+\xi_2 t_\vartheta^2\right)}{2\xi_S^3\left(1+t_\vartheta^2\right)} \geq 0 \, . \tag{4.164}$$

In order to obtain minimum conditions w.r.t. all field directions, we simply apply the ϑ-extrema of the 2HDM- and PQ-2HDM directions, i.e. $\vartheta_{\rm THI}$ and $\vartheta_{\rm PQTHI}$. This

amounts to a total of four minimum condition for the PQ-direction:

$$
\begin{aligned}
&\textbf{PQI:}\\
&\kappa_{1s} \equiv \lambda_{1S} \geq 0\,,\\
&\kappa_{2s} \equiv \lambda_{2S} \geq 0\,,\\
&(\kappa_{s1} + \kappa_{s2})\,(\lambda_{1S}\kappa_{s2} + \lambda_{2S}\kappa_{s1}) \geq 0\,,\\
&(\kappa_{s1} + \kappa_{s2})\,(\lambda_1 + \lambda_2 - 2\lambda_{34}) \geq 0\,,
\end{aligned}
$$

where the first two correspond to the 2HDM-$h_{1,2}$ directions and the last two conditions correspond to the PQTHI-sh_{12} direction and to the 2HDM-h_{12} direction, respectively. By considering the last two conditions, we cannot make a conclusive statement whether κ_{s1} and κ_{s2} are positive or negative. This can only be determined if either $\lambda_{1,2} \geq \lambda_{34}$ or $\lambda_{1,2} \leq \lambda_{34}$ is given. Thus, the last two conditions can be neglected. Moreover, we note that these conditions vanish by taking the limit to case (II). The absence of the portal couplings and the non-minimal coupling hierarchy, i.e. $\xi_S \gg \xi_{1,2}$, are mainly responsible for an inflationary valley to exist in the PQ-direction. For completeness we refer to the above minimum conditions as the inflationary conditions and add case (II) as a another condition in our model.

Since we are considering four inflationary trajectories, we need an adequate description of the inflaton field ϕ which we identify as the PQ-scalar s. Therefore, we canonically normalize the inflaton field s with the following field redefinitions for inflation in the s-, sh_1-, sh_2- and sh_{12} direction, respectively

$$\Omega^2 \frac{d\chi_s}{ds} = \sqrt{\Omega^2 + 6\xi_S^2 \frac{s^2}{M_p^2}}\,, \tag{4.165}$$

$$\Omega^2 \frac{\chi_{sh_i}}{ds} = \sqrt{b_i \left(\Omega_i^2 + 6\xi_S^2 \frac{s^2}{M_p^2}\right)}\,. \tag{4.166}$$

By integration we obtain the canonically normalized fields $\chi_{s,sh_1,sh_2,sh_{12}}$

$$\frac{\sqrt{\xi_S}}{M_p}\chi_s = \sqrt{1+6\xi_S}\,\mathrm{arcsinh}\left(\sqrt{1+6\xi_S}\,u(s)\right) - \sqrt{6\xi_S}\,\mathrm{arctanh}\left(\frac{\sqrt{6\xi_S}\,u(s)}{\sqrt{1+(1+6\xi_S)\,u^2(s)}}\right)\,, \tag{4.167}$$

$$\frac{1}{M_p}\sqrt{\frac{\xi_S}{b_i}}\chi_{sh_i} = \sqrt{1+6\xi_S}\,\mathrm{arcsinh}\left(\sqrt{\frac{1+6\xi_S}{b_i}}u(s)\right) - \sqrt{6\xi_S}\,\mathrm{arctanh}\left(\frac{\sqrt{6\xi_S}\,u(s)}{\sqrt{b_i+(1+6\xi_S)\,u^2(s)}}\right) \tag{4.168}$$

inflation along	Potential (4.148) minimized at	Inflationary conditions	Einstein frame slow roll potential
$s\,h_1$	$\gamma_0 = \arctan\left(\sqrt{-\frac{\lambda_{1S}}{\lambda_1}}\right)$ $\vartheta_0 = 0$	$\kappa_{s1} \geq 0\,,\ \kappa_{s2} \leq 0$ $\kappa_{1s} \leq 0\,,\ \kappa_{2s} \geq 0$	$\frac{\lambda_{sh_1}}{8} s^4 \left(1 + \xi_S \frac{s^2}{M_P^2}\right)^{-2}$
$s\,h_2$	$\gamma_0 = \arctan\left(\sqrt{-\frac{\lambda_{2S}}{\lambda_2}}\right)$ $\vartheta_0 = \frac{\pi}{2}$	$\kappa_{s1} \leq 0\,,\ \kappa_{s2} \geq 0$ $\kappa_{1s} \geq 0\,,\ \kappa_{2s} \leq 0$	$\frac{\lambda_{sh_2}}{8} s^4 \left(1 + \xi_S \frac{s^2}{M_P^2}\right)^{-2}$
$s\,h_{12}$	$\gamma_0 = \arctan\left(\sqrt{-\frac{\kappa_{s2}+\kappa_{s2}}{\lambda_1\lambda_2-\lambda_{34}^2}}\right)$ $\vartheta_0 = \arctan\left(\sqrt{\frac{\kappa_{s1}}{\kappa_{s2}}}\right)$	$\kappa_{s1} \leq 0\,,\ \kappa_{s2} \leq 0$ $\kappa_{1s} \leq 0\,,\ \kappa_{2s} \leq 0$	$\frac{\lambda_{sh_{12}}}{8} s^4 \left(1 + \xi_2 \frac{s^2}{M_P^2}\right)^{-2}$
s	$\gamma_0 = 0$ $\vartheta_0 = \{0, \frac{\pi}{2}\}$	$\kappa_{1s} \geq 0\,,\ \kappa_{2s} \geq 0$ $\vee\ \lambda_{1S,2S} \ll \lambda_S$	$\frac{\lambda_S}{8} s^4 \left(1 + \xi_S \frac{s^2}{M_P^2}\right)^{-2}$

Table 4.2.: Conditions and characteristics for PQI and PQTHI, i.e. s- and $sh_{1,2,12}$-inflation, with $\xi_S \gg \xi_{1,2}$.

with $u(s) \equiv \sqrt{\xi_S}s/M_p$. By taking the inverse of the canonically normalized fields, we can write the inflationary scalar potential in Einstein frame for PQI and PQTHI in the usual form:

$$V_{s,sh_i}(\chi_i) = \frac{\tilde{\lambda}}{8} \frac{s^4(\chi_i)}{\left(1 + \xi_S \frac{s^2(\chi_i)}{M_p^2}\right)^2}\,, \tag{4.169}$$

where $\tilde{\lambda}$ is given by the following inflationary directions:

$$\tilde{\lambda} = \begin{cases} \lambda_S & \text{(PQI)} \\ \lambda_S - \dfrac{\lambda_{iS}^2}{\lambda_i} & \text{(PQTHI-}sh_i\text{)} \\ \lambda_S - \dfrac{\lambda_1\lambda_{2S}^2 + \lambda_{1S}^2\lambda_2 - 2\lambda_{1S}\lambda_{2S}\lambda_{34}}{\lambda_1\lambda_2 - \lambda_{34}^2} & \text{(PQTHI-}sh_{12}\text{)} \end{cases}. \tag{4.170}$$

In Table 4.2 we summarize the extrema, inflationary conditions and Einstein frame slow-roll potential for PQI and PQTHI. We show the two inflationary scenarios in figure 4.5 which represents PQI (left) and PQTHI (right). As discussed in the previous section (see sec. 4.3.1), the inflationary predictions A_s, n_s and r are constrained by PLANCK/BICEP data [61, 60, 72]. According to our naturalness philosophy, we demand the non-minimal coupling to be constrained by $\xi_S \lesssim 1$ which is shown in figure 4.6. Thus, A_s sets the following limits to ξ_S and $\tilde{\lambda}$

$$8.5 \times 10^{-3} \lesssim \xi \lesssim 1 \ \text{ implying } \ 9 \times 10^{-10} \gtrsim \tilde{\lambda} \gtrsim 4.5 \times 10^{-13}\,. \tag{4.171}$$

In order to determine n_s and r we require the number of e-folds from some time t_* where

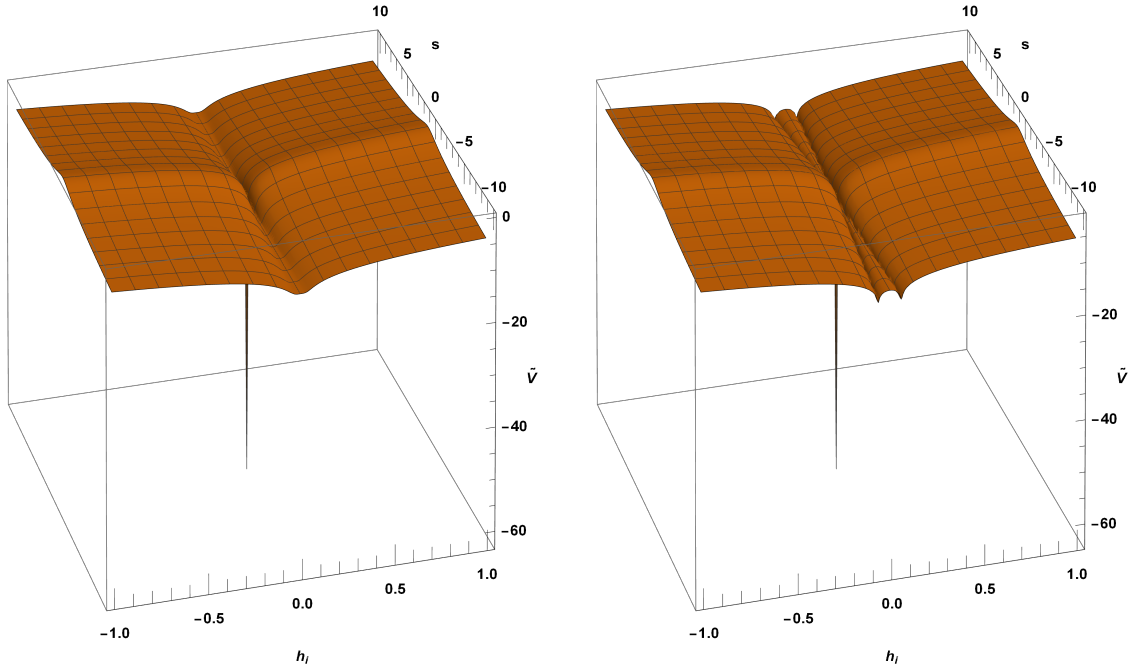

Figure 4.5.: Decadic log Einstein frame scalar potential depicting PQI (left) and PQTHI (right) in units of M_p as a function of the PQ-scalar s and the two Higgs fields h_1 and h_2.

the scale $k_* = a_* \mathcal{H}_*$ exited the horizon to the time where inflation ended denoted by $k_{\text{end}} = a_{\text{end}} \mathcal{H}_{\text{end}}$. This is defined by

$$N_* \equiv \log\left(\frac{a_{\text{end}}}{a_{k_*}}\right) = \int_{\chi_I}^{\chi_{\text{end}}} \frac{d\chi}{\sqrt{2\epsilon}}\,, \tag{4.172}$$

which can be solved exactly by the Klein-Gordon equation

$$\frac{d^2\chi}{dN^2} + 3\frac{d\chi}{dN} - \frac{1}{2M_p^2}\left(\frac{d\chi}{dN}\right)^3 + \sqrt{2\epsilon}\left(3M_p - \frac{1}{2M_p}\left(\frac{d\chi}{dN}\right)^2\right). \tag{4.173}$$

During inflation, the largest scales exit the horizon at k_* which re-enter the horizon at a later time, i.e. at matter or radiation domination, cf. Ref. [79]. In fact, the largest scales are the last to re-enter the horizon which corresponds to scales of our current horizon, i.e. $k_0 = a_0 \mathcal{H}_0$. The required amount of e-folds for solving the horizon problem is therefore related to the complete expansion history of the universe and is given by [80]

$$\frac{k_*}{k_0} \equiv \frac{k_*}{a_0 \mathcal{H}_0} = \frac{a_{k_*} \mathcal{H}_{k_*}}{a_0 \mathcal{H}_0} = \frac{a_{k_*}}{a_{\text{end}}} \frac{a_{\text{end}}}{a_{\text{eq}}} \frac{\mathcal{H}_{k_*}}{\mathcal{H}_{\text{eq}}} \frac{a_{\text{eq}} \mathcal{H}_{\text{eq}}}{a_0 \mathcal{H}_0}\,, \tag{4.174}$$

where the subscripts "eq" and "0" denote matter-radiation equality and the present time, respectively. With the ratio $a_{k_*}/a_{\text{end}} = \exp(-N_*)$, we identify the number of e-folds during

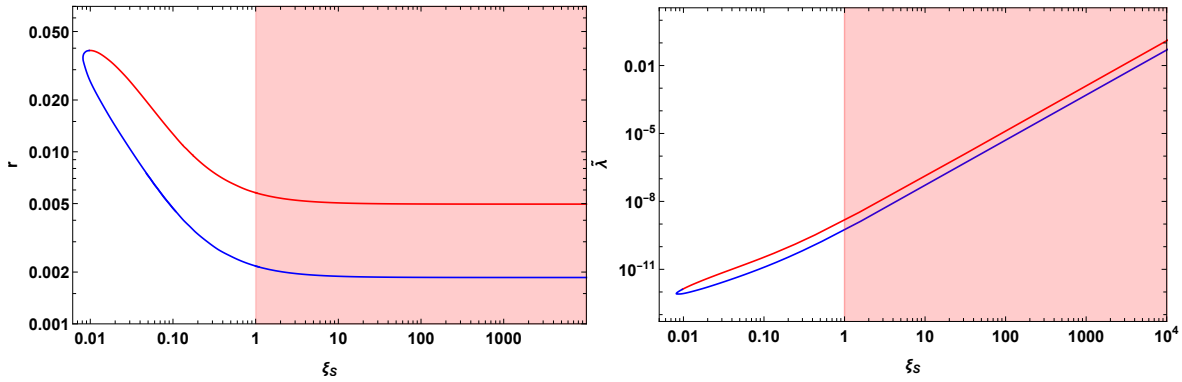

Figure 4.6.: Shown are the 95% C.L. contours of r vs. ξ_S (left) and the effective quartic coupling for inflation $\tilde{\lambda}$ vs. ξ_S at the pivot scale $k_* = 0.002$ Mpc^{-1}. The red shaded region given by $\xi_S > 1$ indicates the unnatural regime according to our naturalness philosophy. The red and blue curves indicate constraints given by the redder spectrum and the bluer spectrum of n_s [61, 72].

inflation N_* by reformulating eq. (4.174) to find [80]

$$N_* = -\log\frac{k_*}{a_0\mathcal{H}_0} + \log\frac{a_{\rm end}}{a_{\rm eq}} + \log\frac{\mathcal{H}_{k_*}}{\mathcal{H}_{\rm eq}} + \log\frac{a_{\rm eq}\mathcal{H}_{\rm eq}}{a_0\mathcal{H}_0}\,. \tag{4.175}$$

By using the slow-roll approximation for the Hubble rate during inflation, i.e. $\mathcal{H}_{k_*} \simeq \sqrt{V_{k_*}/3\,M_p^2}$, we obtain [80]

$$N_* = -\log\frac{k_*}{a_0\mathcal{H}_0} + \log\frac{a_{\rm end}}{a_{\rm eq}} + \log\sqrt{\frac{V_{k_*}}{3\,M_p^2}}\frac{1}{\mathcal{H}_{\rm eq}} + \log\frac{a_{\rm eq}\mathcal{H}_{\rm eq}}{a_0\mathcal{H}_0}\,. \tag{4.176}$$

In 2hdSMASH we adopt the simplicity of the expansion history of the universe from SMASH [7] (see also figure 2.1). Based on the smallness of the non-minimal couplings, they can be neglected by the end of inflation. Correspondingly, preheating and reheating occur in an approximate quartic potential, where the universe is radiation-dominated. This has been worked out for SMASH in detail by elaborate lattice simulations where it was shown that after a few oscillations the scalar potential is approximately quartic [7, 45].

By using the relation

$$\log\frac{a_{\rm end}}{a_{\rm eq}} = \log\frac{a_{\rm end}}{a_0} + \log\frac{a_0}{a_{\rm eq}}\,, \tag{4.177}$$

we can simplify the number of e-folds as follows

$$N_* = -\log\frac{k_*}{a_0\mathcal{H}_0} + \log\frac{a_{\rm end}}{a_0} + \log\sqrt{\frac{V_{k_*}}{3\,M_p^2}} + \log\frac{1}{\mathcal{H}_0}\,. \tag{4.178}$$

The ratio a_{end}/a_0 relates the scale of the end of inflation with the scale of the present time which is given by [81]

$$\frac{a_{\text{end}}}{a_0} = \frac{a_{\text{end}}}{a_{\text{RD}}}\frac{a_{\text{RD}}}{a_{\text{end}}} = \left(\frac{g_{*s,\text{RD}}}{g_{*s,0}}\right)^{-1/3}\left(\frac{g_{*\rho,\text{RD}}}{g_{*\rho,0}}\right)^{1/4}\left(\frac{\rho_{0,\text{RD}}}{\rho_{\text{end}}}\right)^{1/4}\left(\frac{a_{\text{end}}}{a_{\text{RD}}}\right)^{(1-3w)}, \tag{4.179}$$

where the subscript "RD" denotes radiation domination, $g_{*,\rho}$ and $g_{*,s}$ denote the number of relativistic degrees of freedom for the energy density and entropy, respectively. Since the universe is radiation-dominated by the end of inflation, the energy of state parameter $w = p/\rho$ approaches $1/3$ instantaneously in the epoch of preheating for which we can approximate eq. (4.179)

$$\frac{a_{\text{end}}}{a_0} \simeq \left(\frac{g_{*s}(T_R)}{g_{*s}(T_0)}\right)^{-1/3}\left(\frac{g_{*\rho}(T_R)}{g_{*\rho}(T_0)}\right)^{1/4}\left(\frac{\rho_{0,\text{RD}}}{V_{\text{end}}}\right)^{1/4}, \tag{4.180}$$

where the subscript "R" denotes reheating. The corresponding number of relativistic degrees of freedom are given by [82]

$$g_{*s}(T_0) \simeq 3.91\,,\; g_{*\rho}(T_0) \simeq 2\,,\; g_{*s}(T_R) \simeq g_{*\rho}(T_R) \simeq 124.5 \tag{4.181}$$

and the present time energy density of radiation $\rho_{0,\text{RD}}$ is given by [82]

$$\rho_{0,\text{RD}} = \frac{\pi^2 T_0^4}{15} \simeq 2.02 \times 10^{-15}\,\text{eV}^4\,. \tag{4.182}$$

Furthermore, we give the updated values of the present time Hubble parameter $\mathcal{H}_0$ and Hubble scale $k_0 = a_0\mathcal{H}_0$ by Ref. [37]

$$\begin{aligned} &\mathcal{H}_0 \simeq 5.9 \times 10^{-61}\, h\, M_p \qquad \text{with} \quad h \simeq 0.674\,, \\ &a_0\mathcal{H}_0 \simeq 22.47 \times 10^{-5}\,\text{Mpc}^{-1}\,, \end{aligned} \tag{4.183}$$

where h is the Hubble constant. The number of e-folds can now be approximated and reads [80, 83]

$$\begin{aligned} N_* &\simeq 61.25 - \log\frac{k_*}{a_0\mathcal{H}_0} - \log\frac{10^{16}\,\text{GeV}}{V_{k_*}^{1/4}} + \log\frac{V_{k_*}^{1/4}}{V_{\text{end}}^{1/4}} \\ &\simeq 59 - \log\left(\frac{k_*}{10^{-3}\,\text{Mpc}^{-1}}\right) - \log\left(\frac{10^{-4}\,\text{Mpc}^{-1}}{a_0\mathcal{H}_0}\right) - \log\frac{10^{16}\,\text{GeV}}{V_{k_*}^{1/4}} + \log\frac{V_{k_*}^{1/4}}{V_{\text{end}}^{1/4}}\,, \end{aligned} \tag{4.184}$$

where we included the maximum horizon of the observable universe given by the upper bound $V_{k_*}^{1/4} \lesssim 10^{16}$ GeV, cf. [6, 7, 82]. The scale of horizon exit is $k_* = 0.002\ \text{Mpc}^{-1}$ which corresponds to the largest observable scales in the CMB measured by Planck/BICEP [61, 72].

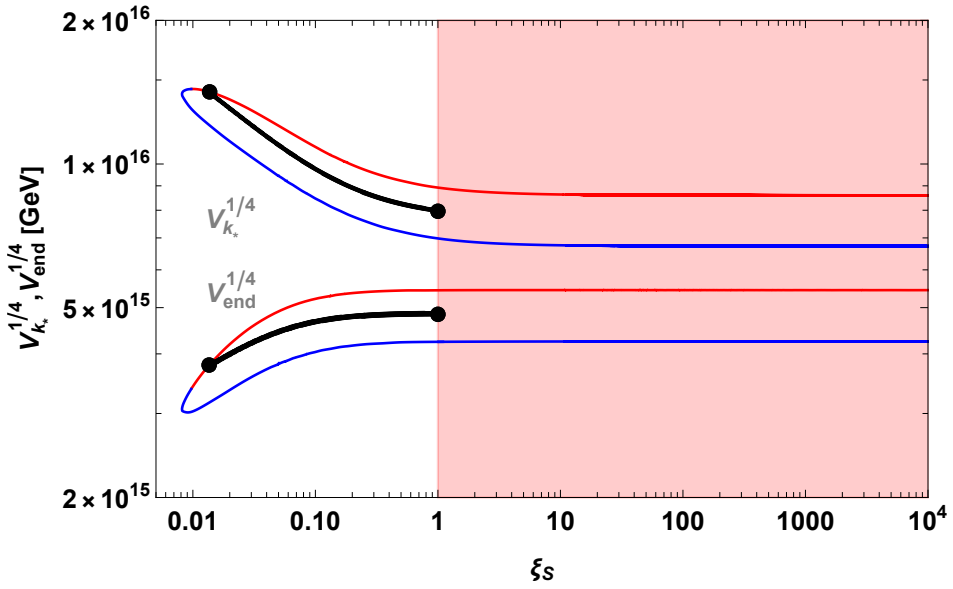

Figure 4.7.: Shown are the 95% C.L. contours of $V_{k_*}^{1/4}$ and $V_{\rm end}^{1/4}$ vs. ξ_S at the pivot scale $k_* = 0.002\,\text{Mpc}^{-1}$. The red shaded region given by $\xi_S > 1$ indicates the unnatural regime according to our naturalness philosophy. The red and blue curves indicate constraints given by the redder spectrum and the bluer spectrum of n_s [61, 72]. The black solid curves take the 2hdSMASH expansion history of our universe into account where inflation is followed by immediate radiation-domination. Correspondingly, the black dots specify the range of validity for a consistent expansion history.

With the constants of eq. (4.183) we obtain

$$N_* \simeq 59.06 - \log\frac{10^{16}\,\text{GeV}}{V_{k_*}^{1/4}} + \log\frac{V_{k_*}^{1/4}}{V_{\rm end}^{1/4}}\,, \tag{4.185}$$

which illustrates that only the energy scales $V_{k_*}^{1/4}$ and $V_{\rm end}^{1/4}$ are relevant. By utilizing the the Planck constraints to fit the quartic coupling $\tilde{\lambda}$ to A_s we can determine N_* of eq. (4.185) which must match the number of e-folds obtained from solving the inflaton's eom from eq. (4.173). Correspondingly, the energy scales $V_{k_*}^{1/4}$ and $V_{\rm end}^{1/4}$ are determined. In figure 4.7 we show this correspondence of $V_{k_*}^{1/4}$ and $V_{\rm end}^{1/4}$ as a function of the non-minimal coupling ξ_S where the solid black curve manifests this result. Typical values of $V_{k_*}^{1/4}$ and $V_{\rm end}^{1/4}$ are in the range of

$$8\times10^{15}\,\text{GeV} \lesssim V_{k_*}^{1/4} \lesssim 1.4\times10^{16}\,\text{GeV}\,, \tag{4.186}$$

$$3.8\times10^{15}\,\text{GeV} \lesssim V_{\rm end}^{1/4} \lesssim 4.8\times10^{15}\,\text{GeV} \tag{4.187}$$

for

$$1.35 \times 10^{-2} \lesssim \xi_S \lesssim 1 \quad \text{implying} \quad 9 \times 10^{-10} \gtrsim \tilde{\lambda} \gtrsim 2.2 \times 10^{-12}\,. \tag{4.188}$$

These ranges are indicated by the black dots in figure 4.7 for which we can compute the corresponding range of the number of e-folds N_* from eq. (4.185)

$$59.3 \lesssim N_* \lesssim 60.7\,. \tag{4.189}$$

We show our result in figure 4.8 where the thick red curve is obtained by eq. (4.185) which accounts for the numerically determined expansion history[9]. The black solid lines have been acquired by solving the Klein-Gordon equation (4.173) without taking the expansion history of our universe into account. The red curve is close to $N = 60$ as indicated in eq. (4.189).

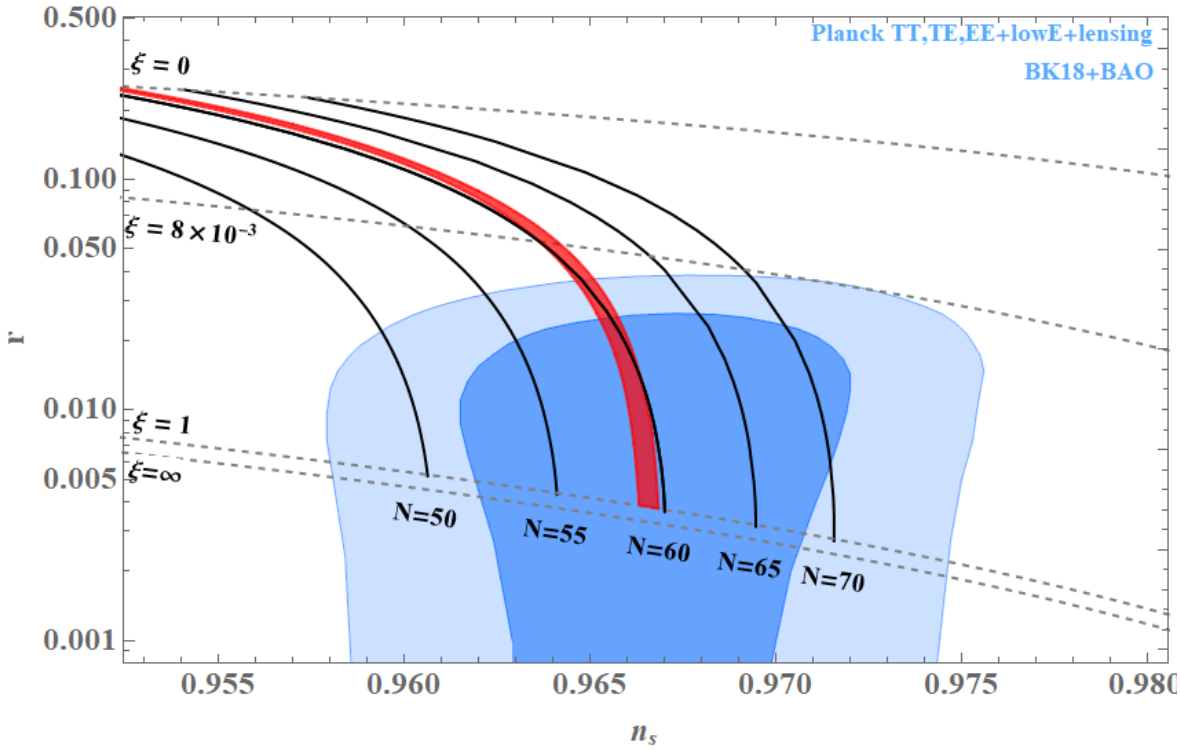

Figure 4.8.: Shown are the 95% and 68% C.L. contours of r vs. n_s constrained by PLANCK/BICEP [61, 60, 72] (shaded blue), the isocontours of constant ξ (gray dashed), the isocontours of constant N (solid black) and the inflationary predictions by 2hdSMASH for PQI/PQTHI taking into account the numerically determined expansion history of the universe (thick red).

[9] We utilized a numerical code from Ref. [7] to obtain the red curve shown in figure 4.8.

Correspondingly, we provide the range of n_s and r for PQI and PQTHI in 2hdSMASH

$$\xi_S \simeq 1 \Rightarrow \begin{cases} 0.9664 \lesssim n_s \lesssim 0.9668 \\ 0.0037 \gtrsim r \gtrsim 0.0036 \end{cases} \quad , \quad \xi_S \simeq 1.35 \times 10^{-2} \Rightarrow \begin{cases} 0.9646 \lesssim n_s \lesssim 0.9651 \\ 0.037 \gtrsim r \gtrsim 0.036 \end{cases} \quad . \tag{4.190}$$

5. Connecting inflation with TeV Scale Particle Physics

This section is dedicated to make the connection between inflationary constraints and low energy constraints. For this reason, we consider the one-loop RGEs (see Appendix E) which run the 2hdSMASH parameters from low- to high-scale and meet the constraints at their respective scales.

As discussed in section 4.3.2, we require amongst others $\lambda_S(M_p) \lesssim 10^{-10}$ for successful inflation. Moreover, there are two inflationary scenarios realized in 2hdSMASH, namely PQI and PQTHI, which differ by sign and size of the portal couplings. These constraints must be met at the Planck scale. In order to account for thermal leptogenesis and BAU, we obtain constraints on the neutrino Yukawa couplings Y_ν and Y_N which influence the RG evolution of the portal couplings. As we will see, this effect will only consider PQI while PQTHI scenarios will face the challenge to run the portal couplings stable all the way up to the Planck scale. According to our naturalness philosophy, we further demand that the portal couplings do not impact Higgs phenomenology through large radiative corrections. Hence, the portal couplings are very important in connecting inflation with particle phenomenology. Along these lines, we also need to attest for vacuum stability and perturbative unitarity. This is done by obeying the BfB and perturbative unitarity conditions for all energy scales until the Planck scale, which ensures high-scale validity. By breaking perturbative unitarity, Landau poles emerge which lead to a breakdown of predictivity. If vacuum stability is not guaranteed, our universe would not correspond to the universe we know today. We will discuss these intricacies in the following sections of this chapter.

We structure the sections as follows: In section 5.1 we will discuss the stability requirements for λ_S by considering the RG running effects of the right handed neutrino Yukawa and portal couplings. In section 5.2 we discuss the constraints from thermal leptogenesis and BAU and their impact on RG running. In section 5.3 we will analyze the running of the portal couplings and give conditions which motivate PQI and PQTHI. Therefore, we give three benchmark points which underline our considerations and illustrate the interconnection of inflation and Higgs phenomenology. In section 5.4 we discuss vacuum-stability, perturbativity and high-scale validity by identifying the effective 2HDM model in our RG-analysis. Since all other couplings are fixed, i.e. portal couplings $\lambda_{1S,2S,12S}$, neutrino Yukawa couplings

$Y_{\nu,N}$ and PQ self-coupling λ_S, we consider the remaining 2HDM couplings $\lambda_{1,2}$ and λ_{34}. In particular we pay attention to the stability of λ_2 which tends to run negative. We will argue that λ_3 and λ_{34} can cure this instability while keeping λ_1 fixed. This is illustrated by representative benchmarks. In section 5.5 we accumulate all of the analysis and provide benchmark points which accommodate inflation, theoretical and experimental constraints while presenting interesting Higgs phenomenology relevant for HL-LHC and future colliders.

5.1. Stability analysis of λ_S

In this section we want to outline the stability condition on the running of λ_S for successful inflation. This in turn will lead to conditions on the Higgs portal couplings λ_{1S}, λ_{2S}, λ_{12S} and the right handed Yukawa couplings Y_N. We give to one-loop accuracy, the renormalization group evolution of $\lambda_S(\mu)$ (see Appendix E)

$$(4\pi)^2 \frac{d}{d\ln\mu}\lambda_S = \tag{5.1}$$
$$10\lambda_S^2 + 4\lambda_{1S}^2 + 4\lambda_{2S}^2 + 8\lambda_{12S}^2 - 2\mathrm{Tr}\left(Y_N^\dagger Y_N Y_N^\dagger Y_N\right) + 2\lambda_S \mathrm{Tr}\left(Y_N^\dagger Y_N\right).$$

As discussed in section 4.3.2, we require for successful inflation $\lambda_S(M_p) \lesssim 10^{-10}$ [7]. Such a small quartic coupling can in fact suffer from RG-running instability, i.e. large enhancements of λ_S at high energies, thus spoiling inflation. Therefore, we require $\lambda_S(m_s) \sim \lambda_S(M_p)$ for stability reasons. Imposing this requirement on eq. (5.1) leads to constraints on the squared Higgs portal couplings $\lambda_{1S,2S,12S}^2$ and on the trace of right handed neutrino Yukawas $\mathrm{Tr}\left(Y_N^\dagger Y_N Y_N^\dagger Y_N\right)$, as we will argue now.

As a first observation, we can neglect the terms proportional to λ_S on the right hand side of eq. (5.1). This is per our request for negligible running of λ_S. Furthermore, the RG running effects of the portal couplings and the right handed neutrino Yukawas are taken to be negligible due to RG stability. With these reasonable assumptions, we can integrate eq. (5.1) and find

$$\frac{\lambda_S(\mu)}{\lambda_S(m_s)} \approx \tag{5.2}$$
$$1 + \frac{1}{4\pi^2\lambda_S(m_s)}\left[\lambda_{1S}^2(m_s) + \lambda_{2S}^2(m_s) + 2\lambda_{12S}^2(m_s) - \frac{1}{2}\mathrm{Tr}\left(Y_N^\dagger Y_N Y_N^\dagger Y_N\right)_{m_s}\right]\log\frac{\mu}{m_s}.$$

From eq. (5.2) we can see that the portal couplings enhance, while the right handed neutrino Yukawas diminish λ_S. This endangers vacuum stability (cf. Ref. [7]) and can be avoided in one of two ways. Either the portal coupling contribution is greater than the Yukawa contribution or both contributions are negligible compared to λ_S. By choosing the latter, we avoid

tremendous fine tuning at the matching scale m_s which leads to the following constraints

$$\left.\begin{array}{l} |\lambda_{1S}(m_s)| \\ |\lambda_{2S}(m_s)| \\ |\lambda_{12S}(m_s)| \\ \sqrt{\mathrm{Tr}\left(Y_N^\dagger Y_N Y_N^\dagger Y_N\right)_{|m_s}} \end{array}\right\} \ll \sqrt{\lambda_S(m_s)} \approx 10^{-5}\,, \tag{5.3}$$

implying $\lambda_S(M_P) \approx \lambda_S(m_s) \approx 10^{-10}$ as expected.

5.2. RG-analysis with BAU and thermal leptogenesis

In the previous section we derived an upper bound on Tr $\left(Y_N^\dagger Y_N Y_N^\dagger Y_N\right)$ at the scale m_s (see eq. (5.3)). This upper bound can be further specified for higher energy domains, e.g. $\mu \simeq 30M_p$, in order to investigate the minimum condition of λ_S [7]. Therefore, by considering $\mu \simeq 30M_p$ we obtain

$$Y_N \lesssim \left(\frac{8\pi^2\lambda_S}{163\log\left(\frac{30M_{\mathrm{P}}}{m_s}\right)}\right)^{1/4}\,, \tag{5.4}$$

where $Y_{N,33} = Y_{N,22} = 3Y_{N,11}$ accommodates vanilla leptogenesis with hierarchical right-handed neutrinos. By considering the right-handed neutrino masses given by

$$M_{N,i} = \frac{Y_{N,i}v_S}{\sqrt{2}} \tag{5.5}$$

with $M_{N,3} = M_{N,2} = 3M_{N,1}$, we can convert the upper bound of eq. (5.4) to an upper bound on $M_{N,1}$:

$$M_{N,1} \lesssim \frac{\sqrt{2}}{v_S}\left(\frac{8\pi^2\lambda_S}{163\log\left(\frac{30M_{\mathrm{P}}}{m_s}\right)}\right)^{1/4}\,. \tag{5.6}$$

The CP-violating and out-of-equilibrium decay of the lightest right-handed neutrino $N_1 \to l\Phi_1$ produces BAU via thermal leptogenesis [25, 36, 7]. This is quantified by the CP-asymmetry ϵ_1 which is given by [84, 85, 86, 87]:

$$\epsilon_1 = \frac{\Gamma_D\left(N_1 \to l\Phi_1\right) - \Gamma_D\left(N_1 \to l^*\Phi_1^*\right)}{\Gamma_D\left(N_1 \to l\Phi_1\right) + \Gamma_D\left(N_1 \to l^*\Phi_1^*\right)} \simeq \frac{1}{8\pi}\frac{\sum_j \mathrm{Im}\left[\left(Y_\nu Y_\nu^\dagger\right)_{1j}^2\right]}{\left(Y_\nu Y_\nu^\dagger\right)_{11}}\, g\left(x_{1j}\right) \tag{5.7}$$

where $g_{1j}\left(x_{1j}\right)$ is given as

$$g_{1j}\left(x_{1j}\right) = \sqrt{x_{1j}}\left(\frac{2-x_{1j}}{x_{1j}-1} + (1+x_{1j})\log\left(\frac{1+x_{1j}}{x_{1j}}\right)\right) \quad \text{with} \quad x_{1j} = \frac{M_j^2}{M_1^2}\,. \tag{5.8}$$

For $x_{1j} > 1$ we can approximate the CP-asymmetry as follows [87]:

$$\epsilon_1 \simeq -\frac{3}{16\pi}\frac{\sum_j \mathrm{Im}\left[\left(Y_\nu Y_\nu^\dagger\right)^2_{1j}\right]}{\left(Y_\nu Y_\nu^\dagger\right)_{11}}\left(\frac{M_1}{M_j}\right) = -\frac{3M_1}{16\pi}\frac{\sum_j \mathrm{Im}\left[\left(Y_\nu m_\nu^\dagger Y_\nu^\dagger\right)^2_{1j}\right]}{\left(Y_\nu Y_\nu^\dagger\right)_{11}}\,, \tag{5.9}$$

where we used eq. (3.20) to substitute the light neutrino mass matrix m_ν. Based on the observed BAU we need to place an upper bound on ϵ_1. Therefore, we further simplify ϵ_1 by using the Casas-Ibarra parametrization for the light neutrino Yukawa coupling Y_ν:

$$Y_\nu = \frac{\sqrt{2}}{v_1} D_{\sqrt{M}}\, R\, D_{\sqrt{m}}\, U_\nu^\dagger\,, \tag{5.10}$$

where $D_{\sqrt{A}} \equiv \mathrm{diag}\left(\sqrt{a_1}, \sqrt{a_2}, \sqrt{a_3}\right)$ and R is an orthogonal (complex) matrix with $R^\dagger R = \mathbb{1}$. In particular, we use the fact that we sum over two right-handed neutrinos and use the orthogonality condition $\sum_j R^2_{1j} = 1$. We can therefore approximate the upper bound as:

$$|\epsilon_1| \lesssim \frac{3}{16\pi}\frac{M_1}{v_2^2}\left(m_3 - m_1\right)\,. \tag{5.11}$$

For simplification we set $m_1 \simeq 0$ and therefore get:

$$|\epsilon_1| \lesssim \frac{3}{16\pi}\frac{M_1}{v_2^2} m_3\,. \tag{5.12}$$

This upper bound on ϵ_1 can be translated into a lower bound on the lightest right-handed neutrino mass $M_{N,1}$, i.e. Davidson-Ibarra bound [87]:

$$M_{N,1} \gtrsim \frac{5\times 10^8\ \mathrm{GeV}}{1+t_\beta^2}\,, \tag{5.13}$$

which translates into a lower bound for $Y_{N,11}$

$$Y_{N,11} \gtrsim \frac{7.1\times 10^8\ \mathrm{GeV}}{v_S\left(1+t_\beta^2\right)}\,. \tag{5.14}$$

By combining equations (5.14) and (5.4) we obtain the range for $Y_{N,11}$:

$$\frac{7.1\times 10^8\ \mathrm{GeV}}{v_S\left(1+t_\beta^2\right)} \lesssim Y_{N,11} \lesssim \left(\frac{8\pi^2\lambda_S}{163\log\left(\frac{30M_\mathrm{P}}{m_s}\right)}\right)^{1/4}\,. \tag{5.15}$$

Once $Y_{N,11}$ is constrained by v_S, t_β and λ_S we are left with only nine degrees of freedom, namely $Y_{\nu,ij}$. In order to obtain the left-handed neutrino Yukawa couplings Y_ν, we need to

calculate [88]

$$Y_\nu = \frac{\sqrt{1+t_\beta^2}}{v}\,\mathcal{D}_{\sqrt{M}} O \mathcal{D}_{\sqrt{m_\nu}} U_\nu^\dagger\,, \tag{5.16}$$

where

$$\mathcal{D}_{\sqrt{M}} \equiv \mathrm{diag}\left(\sqrt{M_{N,1}}, \sqrt{3M_{N,1}}, \sqrt{3M_{N,1}}\right)\,, \tag{5.17}$$

$$\mathcal{D}_{\sqrt{m_\nu}} \equiv \mathrm{diag}\left(\sqrt{m_{\nu,1}}, \sqrt{m_{\nu,2}}, \sqrt{m_{\nu,3}}\right) \tag{5.18}$$

denote the diagonalized right-handed Majorana and left-handed Dirac neutrino mass matrix respectively. U_ν is the PMNS-neutrino mixing matrix whose components are given by the best global fits of Ref. [89]. O is a 3×3-orthogonal matrix which is in general complex and consists of three complex angles. However, we follow the same line of reasoning as in Ref. [7] by taking O to be of unity since we can neglect $\mathcal{O}(1)$ contributions for the RGE stability analysis. Furthermore, the left-handed neutrinos are constrained by neutrino oscillation experiments [89] and cosmological neutrino observations [61]. From the PLANCK 2018 [61] constraints we obtain the upper bound on the sum of the neutrino masses:

$$\sum_{i=1}^{3} m_{\nu,i} < 0.12\ \mathrm{eV} \quad (95\%\ \mathrm{C.L.\ Planck\ TT,TE,EE+lowE+lensing+BAO})\,. \tag{5.19}$$

The experimental best fit constraints of neutrino masses from atmospheric and solar mass splitting [89] for normal ordering (NO) are given by:

$$\Delta m_{21}^2\left(10^{-5}\ \mathrm{eV}^2\right) = 7.5^{+0.22}_{-0.2}\ ,\ \Delta m_{31}^2\left(10^{-3}\ \mathrm{eV}^2\right) = 2.55^{+0.02}_{-0.03}\ \ (\text{best fit } \pm 1\sigma, \mathrm{NO})\,. \tag{5.20}$$

We consider a hierarchical mass ordering $m_{\nu,1} < m_{\nu,2} < m_{\nu,3}$ where we take, as mentioned above, $m_{\nu,1} \equiv m_1 \simeq 0$. Then, the left-handed neutrino Yukawa matrix is given by:

$$Y_{\nu,(i+1)j} \simeq \frac{1}{v}\sqrt{\frac{3}{\sqrt{2}} Y_{N,11} m_{\nu,(i+1)}\left(1+t_\beta^2\right) v_S}\; U^*_{\nu,j(i+1)} \quad \text{with} \quad Y_{\nu,1j} \simeq 0\,, \tag{5.21}$$

where $m_{\nu,2}$ and $m_{\nu,3}$ are given by:

$$m_{\nu,2} \simeq \Delta m_{2,1} \simeq 8.66\ \mathrm{meV} \quad , \quad m_{\nu,3} \simeq \sqrt{\Delta m_{2,1}^2 + \Delta m_{3,1}^2} \simeq 51.23\ \mathrm{meV}\,. \tag{5.22}$$

Since $m_{\nu,3} \gg m_{\nu,2} \gg m_{\nu,1}$ and $U^*_{\nu,32,33} \gtrsim U^*_{\nu,ij}$, we only consider $Y_{\nu,32,33}$ for the remainder of this paper, i.e.

$$Y_{\nu,32,33} \simeq \frac{1}{v}\sqrt{\frac{3}{\sqrt{2}} Y_{N,11} m_{\nu,3}\left(1+t_\beta^2\right) v_S}\; U^*_{\nu,32,33}\,. \tag{5.23}$$

The aforementioned nine degrees of freedom are thus constrained by experimental values and by the benchmark relevant parameter t_β. Hence, we can account for BAU by vanilla thermal leptogenesis with hierarchical normal ordering of the light neutrino masses.

There are a few caveats to consider regarding the size of the neutrino couplings in the RG-flow of λ_{1S}. Therefore, we consider the RGE of λ_{1S}:

$$\begin{aligned}\mathcal{D}\lambda_{1S} = \lambda_{1S}\left(-\frac{3}{2}g_1^2 - \frac{9}{2}g_2^2 + 4\lambda_{1S} + 4\lambda_S + 6\lambda_1\right) + \lambda_{2S}\left(4\lambda_3 + 2\lambda_4\right) + 8\lambda_{12S}^2 \\ + \lambda_{1S}\left(6Y_b^2 + 2Y_\tau^2 + 2\mathrm{Tr}\left(Y_\nu^\dagger Y_\nu\right) + \mathrm{Tr}\left(Y_N^\dagger Y_N\right)\right) - 4\mathrm{Tr}\left(Y_\nu^\dagger Y_\nu Y_N^\dagger Y_N\right) .\end{aligned} \tag{5.24}$$

As we can see the running is dominated by the size of λ_{1S}, λ_{2S} and $\mathrm{Tr}\left(Y_\nu^\dagger Y_\nu Y_N^\dagger Y_N\right)$ where the latter contributes negatively on the running. For PQTHI-scenarios we do not have to worry about the size of the neutrino Yukawa term since $\lambda_{1S,2S} \gg \mathrm{Tr}\left(Y_\nu^\dagger Y_\nu Y_N^\dagger Y_N\right)$ which is thus negligible. However, for PQI the portal couplings can be of the same size as the neutrino Yukawa term, i.e. $\lambda_{1S,2S} \sim \mathrm{Tr}\left(Y_\nu^\dagger Y_\nu Y_N^\dagger Y_N\right)$, which causes λ_{1S} to run negative at higher energies. In order to secure positive portal couplings at the inflationary scale for PQI, we impose a condition on the initial value of λ_{1S} to guarantee $\lambda_{1S}(M_P) > 0$:

$$\lambda_{1S} \gtrsim \mathrm{Tr}\left(Y_\nu^\dagger Y_\nu Y_N^\dagger Y_N\right) . \tag{5.25}$$

For the remainder of the paper, we will only consider the real entries of Y_ν, i.e. $\mathrm{Re}(Y_{\nu,ij})$, since the RG-analysis, except for Y_ν itself, is independent of the imaginary part. The RG-running of Y_ν is severly suppressed by multiplicatives of its own value at the electroweak scale (see eq. (E.18)). Therefore, its value at the electroweak scale can be approximated to be the same at the inflationary scale. The same applies even more so for Y_N. We demonstrate this fact in figure 5.1 for $Y_{\nu,32,33}$ and $Y_{N,1}$. We can see that the values of the Yukawa couplings are approximately the same at the inflationary scale as they are at the electroweak scale. However, for completeness, we will include the running of the neutrino Yukawas into our RG-analysis but note that their value is almost scale-invariant, as we would expect from looking at the RGEs of eqns (E.18)-(E.19) of appendix E.

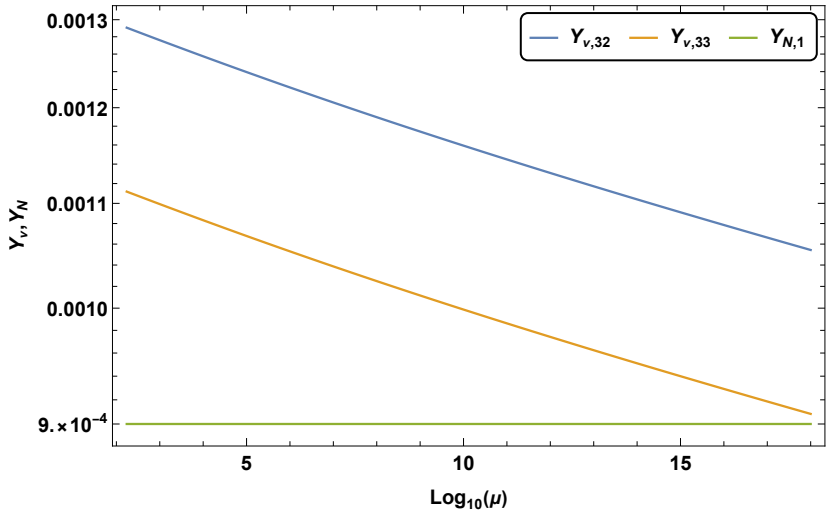

Figure 5.1.: Shown are the the RG-running of the largest components of the Dirac neutrino couplings $Y_{\nu,32,33}$ and the main Majorana neutrino coupling $Y_{N,1}$ with $t_\beta = 5.5$, $\lambda_S = 10^{-10}$ and $v_S = 10^{10}$ GeV. The renormalization scale is set by the top pole mass $m_t = (172.5 \pm 0.7)$ GeV given by Ref. [37] to run from low- to high scale.

5.3. Interconnection of portal couplings

In this section we consider the effects of the one-loop RG running of the portal couplings and make the connection between inflation and Higgs phenomenology. We evolve the couplings from the electroweak scale all the way up to the Planck scale and discuss the intricacies of satisfying the constraints for successful inflation (see Table 4.2) while accommodating a 125 GeV Higgs with additional heavy Higgses at the electroweak/TeV scale. In particular, we will discuss the running of the portal couplings and its impact on the inflationary field direction with regard to inflationary conditions (see Table 4.2 for details). Therefore, we pay attention to the size of the portal coupling and consider its sign at the Planck scale. We introduce in Table 5.1 benchmark points representing inflation in the sh_{12}-, sh_2- and s-direction which satisfy our considerations and convey the statement of our discussion.

As discussed in section 3.9 we determined that the squared masses of the heavy Higgses strongly depend on $\lambda_{12S} v_S^2$. In fact, a tiny value for λ_{12S} is preferred by high-scale validity analysis [90, 91] since $\lambda_{12S} v_S^2$ resembles a soft breaking parameter in a softly broken $U(1)$-symmetric 2HDM[1] [25, 34]. Therefore, we first consider the RG running of λ_{12S}. We can already see that the running of λ_{12S} is proportional to itself:

$$\mathcal{D}\lambda_{12S} = \lambda_{12S}\left(-\frac{3}{2}g_1^2 - \frac{9}{2}g_2^2 + 2\lambda_3 + 4\lambda_4 + 2\lambda_S + 4(\lambda_{1S} + \lambda_{2S}) + 3Y_t^2 + 3Y_b^2 + Y_\tau^2\right) . \quad (5.26)$$

[1] In section 3.7 we describe the effective low-energy matching of 2hdSMASH to a softly broken $U(1)$-symmetric 2HDM.

Parameters	**BP-sh_{12}**	**BP-sh_2**	**BP-s**
λ_1	0.07	0.07	0.07
λ_2	0.263	0.316	0.258
λ_3	0.60	0.54	0.54
λ_4	-0.40	-0.14	-0.14
λ_S	6.5×10^{-10}	4.44×10^{-10}	10^{-10}
λ_{1S}	-6.59×10^{-6}	5.57×10^{-6}	4.8×10^{-14}
λ_{2S}	10^{-15}	-4.27×10^{-6}	10^{-15}
λ_{12S}	2.5×10^{-16}	2.5×10^{-16}	2.5×10^{-16}
$\tan\beta$	5.5	5.5	26
$Y_{N,1}$	9×10^{-4}	9×10^{-4}	4×10^{-5}
$Y_{\nu,3}$	5.18×10^{-3}	5.18×10^{-3}	1.09×10^{-3}
v_S	3×10^{10}	3×10^{10}	3×10^{10}
m_h (GeV)	125.2	125.1	125.1
m_H (GeV)	799.4	798.8	1711.5
m_s (GeV)	6.6×10^5	6.3×10^5	3×10^5
m_A (GeV)	799.5	799.5	1711.5
$m_{H^\pm}$ (GeV)	807.0	802.2	1712.8

Table 5.1.: Three benchmarks passing theoretical and experimental constraints representative for inflation in sh_{12}-, sh_2- and s-direction. The top pole mass is given by Ref. [37] to be $m_t = (172.5 \pm 0.7)$ GeV.

By considering the value of λ_{12S} at the electroweak scale we determine the size of heavy Higgs masses since we fix the PQ-breaking scale at $v_S = 3 \times 10^{10}$ GeV. Hence, λ_{12S} is chosen to be tiny as argued in section 3.9 to acquire a phenomenologically viable model which can be tested at the HL-LHC or future colliders. This smallness is associated with an enhanced Poincaré symmetry which we have discussed in section 3.7. The size of λ_{12S} will be preserved all the way up to the Planck scale, thus justifying the considerations of Section 4.3. By analyzing the RG evolution of λ_{1S} and λ_{2S} we can determine whether we satisfy PQI or PQTHI directions at the Planck scale. The RGEs of λ_{1S} and λ_{2S} are given by:

$$\begin{aligned}\mathcal{D}\lambda_{1S} = {} & \lambda_{1S}\left(-\frac{3}{2}g_1^2 - \frac{9}{2}g_2^2 + 4\lambda_{1S} + 4\lambda_S + 6\lambda_1\right) + \lambda_{2S}\left(4\lambda_3 + 2\lambda_4\right) + 8\lambda_{12S}^2 \\ & + \lambda_{1S}\left(6Y_b^2 + 2Y_\tau^2 + 2\mathrm{Tr}\left(Y_\nu^\dagger Y_\nu\right) + \mathrm{Tr}\left(Y_N^\dagger Y_N\right)\right) - 4\mathrm{Tr}\left(y_\nu^\dagger Y_\nu Y_N^\dagger Y_N\right), \qquad (5.27) \\ \mathcal{D}\lambda_{2S} = {} & \lambda_{2S}\left(-\frac{3}{2}g_1^2 - \frac{9}{2}g_2^2 + 4\lambda_{2S} + 4\lambda_S + 6\lambda_2\right) + \lambda_{1S}\left(4\lambda_3 + 2\lambda_4\right) + 8\lambda_{12S}^2 \\ & + \lambda_{2S}\left(6Y_t^2 + \mathrm{Tr}\left(Y_N^\dagger Y_N\right)\right). \qquad (5.28)\end{aligned}$$

Since λ_{12S}, Y_N and Y_ν are very small, we can safely neglect terms involving them. Thus, we can rewrite the RGEs of the portal couplings as follows:

$$\mathcal{D}\lambda_{1S} \simeq \lambda_{1S}\left(-\frac{3}{2}g_1^2 - \frac{9}{2}g_2^2 + 4\lambda_{1S} + 4\lambda_S + 6\lambda_1 + 6y_b^2 + 2y_\tau^2\right) + \lambda_{2S}\left(4\lambda_3 + 2\lambda_4\right), \tag{5.29}$$

$$\mathcal{D}\lambda_{2S} \simeq \lambda_{2S}\left(-\frac{3}{2}g_1^2 - \frac{9}{2}g_2^2 + 4\lambda_{2S} + 4\lambda_S + 6\lambda_2 + 6y_t^2\right) + \lambda_{1S}\left(4\lambda_3 + 2\lambda_4\right). \tag{5.30}$$

There are two terms to consider, namely the first term which is proportional to the evolving portal coupling itself and the second term which is proportional to the other portal coupling. We notice that the combination of both terms will determine the size of the portal coupling at the Planck scale. Unfortunately, we cannot solve these RGEs analytically but we can analyze their contributions and make a statement about the size and the behavior of their evolution so that we end up with the required conditions for PQI or PQTHI at the Planck scale. There are three separate scenarios concerning the size of the portal couplings, i.e.

$$|\lambda_{1S}| < |\lambda_{2S}| \;\;,\;\; |\lambda_{1S}| > |\lambda_{2S}| \;\;,\;\; |\lambda_{1S}| \sim |\lambda_{2S}|\,, \tag{5.31}$$

where only two of them will be our main focus. Therefore, we will consider without loss of generality benchmarks BP-sh_{12} and BP-sh_2 - BP-s of Table 5.1 for the cases $|\lambda_{1S}| > |\lambda_{2S}|$ and $|\lambda_{1S}| \sim |\lambda_{2S}|$ respectively. Starting with the latter will help clarify the various contributions to the RGEs of λ_{1S} and λ_{2S}.

$|\lambda_{1S}| \sim |\lambda_{2S}|$: Both portal couplings will influence the running of each other. Therefore it is necessary to analyze which contributions will have the dominant influence. Since the top Yukawa coupling is larger than the bottom- and the τ-Yukawa couplings, the influence of λ_{2S} will dominate the evolution of λ_{1S}. Hence, λ_{1S} will evolve towards the value of λ_{2S} when approaching the Planck scale. This can be circumvented by approximating the RGEs further and modifying the portal couplings accordingly. By comparison, we can neglect $Y_{b,\tau}$, $\lambda_{1,2,S}$ and $g_{1,2}$ since the portal couplings are equal in size and the top Yukawa term dominates the running of λ_{2S}. This is due to the fact that the top Yukawa dominates in the low-energy regime and becomes in comparison less dominant in the high energy regime. Thus, the running of λ_{2S} affects the running of λ_{1S} by the coupling term involving λ_3 and λ_4. We therefore assume λ_3 and λ_4 not to grow significantly when approaching the Planck scale[2]. Hence, the RGEs of $\lambda_{1S,2S}$ for $|\lambda_{1S}| \sim |\lambda_{2S}|$ can be approximated to:

$$\mathcal{D}\lambda_{1S} \approx \lambda_{2S}\left(4\lambda_3 + 2\lambda_4\right), \tag{5.32}$$

$$\mathcal{D}\lambda_{2S} \approx 6\lambda_{2S}y_t^2\,. \tag{5.33}$$

[2]We require λ_3 and λ_4 to run perturbative to high energies and thus prefer that exponential growth near the Planck scale is suppressed.

The running of λ_{2S} will dominate unless we implement a correction to the initial value of λ_{1S} so that both portal couplings will preserve their respective sign and size at the Planck scale. Considering the chain rule, we can reformulate the two RGEs in order to obtain a differential equation:

$$\mathcal{D}\lambda_{1S} = \frac{\partial\lambda_{1S}}{\partial\lambda_{2S}}\mathcal{D}\lambda_{2S} \approx \lambda_{2S}\,(4\lambda_3 + 2\lambda_4) \tag{5.34}$$

$$\Rightarrow \frac{\partial\lambda_{1S}}{\partial\lambda_{2S}} \approx \frac{2\lambda_3 + \lambda_4}{3y_t^2}\,. \tag{5.35}$$

By integrating both sides, we obtain the necessary correction for λ_{1S} to counter the effect of the top Yukawa:

$$\delta\lambda_{1S} \approx \frac{\lambda_{2S}\,(2\lambda_3 + \lambda_4)}{3y_t^2}\,, \tag{5.36}$$

where $|\lambda_{1S}| \simeq |\lambda_{2S}|$. Hence, the initial value for λ_{1S} is given by:

$$|\lambda_{1S}^{\text{corr.}}(\mu_{EW})| = |\lambda_{1S} + \delta\lambda_{1S}|_{\mu_{EW}} \approx \left|\lambda_{2S} \times \left(1 + \frac{2\lambda_3 + \lambda_4}{3y_t^2}\right)\right|_{\mu_{EW}}\,, \tag{5.37}$$

where μ_{EW} is the electroweak scale and $\lambda_{1S}^{\text{corr.}}$ is the corrected value of λ_{1S}. This correction causes both RGEs to be of equal size and preserve their respective sign at the Planck scale. Therefore, this case describes inflation in the sh_1 or sh_2 direction where either portal coupling differs by sign change. For illustration we consider the case where $\lambda_{1S} > 0$ and $\lambda_{2S} < 0$ given by benchmark point BP-sh_2. In figure 5.2 we can see the running of both portal cou-

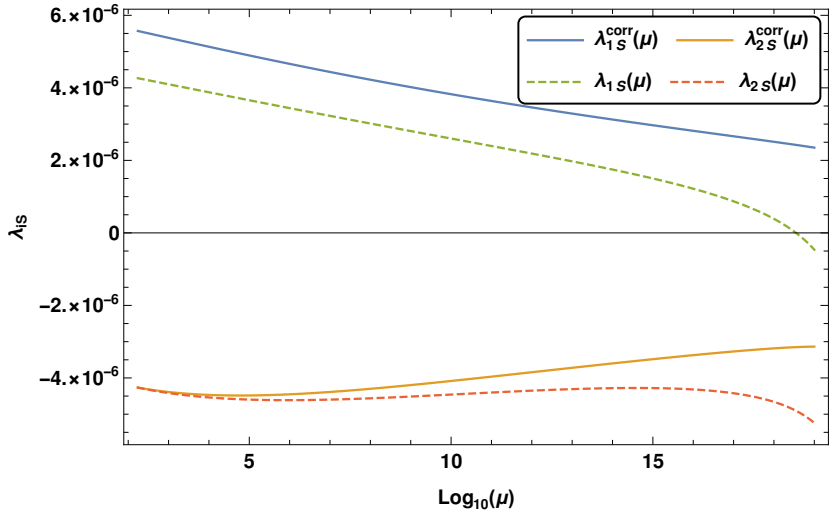

Figure 5.2.: RG evolution of λ_{1S} and λ_{2S} of BP-sh_2 where $|\lambda_{1S}| \sim |\lambda_{2S}|$ with opposite signs. Here, the initial value of $\lambda_{1S}^{\text{corr}}$ is given by eq. (5.37) which affects the running of λ_{1S} positively compared to the running where no correction is applied.

plings with and without a correction applied to $\lambda_{1S}(\mu)$. As described above, we can see that the correction preserves the sign of both portal couplings all the way up to the Planck scale. The same line of reasoning applies to sh_1 by switching signs of λ_{1S} and λ_{2S}. For the benchmark point BP-s of Table 5.1 both portal couplings are taken positive. However, the running of λ_{1S} and λ_{2S} is dominantly determined by the left- and right-handed Yukawa couplings. In section 5.2 we discussed the appropriate initial value λ_{1S} needs (see eq. (5.25)) in order for both portal couplings to remain positive at the Planck scale.

$|\lambda_{1S}| > |\lambda_{2S}|$: In general, this case describes either PQI or PQTHI-sh_{12} since both portal couplings will be either positive (PQI) or negative (PQTHI-sh_{12}) at the Planck scale, as we will argue now. For PQI, we consider tiny portal couplings which is represented in benchmark BP-s. Therefore, we will refer to PQTHI-sh_{12} for a more general discussion where portal couplings are assumed to be sizable compared to PQI. We consider BP-sh_{12} of table 5.1, where $\lambda_{1S} < 0$ and $\lambda_{2S} > 0$ but differ in size, i.e. $|\lambda_{1S}| > |\lambda_{2S}|$ at the electroweak scale. Thus, we can approximate the RGEs of λ_{1S} and λ_{2S} by

$$\mathcal{D}\lambda_{1S} \approx \lambda_{1S}\left(-\frac{3}{2}g_1^2 - \frac{9}{2}g_2^2 + 4\lambda_{1S} + 4\lambda_S + 6\lambda_1 + 6y_b^2 + 2y_\tau^2\right) + \dots, \tag{5.38}$$

$$\mathcal{D}\lambda_{2S} \approx \lambda_{1S}\left(4\lambda_3 + 2\lambda_4\right) + \dots, \tag{5.39}$$

where only contributions of λ_{1S} are considered since λ_{2S} is sub-dominant in comparison. This approximation is illustrated in Figure 5.3 where λ_{2S} approaches the value of λ_{1S} and they become equal at the Planck scale.

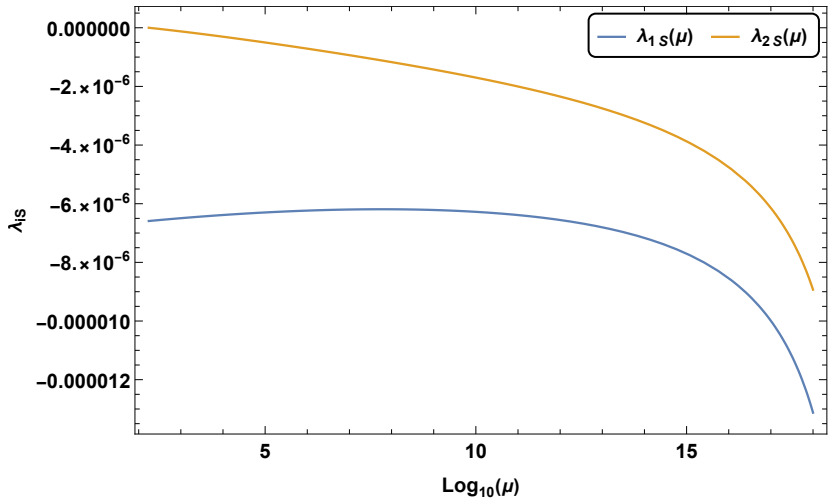

Figure 5.3.: RG evolution of portal couplings λ_{1S} and λ_{2S} for sh_{12}-inflation using BP-sh_{12} from Table 5.1. The top pole mass $m_t = (172.5 \pm 0.7)$ GeV given by Ref. [37] is used to set the renormalization scale for the benchmarks to run from low- to high scale.

5.4. Stability analysis

In this section we analyze vacuum stability, perturbative unitarity and high-scale validity of 2hdSMASH. Vacuum stability is mostly endangered by λ_2 running negative. For a Type-II 2HDM, the Higgs doublet Φ_2 couples to the top-quark which can force λ_2 into negative values. The same phenomenon has been observed in the SM, which is regarded as the top-quark instability. We show, that we can circumvent this problem by stabilizing the running of λ_2 with the mixing parameter λ_{34}. For that reason, we consider the necessary BfB condition of the 2HDM

$$\lambda_{34} \geq -\sqrt{\lambda_1 \lambda_2}\,, \tag{5.40}$$

which we can translate into the following form

$$\frac{\lambda_{34}^2}{\lambda_1} \geq -\lambda_2\,. \tag{5.41}$$

We identify in eq. (5.41) the parameter δ given by

$$\delta \equiv \frac{\lambda_{34}^2}{\lambda_1}\,, \tag{5.42}$$

which we will use to stabilize the running effects of λ_2 as we will argue in the following.

The instability can be understood by considering the one-loop RGE of λ_2:

$$\begin{aligned}\mathcal{D}\lambda_2 = &\frac{3}{4}g_1^4 + \frac{3}{2}g_1^2 g_2^2 + \frac{9}{4}g_2^4 - \frac{9}{5}g_1^2\lambda_2 - 9g_2^2\lambda_2 + 12\lambda_2^2 + 2\lambda_{2s}^2 \\ &+ 4\lambda_3^2 + 4\lambda_3\lambda_4 + 2\lambda_4^2 + 12\lambda_2 Y_t^2 - 12Y_t^4\,,\end{aligned} \tag{5.43}$$

where the dominant negative top Yukawa contribution $\propto Y_t^4$ is competing with other dominant quartic coupling terms. It proves useful to consider λ_3 and λ_4 for stabilization since it contributes positively to its RG-running and λ_1 is absent. However, enhancing λ_1 would only contribute indirectly to the RG-running of λ_2 by its mediator couplings λ_3 and λ_4. Hence, we fix λ_1 and vary λ_3 and λ_4 for stabilization. By considering the RGE of λ_1, we recognize that the same λ_3 and λ_4 contributions affect its running

$$\begin{aligned}\mathcal{D}\lambda_1 = &\frac{3}{4}g_1^4 + \frac{3}{2}g_1^2 g_2^2 + \frac{9}{4}g_2^4 - \lambda_1\left(3g_1^2 + 9g_2^2\right) + 12\lambda_1^2 + 4\lambda_3\lambda_4 + 4\lambda_3^2 + 2\lambda_4^2 + 2\lambda_{1S}^2 \\ &+ 12\lambda_1 Y_b^2 - 12Y_b^4 + 4\lambda_1 Y_\tau^2 - 4Y_\tau^4 + 4\lambda_2 \mathrm{Tr}\left(Y_\nu^\dagger Y_\nu\right) - 4\mathrm{Tr}\left(Y_\nu^\dagger Y_\nu Y_\nu^\dagger Y_\nu\right)\,,\end{aligned} \tag{5.44}$$

where negative terms, such as the down-type Yukawa contribution is sub-dominant in comparison. Therefore, any enhancement of λ_3 and λ_4 will enhance λ_1 by going to higher energies and thus endangering perturbative unitarity. This can be avoided by applying the

perturbative unitarity bounds for λ_1 and λ_{34}, such that

$$|\delta| \equiv \left| \frac{\lambda_{34}^2(\mu)}{\lambda_1(\mu)} \right| < 8\pi \ , \ \forall \mu \tag{5.45}$$

is bounded from above. Furthermore, we have to ensure that we maintain a 125 GeV light Higgs. Its mass is approximately

$$m_h^2 \approx \frac{v_S^2}{\left(1+t_\beta^2\right)^2} \left[\lambda_1 + t_\beta^4 \, \lambda_2 + 2\, t_\beta^2 \, \lambda_{34} \right] , \tag{5.46}$$

where portal terms are neglected for now. We can see that for $t_\beta > 1$, as considered in our case, the λ_2 term is t_β^2 times larger than the one with λ_{34}. Therefore, any enhancement in λ_{34} is met with a slight decrease in λ_2 since its decrease will counterbalance the increase of λ_{34} by a factor of t_β^2. Thus, λ_{34} is capable to influence the RG-running of λ_2 without violating Higgs phenomenology.

There are two intertwining effects which stabilize the RG-running of λ_2, namely

1) initial values given to λ_2, λ_3 and λ_4 and

2) an RG-running effect caused by λ_3 and λ_4.

Both effects, namely 1) and 2), contribute to the RG stabilization of λ_2 and are interconnected. Here, the emphasis is on the RG-running effects since they are responsible to uplift λ_2 from its negative top Yukawa running term at energy scales $\mu \gtrsim m_t$. In order to gain some analytical understanding, we consider the Coleman-Weinberg potential, cf. Ref. [92], which we will utilize to acquire $\lambda_2(\mu)$, i.e. the integrated version[3] of $\mathcal{D}\lambda_2$, to identify the dominant RG-running contributions. The full expression of the Coleman-Weinberg potential is given in appendix F, whose general analytical form is given by

$$\begin{aligned} V_{\rm CW}(\phi_i) = & \frac{1}{64\pi^2} \\ & \times \left(\sum_b g_b m_b^4(\phi_i) \left[\log\left(\frac{m_b^2(\phi_i)}{\Lambda^2} \right) - \frac{3}{2} \right] - \sum_f g_f m_f^4(\phi_i) \left[\log\left(\frac{m_f^2(\phi_i)}{\Lambda^2} \right) - \frac{5}{2} \right] \right) , \end{aligned} \tag{5.47}$$

where $g_{f/b}$ are the degrees of freedom and $m_{f/b}$ are the masses of fermions/bosons. By performing a matching to an effective tree-level potential in the h_2-direction

$$V_{\rm eff} \simeq V_0 + V_{\rm CW} \simeq \frac{\lambda_2^{\rm eff} h_2^4}{8} \tag{5.48}$$

[3]This can be verified by using the *Callan-Symanzik* equation.

with

$$V_0 \simeq \frac{\lambda_2 h_2^4}{8}\,, \tag{5.49}$$

where $h_1 \simeq s \simeq 0$, we acquire an RG-improved potential for h_2. As a result we obtain the effective coupling λ_2^{eff} by computing

$$\lambda_2^{\text{eff}} = \frac{8}{h_2^4} V_{\text{eff}}(h_2)\,, \tag{5.50}$$

which is given by

$$\begin{aligned}\lambda_2^{\text{eff}} \simeq \lambda_2(m_t) + \frac{\lambda_{2S}^2\left(\log\left(\frac{h_2^2\lambda_{2S}}{2m_t^2}\right)-\frac{3}{2}\right)+\lambda_3^2\left(\log\left(\frac{h_2^2\lambda_3}{2m_t^2}\right)-\frac{3}{2}\right)}{16\pi^2} \\ + \frac{(\lambda_3+\lambda_4)^2\left(\log\left(\frac{h_2^2(\lambda_3+\lambda_4)}{2m_t^2}\right)-\frac{3}{2}\right)+6\left(\lambda_2^2\left(\log\left(\frac{27h_2^2\lambda_2}{16m_t^2}\right)-\frac{3}{2}\right)-Y_t^4\left(\log\left(\frac{h_2^2Y_t^2}{2m_t^2}\right)-\frac{3}{2}\right)\right)}{16\pi^2}\,,\end{aligned} \tag{5.51}$$

where we neglected the sub-dominant gauge couplings $g_{1,2,3}$. Furthermore, we can neglect the portal coupling term $\propto \lambda_{2S}^2$ since its contribution is small in comparison[4]. Thus, we find

$$\begin{aligned}\lambda_2^{\text{eff}} \approx \lambda_2(m_t) + \frac{\lambda_3^2\left(\log\left(\frac{h_2^2\lambda_3}{2m_t^2}\right)-\frac{3}{2}\right)+(\lambda_3+\lambda_4)^2\left(\log\left(\frac{h_2^2(\lambda_3+\lambda_4)}{2m_t^2}\right)-\frac{3}{2}\right)}{16\pi^2} \\ + \frac{6\left(\lambda_2^2\left(\log\left(\frac{27h_2^2\lambda_2}{16m_t^2}\right)-\frac{3}{2}\right)-Y_t^4\left(\log\left(\frac{h_2^2Y_t^2}{2m_t^2}\right)-\frac{3}{2}\right)\right)}{16\pi^2}\end{aligned} \tag{5.52}$$

with running scale $\mu \equiv h_2$. We can identify four stabilizing contributions, namely $\lambda_2(m_t)$, λ_2^2, λ_{34}^2 and λ_3^2. The former two, i.e. $\lambda_2(m_t)$ and λ_2^2, are capable of stabilizing its running when large initial conditions are applied. Moreover, we can see that contributions proportional to λ_{34}^2 and λ_3^2, enter quadratically as well and provide a further source of stabilization. In the case where λ_4 is negative, as we consider in our benchmarks, the most important parameter for RG-running stability becomes λ_3 which enters quadratically in two terms of eq. (5.52). This phenomenon is illustrated in figure 5.4 where $\lambda_2(\mu)$ is depicted for benchmark points BP-sh_2' and BP-sh_2'' of table 5.2. Naively, we would expect that benchmark BP-sh_2' has a sub-dominant effect on the running of λ_2 compared to BP-sh_2''. Despite the fact, that the initial value of λ_2 is smaller in comparison, the dominance of λ_3 causes $\lambda_2(\mu)$ to run higher. This leaves BP-sh_2' with the biggest impact. Moreover, we can associate the tree-level stability

[4]We list in table 5.2 three benchmarks, which represent the most extreme case where portal couplings are sizable, i.e. benchmarks for PQTHI-sh_2. The contribution of the shown portal couplings is sub-dominant to eq. (5.51).

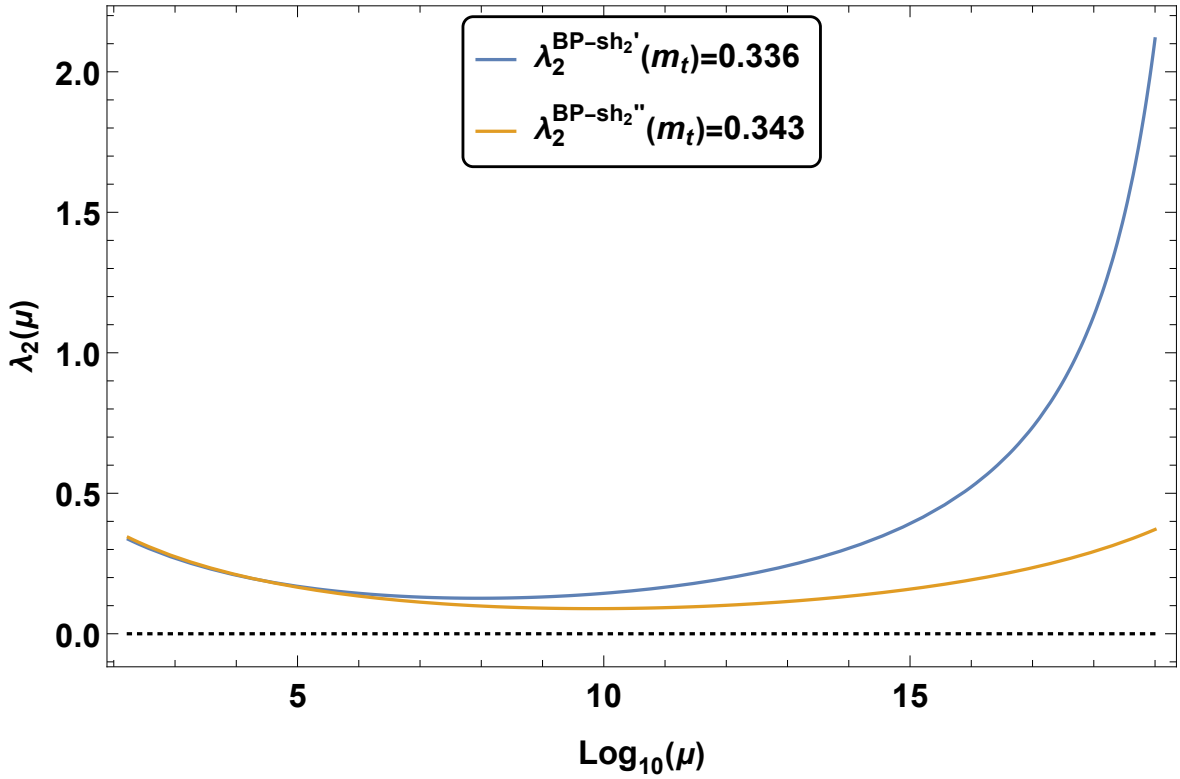

Figure 5.4.: Shown are $\lambda_2(\mu)$ from benchmark BP-sh_2' and BP-sh_2'' given in table 5.2. The top pole mass $m_t = (172.5 \pm 0.7)$ GeV given by Ref. [37] is used to set the renormalization scale for the benchmarks to run from low- to high scale.

condition of eq. (5.41) to an RG-running stability condition

$$\delta(\mu) + \lambda_2(\mu) \geq 0 \quad , \quad \forall \mu \,, \tag{5.53}$$

where negative $\lambda_2(\mu)$ can be counterbalanced by $\delta(\mu)$. This effect can be seen in figure 5.5 by considering benchmarks BP-sh_2 and BP-sh_2' of table 5.2. The tree-level effect is given by BP-sh_2 and depicted in figure 5.5 (left) with $\delta^{\text{BP-}sh_2} > \lambda_2^{\text{BP-}sh_2}$. By comparison, we can see in figure 5.5 (right) the RG-running effect of benchmark BP-sh_2' which is mainly caused by the term $\sim \lambda_3^2$ of eq. (5.52). In our analysis we neglected terms $\propto \lambda_{2S}^2$ in the RG-running of λ_2. This is due to the fact, that λ_{2S} is constrained by another stability condition, namely

$$\tilde{\lambda}_S \equiv \lambda_S - \frac{\lambda_{2S}^2}{\lambda_2} \geq 0 \,. \tag{5.54}$$

This stability condition would be violated if we chose $\lambda_{2S}^2 \sim \lambda_2$, since $\lambda_S \sim 10^{-10}$. Thus, the portal coupling is constrained to be $\lambda_{2S} \lesssim \sqrt{\lambda_S}$ (see sec. 5.1). We show in figure 5.6 the RG-evolution of $\tilde{\lambda}_S$ and its scale-invariance. We note, that λ_3 and

Parameters	**BP-sh_2**	**BP-sh_2'**	**BP-sh_2''**
λ_1	0.07	0.07	0.07
λ_2	0.316	0.336	0.343
λ_3	0.54	0.54	0.44
λ_4	-0.14	-0.44	-0.44
λ_S	4.44×10^{-10}	4.44×10^{-10}	4.44×10^{-10}
λ_{1S}	5.57×10^{-6}	5.57×10^{-6}	5.57×10^{-6}
λ_{2S}	-4.27×10^{-6}	-4.27×10^{-6}	-4.27×10^{-6}
λ_{12S}	2.5×10^{-16}	2.5×10^{-16}	2.5×10^{-16}
$\tan\beta$	5.5	5.5	5.5
$Y_{N,1}$	9×10^{-4}	9×10^{-4}	9×10^{-4}
$Y_{\nu,3}$	5.18×10^{-3}	5.18×10^{-3}	5.18×10^{-3}
v_S	3×10^{10}	3×10^{10}	3×10^{10}
m_h (GeV)	125.1	125.1	125.2
m_H (GeV)	798.7	799.5	799.7
m_s (GeV)	6.3×10^5	6.3×10^5	6.3×10^5
m_A (GeV)	799.5	799.5	799.5
$m_{H^\pm}$ (GeV)	802.1	807.7	807.7

Table 5.2.: List of three benchmarks representing the most extreme case of portal coupling configuration which pass theoretical and experimental constraints and differ by λ_2, λ_3 and λ_4.

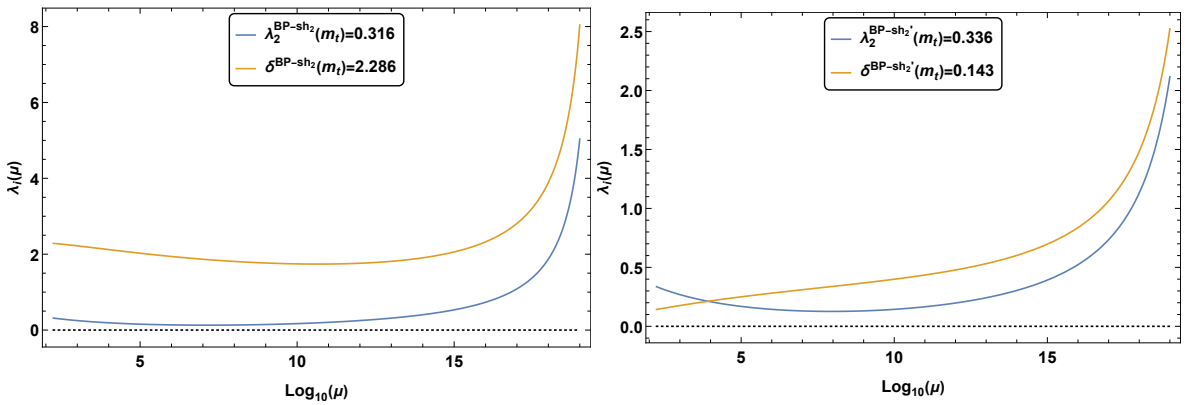

Figure 5.5.: Shown are the RG-running of λ_2 and δ given by benchmark BP-sh_2 (left) and the RG-running of λ_2 and δ given by benchmark BP-sh_2' of table 5.2. The renormalization scale is set at the top pole mass $m_t = (172.5 \pm 0.7)$ GeV, cf. Ref. [37], to run from low- to high scale.

λ_{34} are mainly responsible for stabilizing the RG-running of λ_2. By erasing λ_1, λ_3, λ_4, λ_{1S} and λ_{12S} from our model, we would recover the SMASH model. In particular, in the absence of λ_3 and λ_4, the RG-running of λ_2 in 2hdSMASH becomes the RGE of λ_H in SMASH. By comparison, 2hdSMASH provides further parameters for stabilization, i.e. λ_3 and λ_4, which is depicted in figure 5.7. We conclude, the

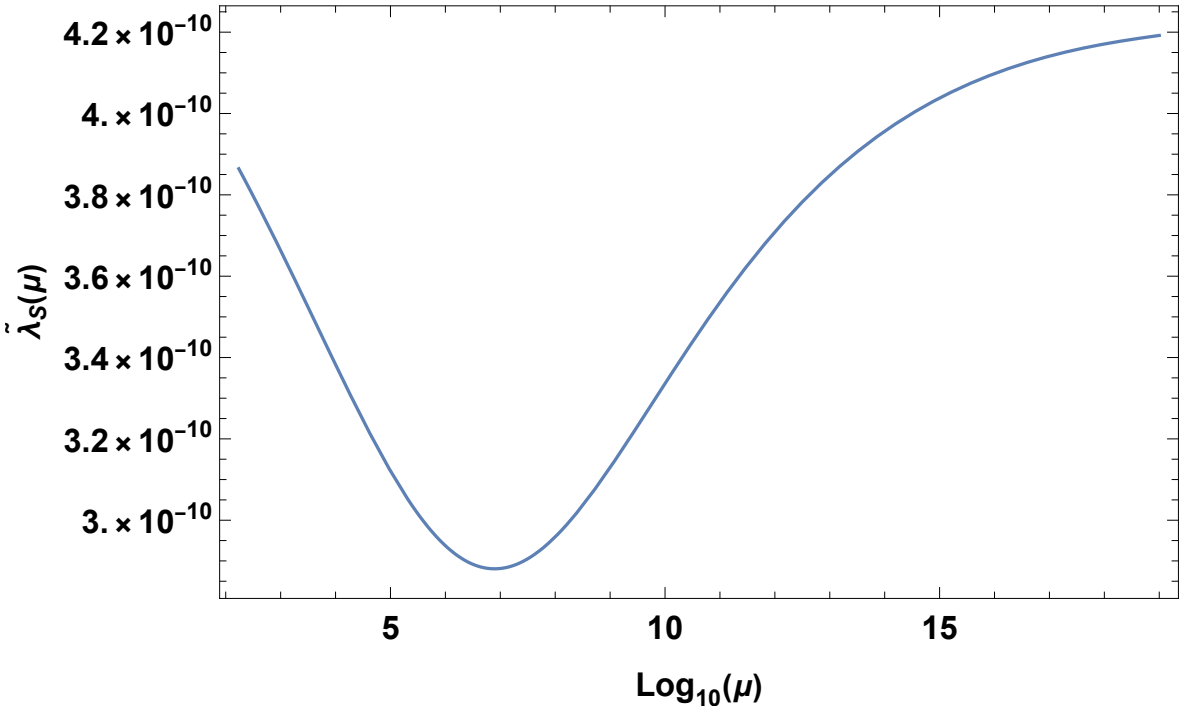

Figure 5.6.: RG-evolution of $\tilde{\lambda}_S(\mu) \equiv \lambda_S(\mu) - \frac{\lambda_{2S}^2(\mu)}{\lambda_2(\mu)}$ from benchmark BP-sh_2. The renormalization scale is set at the top pole mass $m_t = (172.5 \pm 0.7)$ GeV, cf. Ref. [37], to run from low- to high scale.

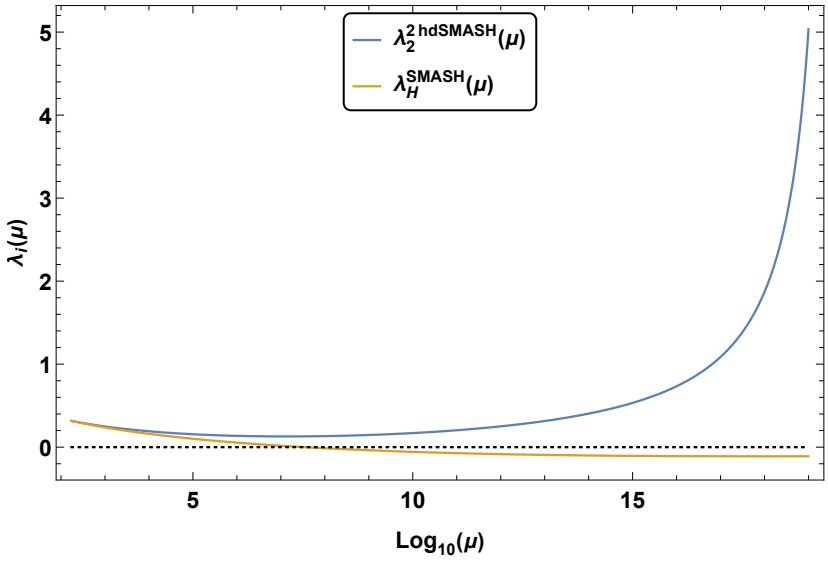

Figure 5.7.: Depicted are the RG evolutions of $\lambda_2(\mu)$ for 2hdSMASH (blue solid curve) and SMASH (orange solid curve) for PQTHI using BP-sh_2 of Table 5.1. The renormalization scale is set at the top pole mass $m_t = (172.5 \pm 0.7)$ GeV, cf. Ref. [37], to run from low- to high scale.

mixing parameters λ_3 and λ_4 assist stabilizing the RG-running of λ_2. Furthermore, the two intertwining effects, i.e. tree-level initial conditions and RG-effects, provide

an analytic understanding how $\lambda_2(\mu)$ behaves. The analysis of this section is representative of the analysis done for all benchmarks acquired in section 5.5. We chose benchmarks of type PQTHI-sh_2 in table 5.2 as an extreme case where portal couplings become sizable and thus provide a more general discussion. We were able to see that portal couplings are constrained and have a sub-dominant effect. This can be seen on tree-level by the following relation

$$\lambda_2 + \frac{1}{2}\left(\delta - \frac{\lambda_{2S}^2}{\lambda_S}\right) \geq 0\,, \tag{5.55}$$

where δ is typically larger. Moreover, we demand that perturbative unitarity constraints (3.25)-(3.30) must be obeyed along the RG evolution, thus ensuring high-scale validity by avoiding Landau-Poles, cf. Ref. [34]. In section 5.5, we give benchmark points which satisfy all theoretical constraints at tree- and one-loop level. The analysis of this section can be easily adopted to scenarios where we consider PQI and other PQTHI directions.

5.5. Benchmarks points

The discussion of inflation in chapter 4 and its connection to electroweak physics by means of RG-analysis in sections 5.1-5.4, culminates to the discussion of benchmark points which satisfy theoretical and experimental constraints. We present benchmarks which are consistent with BfB- and perturbative unitarity conditions from electroweak- all the way up to the Planck scale, thus providing high-scale validity and vacuum stability. Furthermore, the benchmarks are tested against experimental constraints from B-physics and collider experiments on the Higgs sector, thus ensuring 2hdSMASH to be phenomenologically viable.

For this part of the analysis, 2hdSMASH was implemented in `SARAH-v4.14.4` [93], `SPheno-v4.0.4` [94], `HiggsSignals-v2` [95] and `HiggsBounds-v5` [96]. With `SARAH-v4.14.4`, the necessary equations were provided to use in `SPheno-v4.0.4`, such as the RGEs given in appendix E, the scalar- and fermionic masses and its decays. For a given benchmark, this was computed with `SPheno-v4.0.4` and checked with `HiggsSignals-v2` to account for a low-energy signal-strength measurement of the 125 GeV SM-like Higgs scalar at the LHC. Furthermore, the same `SPheno` output was cross-checked with `HiggsBounds-v5` against constraints from heavy Higgs searches at LEP, Tevatron and LHC. With the benchmarks **BP1-BP5** listed in table 5.3 we cover all interesting parameter configurations which also allow

Parameters	**BP1**	**BP2**	**BP3**	**BP4**	**BP5**
λ_1	0.07	0.07	0.07	0.07	0.07
λ_2	0.316	0.263	0.257	0.258	0.257
λ_3	0.54	0.60	0.24	0.54	0.24
λ_4	-0.14	-0.4	0.27	-0.14	-0.28
λ_S	4.44×10^{-10}	6.5×10^{-10}	1.0×10^{-10}	1.0×10^{-10}	1.0×10^{-10}
λ_{1S}	5.57×10^{-6}	-6.59×10^{-6}	4.8×10^{-14}	4.8×10^{-14}	3.6×10^{-13}
λ_{2S}	-4.27×10^{-6}	1.0×10^{-15}	1.0×10^{-15}	1.0×10^{-15}	1.0×10^{-15}
λ_{12S}	2.5×10^{-16}	2.5×10^{-16}	2.5×10^{-16}	2.5×10^{-16}	2.5×10^{-16}
$\tan\beta$	5.5	5.5	26	26	18
$Y_{N,1}$	9×10^{-4}	9×10^{-4}	4×10^{-5}	4×10^{-5}	10^{-4}
$Y_{\nu,3}$	5.175×10^{-3}	5.175×10^{-3}	1.09×10^{-3}	1.09×10^{-3}	1.2×10^{-3}
v_S	3.0×10^{10}	3.0×10^{10}	3.0×10^{10}	3.0×10^{10}	3.0×10^{10}
m_h (GeV)	125.1	125.1	125.2	125.2	125.1
m_H (GeV)	798.7	799.4	1711.5	1711.5	1425.2
m_s (GeV)	6.3×10^5	6.7×10^5	3.0×10^5	3.0×10^5	3.0×10^5
m_A (GeV)	799.5	799.5	1711.5	1711.5	1425.2
$m_{H^\pm}$ (GeV)	802.1	807.0	1709.1	1712.8	1422.2

Table 5.3.: List of benchmarks passing the theoretical constraints and experimental constraints as discussed in the text with a pole top mass of $m_t = (172.5 \pm 0.7)$ GeV according to Ref. [37].

for PQI and PQTHI. The 2HDM couplings λ_1-λ_4 are of $\mathcal{O}(1)$ such that the SM-like Higgs mass $m_h = (125.10 \pm 0.14)$ GeV [37] is obtained. Furthermore, we consider $\tan\beta \gtrsim 5.5$ to accommodate the constraint on the axion decay constant f_a as discussed in appendix A. There is a stringent constraint from $B \to X_s\gamma$ [97] on the charged Higgs sector of the Type-II 2HDM which provides a lower bound on the charged Higgs masses

$$m_{H^\pm} > 650\,\text{GeV}\,. \tag{5.56}$$

This lower bound was recently corrected to be higher in Type-II 2HDM models by computation of $(B \to X_s\gamma)$ at NNLO QCD level [98]

$$m_{H^\pm} > 800\,\text{GeV}\,. \tag{5.57}$$

For choosing $\lambda_{12S} \simeq \mathcal{O}(\frac{v}{v_S})^2$, as discussed in section 3.9 (cf. Ref. [26]), the heavy Higgs sector becomes nearly degenerate with $m_H \approx m_A \approx m_{H^\pm}$. The constraints from electroweak precision tests, namely S, T, U variables, are satisfied for the nearly degenerate mass spectrum of the neutral heavy Higgs sector. We note that the charged Higgs mass has a small mass splitting compared to the other heavy

Higgses which is conceived by considering the change in value for λ_4 of table 5.3. The portal couplings λ_{1S} and λ_{2S} do not have a sizable effect on the scalar masses. However, they are considered in the RG-analysis and connect inflation with particle phenomenology, as discussed in section 5.3. The portal couplings are chosen such that successful inflation is guaranteed and constraints from neutrino physics for thermal leptogenesis and BAU are considered for RG-evolution. The neutrino Yukawa couplings given in table 5.3 satisfy the constraints from neutrino oscillation experiments and BAU as discussed in sec. 5.2. Moreover, the portal couplings are naturally small which protects the SM-like Higgs mass from high-scale radiative corrections. The benchmarks given in table 5.3 are in the TeV range which is established by $\lambda_{12S} \simeq \mathcal{O}(\frac{v}{v_S})^2$. Due to this relation, $\lambda_{12S} v_S^2$ is of order $\mathcal{O}(v^2)$ and resembles a soft breaking parameter of the effective 2HDM low-energy theory. This provides an additional parameter to control the mass spectrum without endangering Higgs phenomenology and its RG evolution all the way up to the Planck scale, cf. Ref. [91].

Therefore, the benchmarks provided in table 5.3 facilitate a mass spectrum at the TeV scale which are allowed by theoretical and experimental constraints. The smallness of the portal couplings imply a considerable suppression of Higgs to axion decays. Hence, 2hdSMASH is indistinguishable from other extended Higgs sectors without axion at upcoming collider experiments based on Higgs decays. However, signals from axion dark matter searches may serve as detection probe of 2hdSMASH.

6. Conclusions

In this thesis, we realized the description of successful inflation and subsequent RG-analysis in 2hdSMASH. In particular, we worked out inflationary directions, i.e. PQI and PQTHI, which are compatible with a naturally generated non-minimal coupling to gravity. Correspondingly, we provided an analytical understanding of RG running which aims at preserving the various interesting features of our parameter space at the Planck scale, thereby connecting directly inflationary constraints with particle phenomenology.

After introducing 2hdSMASH, we discussed in chapter 3 the scalar- and neutrino masses, the theoretical constraints, the model's matching to its effective low-energy theory with subsequent alignment limit and the characteristic mass spectrum. The detailed derivation of the scalar masses, which include three CP-even neutral scalars (h, H, s), one CP-odd scalar (A) and two charged CP-even scalars ($H^{\pm}$), were performed in appendix B and agree with Ref. [26] up to factors of $\mathcal{O}(1)$[1]. The analytical expressions of the scalar masses are numerically verified to an accuracy of more than the digits shown in this thesis. Furthermore, we proved that 2hdSMASH effectively reduces to the SM, thus providing a SM-like particle spectrum. The characteristic mass spectrum beyond SM-like physics, was introduced by inflationary considerations and by the naturalness philosophy adopted from Refs. [35, 25] which provides TeV scale particles.

In chapter 4.3, we describe chaotic inflation in 2hdSMASH where the scalar fields are non-minimally coupled to gravity. For a natural explanation of chaotic inflation we impose that these non-minimal couplings ξ_i, $i = 1, 2, s$, are radiatively generated, i.e. $\xi_i \lesssim 1$, as discussed in Ref. [21] in the context of SMASH. By exploiting the parameter space, we found seven inflationary directions, from which three could be dismissed. Those three field space directions belong to the three 2HDM-directions which are incapable of providing inflation with a non-minimal coupling given by $\xi_i \lesssim 1$. This is based on the phenomenological requirement for the 2HDM quartic

[1] We choose a different normalization convention for the scalar fields compared to Ref. [26], i.e. $\Phi_i^0 = \frac{1}{\sqrt{2}}(h_i + v_i + ia_i)$, resulting in differences of factors.

couplings λ_i, $i = 1, 2, 3, 4$ to be of order $\lambda_i \sim \mathcal{O}(1)$ to generate a SM-like Higgs at the electroweak scale. Thus, we exploit the parameter space for PQI and PQTHI which allowed us to provide four viable inflationary directions, i.e. s-inflation and $sh_{1,2,12}$-inflation. Their inflationary predictions are consistent with the expansion history of the universe where during preheating and reheating, that is immediately after the end of inflation, the universe expands radiation-like. This corresponds to the same inflationary predictions SMASH could provide, see Refs. [6, 7, 45]. In fact, 2hd-SMASH provides the same PQ-breaking scale f_a with the same size of non-minimal couplings which makes it compatible with SMASH's expansion history of the universe and serves as a good assumption. Our results have shown that further calculations with high precision, e.g. lattice calculations, might be needed to derive a correct reheating temperature for 2hdSMASH. This is beyond the scope of this thesis and we leave it to future explorations on the model.

In chapter 5 we discussed the connection of inflation and particle physics by means of RG-running. We performed an extensive RG-analysis to respect constraints from inflation, thermal leptogenesis, BAU, Higgs phenomenology, vacuum stability and perturbative unitarity, thus providing a consistent and complete model of cosmology and particle physics. Therefore, we derived analytic expressions and constraints for crucial RG-running parameters, i.e. $\lambda_{1S,2S,12S,S}$ and $\lambda_{1,2,34}$, which allowed us to gain an analytic understanding of the viable parameter space. We were able to constrain the portal couplings and right handed neutrino Yukawa couplings in terms of λ_S:

$$\lambda_{1S,2S,12S}, Y_N < \sqrt{\lambda_S}\,. \tag{6.1}$$

Moreover, we acquired RG constraints for λ_{1S} in a PQI-scenario by respecting thermal leptogenesis and BAU

$$\lambda_{1S} \gtrsim \mathrm{Tr}\left(Y_\nu^\dagger Y_\nu Y_N^\dagger Y_N\right)\,, \tag{6.2}$$

which ensures the portal couplings to remain positive all the way up to the Planck scale. For PQTHI-scenarios, we considered two cases, namely PQTHI-sh_i represented by $|\lambda_{1S}|_{\mu_{\mathrm{ew}}} \simeq |\lambda_{2S}|_{\mu_{\mathrm{ew}}}$ and PQTHI-sh_{12} represented by $|\lambda_{1S}|_{\mu_{\mathrm{ew}}} \lesssim |\lambda_{2S}|_{\mu_{\mathrm{ew}}}$. Considering PQTHI-$sh_i$, we obtained a correction to the initial value of λ_{1S} which counterbalances the negative top Yukawa contribution of λ_{2S},

$$|\lambda_{1S}^{\mathrm{corr.}}(\mu_{EW})| = |\lambda_{1S} + \delta\lambda_{1S}|_{\mu_{EW}} \approx \left|\lambda_{2S} \times \left(1 + \frac{2\lambda_3 + \lambda_4}{3y_t^2}\right)\right|_{\mu_{EW}}\,, \tag{6.3}$$

where $\lambda_{1S}^{\text{corr.}}$ is the corrected initial value of λ_{1S}. In the case of PQTHI-sh_{12}, we found the responsible couplings, i.e. λ_3 and λ_4, which force λ_{2S} to run towards λ_{1S}. Furthermore, we obtained an analytic understanding of RG-running in the 2HDM, where the couplings λ_3 and λ_4 provide RG-running stability. This is ensured by the relation

$$\delta(\mu) + \lambda_2(\mu) \equiv \frac{\lambda_{34}^2(\mu)}{\lambda_1(\mu)} + \lambda_2(\mu) \geq 0 \quad , \quad \forall \mu \tag{6.4}$$

which prevents $\lambda_2(\mu)$ to run negative. We identified two intertwining effects which stabilize $\lambda_2(\mu)$ by 1) the initial value and 2) by RG-effects caused by λ_3^2 and λ_{34}^2. Moreover, we included perturbative unitarity conditions in our RG-analysis which causes the couplings to be bounded from above. Amongst others, we considered the most prominent perturbative unitarity conditions on the couplings which we used for stabilization, i.e.

$$|\lambda_{1,3}(\mu)| < 8\pi \ , \ |\lambda_3(\mu) \pm \lambda_4(\mu)| < 8\pi \ , \ |\delta(\mu)| < 8\pi \, , \tag{6.5}$$

in order to avoid Landau poles. From this elaborate RG-stability analysis we acquired viable benchmark points which account for all theoretical and experimental constraints, i.e. vacuum stability, perturbative unitarity, inflationary cosmology, thermal leptogenesis, BAU and Higgs phenomenology. The latter was confirmed by testing the benchmarks with `HiggsSignals-v2` and `HiggsBounds-v5` which are in accordance with current LEP, Tevatron and LHC data.

Appendices

A. Constraints on the Axion Decay Constant

The axion decay constant f_a faces astrophysical and cosmological constraints. One of which is obtained from the measured duration of the neutrino signal of the supernova SN 1987A. From this signal, an upper bound on the emission rate of axions is provided [48]. Current improved determinations on the axion emission rate [99, 100] are translated into current lower bounds on f_a:

$$f_a \gtrsim \begin{cases} 5.2 \times 10^8\,\mathrm{GeV}\,, \text{ for } \tan\beta \lesssim 0.5\,, \\ 9.8 \times 10^8\,\mathrm{GeV}\,, \text{ for } \tan\beta \gtrsim 5\,. \end{cases} \tag{A.1}$$

There are further restrictions which apply to axion dark matter by considering the early universe which we will argue now.

During inflation the PQ-symmetry is maximally broken and non-thermally restored in the preheating phase, as discussed in SMASH[1] [6, 7]. After the PQ symmetry is restored it is broken again in the radiation dominated era which corresponds to an energy scale of f_a. There are two mechanisms which produce axion dark matter, namely the misalignment mechanism [11, 12, 13] and the decay of topological defects [101, 102]. Topological defects are described by: *i)* strings which are vortex-like defects that are formed at the PQ phase transition and *ii)* domain walls which are surface-like defects to which strings attach when the temperature of the universe reaches the temperature of the QCD phase transition. The domain wall structure in 2hdSMASH is given by the domain wall number $N_{\mathrm{DW}} > 1$. As long as the PQ symmetry is an exact symmetry, these domain walls are stable and thus threaten to overclose the universe. This would be in conflict with standard cosmology [103, 104]. However, the PQ symmetry, like any global symmetry, can be explicitly broken by Planck-suppressed operators which appear in the effective low energy Lagrangian [105, 106, 107, 108] which may resolve the issue with the domain walls but at the same time cause another problem. These Planck-suppressed operators in the ef-

[1] We consider preheating in 2hdSMASH to be similar to preheating in SMASH.

fective low energy Lagrangian affect the axion potential which shifts the minimum away from zero and therefore destroy the solution to the strong CP problem. Most importantly, this can be circumvented by considering the PQ-symmetry as an automatic or accidental symmetry of an exact discrete $Z_{\mathcal{N}}$ symmetry [109]. Therefore, the axion solution can be protected from semi-classical gravity effects by considering a discrete symmetry for $\mathcal{N} \geq 9$ [110, 111, 112, 113, 114, 115, 116]. This allows for a small explicit symmetry breaking term which is needed to make the domain walls with $N_{\mathrm{DW}} > 1$ unstable and thus cosmologically viable. We assume in 2hdSMASH such a $Z_{\mathcal{N}}$ symmetry with $\mathcal{N} \geq 9$. In order to explain all cold dark matter in the universe by axions [116, 117], we require the axion decay constant to be in the range of

$$4.4 \times 10^7\,\mathrm{GeV} \lesssim f_a \lesssim 9.9 \times 10^9\,\mathrm{GeV}, \text{ for } \mathcal{N} = 9, \tag{A.2}$$

$$1.3 \times 10^9\,\mathrm{GeV} \lesssim f_a \lesssim 9.9 \times 10^9\,\mathrm{GeV}, \text{ for } \mathcal{N} = 10. \tag{A.3}$$

which is partly excluded by the SN 1987A constraint for $\mathcal{N} = 9$. The preferred PQ scale range in 2hdSMASH is therefore

$$3.1 \times 10^9\,\mathrm{GeV} \lesssim v_S \lesssim 5.9 \times 10^{10}\,\mathrm{GeV}\,, \text{ for } \tan\beta \lesssim 0.5\,, \tag{A.4}$$

$$5.9 \times 10^9\,\mathrm{GeV} \lesssim v_S \lesssim 5.9 \times 10^{10}\,\mathrm{GeV}\,, \text{ for } \tan\beta \gtrsim 5\,. \tag{A.5}$$

B. Derivation of Scalar Masses

We derive the charged, neutral CP-odd and CP-even scalar masses by diagonalizing the corresponding squared mass matrices respectively. We will see that computing the charged and CP-odd scalar masses is simpler than computing the CP-even scalar masses. In fact, we will have to use an expansion in order of v/v_S for the latter, while the computation of the former is exact. In the following we will start with the derivation of the charged and CP-odd scalar masses, i.e. $H^\pm$ and A, before we move on to the neutral CP-even scalar masses.

For the charged CP-even and the neutral CP-odd masses, we expand the Higgs doublets Φ_i and the PQ-scalar singlet S about their vacuum:

$$\Phi_1 = (h_1^+ \,,\, \frac{1}{\sqrt{2}}(v_1 + h_1 + ia_1))^T \,, \tag{B.1}$$

$$\Phi_2 = (h_2^+ \,,\, \frac{1}{\sqrt{2}}(v_2 + h_2 + ia_2))^T \,, \tag{B.2}$$

$$S = \frac{1}{\sqrt{2}}(v_S + s + ia_S) \,. \tag{B.3}$$

in order to derive the squared mass matrices:

$$\mathcal{M}^2_{H^\pm} = \begin{pmatrix} \frac{v_2\left(v_S^2\lambda_{12S} - \lambda_4 v_1 v_2\right)}{2v_1} & \frac{1}{2}\left(\lambda_4 v_1 v_2 - v_S^2\lambda_{12S}\right) \\ \frac{1}{2}\left(\lambda_4 v_1 v_2 - v_S^2\lambda_{12S}\right) & \frac{v_1\left(v_S^2\lambda_{12S} - \lambda_4 v_1 v_2\right)}{2v_2} \end{pmatrix} \,, \tag{B.4}$$

$$\mathcal{M}^2_{A} = \begin{pmatrix} \frac{v_2 v_S^2\lambda_{12S}}{2v_1} & -\frac{v_S^2\lambda_{12S}}{2} & -v_2 v_S\lambda_{12S} \\ -\frac{v_S^2\lambda_{12S}}{2} & \frac{v_1 v_S^2\lambda_{12S}}{2v_2} & v_1 v_S\lambda_{12S} \\ -v_2 v_S\lambda_{12S} & v_1 v_S\lambda_{12S} & 2v_1 v_2\lambda_{12S} \end{pmatrix} \,, \tag{B.5}$$

which can be diagonalized by considering the characteristic polynomial in an eigenvalue equation:

$$\det\left(\mathcal{M}_i^2 - \mathbb{1}\lambda\right) = 0 \,. \tag{B.6}$$

The obtained eigenvalues correspond to the charged CP-even and neutral CP-odd masses. In the case of the charged CP-even eigenvalues, we acquire a charged Goldstone boson which is "eaten" by the $W^{\pm}$-bosons and a charged Higgs with a squared mass given by:

$$m_{H^{\pm}}^2 = \frac{1}{2}v_S^2\left(\frac{\left(t_\beta^2+1\right)\lambda_{12S}}{t_\beta} - \frac{\lambda_4 v^2}{v_S^2}\right). \tag{B.7}$$

For the CP-odd eigenvalues, we get two pseudo-Nambu-Goldstone bosons and one pseudoscalar Higgs. One of the two pseudo-Nambu-Goldstone bosons is "eaten" by Z-Boson while the other one corresponds to the axion which acquires a mass from the mixing with the neutral pion (see sec. 3.3.2). The pseudoscalar squared Higgs mass is given by:

$$m_A^2 = \frac{2\lambda_{12S}v_S^2}{1+t_\beta^2}\left(\frac{v^2}{v_S^2}t_\beta + \frac{\left(1+t_\beta^2\right)^2}{4t_\beta}\right). \tag{B.8}$$

We proceed with the CP-even scalar masses and derive the squared-mass matrix in the right basis by making an ansatz for the unitary rotation matrix R. The procedure is the following:

1.) Calculate the squared-mass matrix in the correct basis, i.e. the basis-vectors need to be specified with respect to the physical field basis given by (h, β, s):

$$\mathcal{M}_{0^+}'^2 = \begin{pmatrix} \left.\frac{\partial^2 V}{\partial h \partial h}\right|_{v,v_S} & \left.\frac{1}{h}\frac{\partial^2 V}{\partial h \partial \beta}\right|_{v,v_S} & \left.\frac{\partial^2 V}{\partial h \partial s}\right|_{v,v_S} \\ \left.\frac{1}{h}\frac{\partial^2 V}{\partial \beta \partial h}\right|_{v,v_S} & \left.\frac{1}{h^2}\frac{\partial^2 V}{\partial \beta \partial \beta}\right|_{v,v_S} & \left.\frac{1}{h}\frac{\partial^2 V}{\partial \beta \partial s}\right|_{v,v_S} \\ \left.\frac{\partial^2 V}{\partial s \partial h}\right|_{v,v_S} & \left.\frac{1}{h}\frac{\partial^2 V}{\partial s \partial \beta}\right|_{v,v_S} & \left.\frac{\partial^2 V}{\partial s \partial s}\right|_{v,v_S} \end{pmatrix}. \tag{B.9}$$

2.) Make use of the fact that $v/v_S \ll 1$ by factoring out v_S from $\mathcal{M}_{0^+}'^2$:

$$\mathcal{M}_{0^+}'^2 = \tag{B.10}$$
$$v_S^2\begin{pmatrix} \left(\frac{v}{v_S}\right)^2\frac{\left(\lambda_2 t_\beta^4 + 2\lambda_{34}t_\beta^2+\lambda_1\right)}{\left(t_\beta^2+1\right)^2} & \left(\frac{v}{v_S}\right)^2\frac{t_\beta\left((\lambda_2-\lambda_{34})t_\beta^2-\lambda_1+\lambda_{34}\right)}{\left(t_\beta^2+1\right)^2} & \left(\frac{v}{v_S}\right)\frac{\left(\lambda_{2S}t_\beta^2-2\lambda_{12S}t_\beta+\lambda_{1S}\right)}{t_\beta^2+1} \\ \left(\frac{v}{v_S}\right)^2\frac{t_\beta\left((\lambda_2-\lambda_{34})t_\beta^2-\lambda_1+\lambda_{34}\right)}{\left(t_\beta^2+1\right)^2} & \left(\frac{v}{v_S}\right)^2\frac{t_\beta^2(\lambda_1+\lambda_2-2\lambda_{34})}{\left(t_\beta^2+1\right)^2}+\frac{\left(t_\beta^2+1\right)\lambda_{12S}}{2t_\beta} & \left(\frac{v}{v_S}\right)\frac{\left(\left(t_\beta^2-1\right)\lambda_{12S}+t_\beta(\lambda_{2S}-\lambda_{1S})\right)}{t_\beta^2+1} \\ \left(\frac{v}{v_S}\right)\frac{\left(\lambda_{2S}t_\beta^2-2\lambda_{12S}t_\beta+\lambda_{1S}\right)}{t_\beta^2+1} & \left(\frac{v}{v_S}\right)\frac{\left(\left(t_\beta^2-1\right)\lambda_{12S}+t_\beta(\lambda_{2S}-\lambda_{1S})\right)}{t_\beta^2+1} & \lambda_S \end{pmatrix}.$$

3.) Choose the unitary matrix, cf. Ref. [27][1]

$$R = \exp\left\{ A\left(\frac{v}{v_S}\right) + B\left(\frac{v}{v_S}\right)^2 \right\}, \tag{B.11}$$

where $A, B \in \mathbb{R}^{3\times 3}$ with $A^T = -A$ and $B^T = -B$, to diagonalize the squared-mass matrix $\mathcal{M}'^2_{0^+}$.

4.) Match $A\left(\frac{v}{v_S}\right) + B\left(\frac{v}{v_S}\right)^2$ in powers of v/v_S with $\mathcal{M}'^2_{0^+}$:

$$A\left(\frac{v}{v_S}\right) + B\left(\frac{v}{v_S}\right)^2 = \begin{pmatrix} 0 & B_{12}\left(\frac{v}{v_S}\right)^2 & A_{13}\left(\frac{v}{v_S}\right) \\ -B_{12}\left(\frac{v}{v_S}\right)^2 & 0 & A_{23}\left(\frac{v}{v_S}\right) \\ -A_{13}\left(\frac{v}{v_S}\right) & -A_{23}\left(\frac{v}{v_S}\right) & 0 \end{pmatrix} \tag{B.12}$$

with $A_{12} = B_{13} = B_{23} = 0$.

5.) Diagonalize the squared-mass matrix by calculating:

$$\mathcal{D} = R^T \mathcal{M}'^2_{0^+} R \tag{B.13}$$

and expanding $\mathcal{D}$ up to second order in v/v_S, cf. Refs. [26, 27]

$$\mathcal{D} = \sum_{n=0}^{\infty} \frac{\partial^n}{\partial x^n}\left(R^T \mathcal{M}^2_{0^+} R\right)\Big|_{x=0} \frac{x^n}{n!}\Big|_{x=\left(\frac{v}{v_S}\right)} \simeq \tilde{\mathcal{D}} + \mathcal{O}\left(\left(\frac{v}{v_S}\right)^3\right) \tag{B.14}$$

$$\Rightarrow \quad \tilde{\mathcal{D}} = \begin{pmatrix} m_h^2/v_S^2 & 0 & 0 \\ 0 & m_H^2/v_S^2 & 0 \\ 0 & 0 & m_s^2/v_S^2 \end{pmatrix} = \begin{pmatrix} \tilde{\mathcal{D}}_{11} & \tilde{\mathcal{D}}_{12} & \tilde{\mathcal{D}}_{13} \\ \tilde{\mathcal{D}}_{12} & \tilde{\mathcal{D}}_{22} & \tilde{\mathcal{D}}_{23} \\ \tilde{\mathcal{D}}_{13} & \tilde{\mathcal{D}}_{23} & \tilde{\mathcal{D}}_{33} \end{pmatrix}. \tag{B.15}$$

6.) Utilize the fact that we have three equations $\left(\tilde{\mathcal{D}}_{12,13,23} \stackrel{!}{=} 0\right)$ for three parameters $(B_{12}, A_{13,23})$ and solve these equations for these parameters:

$$\tilde{\mathcal{D}}_{12,13,23} \stackrel{!}{=} 0 \implies B_{12}\,,\; A_{13,23}\,. \tag{B.16}$$

[1] This ansatz was introduced in Ref. [27] in order to diagonalize the neutral CP even squared mass matrix of the DFSZ model with a cubic term $\propto c\,\Phi_2^\dagger \Phi_1 S + h.c.$ instead of a quartic term.

7.) Use the results of B_{12}, $A_{13,23}$ to obtain $\tilde{\mathcal{D}}_{11,22,33}$ in order to calculate the masses:

$$\frac{m_h^2}{v_S^2} = \frac{\left(\frac{v}{v_S}\right)^2}{\left(1+t_\beta^2\right)^2}\left[\lambda_1 + t_\beta^4\,\lambda_2 + 2\,t_\beta^2\,\lambda_{34} - \frac{\left(\lambda_{1S} + t_\beta^2\,\lambda_{2S} - 2t_\beta\lambda_{12S}\right)^2}{\lambda_S}\right] + \mathcal{O}\left(\left(\frac{v}{v_S}\right)^4\right), \tag{B.17}$$

$$\frac{m_H^2}{v_S^2} = \frac{\left(1+t_\beta^2\right)\lambda_{12S}}{2t_\beta} + \frac{t_\beta}{\left(1+t_\beta^2\right)^2}\left[\frac{2\left(\left(\lambda_{1S}-\lambda_{2S}\right)t_\beta + \lambda_{12S}\left(1-t_\beta^2\right)\right)^2}{\lambda_{12S}\left(1+t_\beta^2\right) - 2t_\beta\lambda_S} + \left(\lambda_1+\lambda_2-2\lambda_{34}\right)t_\beta\right]\left(\frac{v}{v_S}\right)^2 + \mathcal{O}\left(\left(\frac{v}{v_S}\right)^4\right), \tag{B.18}$$

$$\frac{m_s^2}{v_S^2} = \lambda_S + \frac{t_\beta}{\left(1+t_\beta^2\right)^2}\left[\frac{\left(\lambda_{1S}+\lambda_{2S}t_\beta^2 - 2t_\beta\lambda_{12S}\right)^2}{\lambda_S} - \frac{2t_\beta^2\left(\left(\lambda_{1S}-\lambda_{2S}\right)t_\beta + \lambda_{12S}\left(1-t_\beta^2\right)\right)^2}{\lambda_{12S}\left(1+t_\beta^2\right) - 2t_\beta\lambda_S}\right]\left(\frac{v}{v_S}\right)^2 + \mathcal{O}\left(\left(\frac{v}{v_S}\right)^4\right). \tag{B.19}$$

These analytically derived masses are valid for **BP1**-**BP4** of section 3.9.

8.) The limit of small portal couplings ($\lambda_{1S,2S,12S} \ll 1$) represents the decoupling of the 2HDM from the PQ-scalar singlet. We choose the following ansatz for the unitary matrix R:

$$R = \exp\left\{M\left(\frac{v}{v_s}\right)^2\right\}, \tag{B.20}$$

which makes the components $\left(\mathcal{M}'^2_{0^+}\right)_{12,13,23}$ marginally small since they are weighted up to second order in v/v_s. Thus, we obtain

$$m_h^2 \approx \frac{v^2}{\left(1+t_\beta^2\right)^2}\left(\lambda_1 + \lambda_2 t_\beta^4 + 2\lambda_{34}t_\beta^2\right), \tag{B.21}$$

$$m_H^2 \approx \frac{v_S^2\lambda_{12S}\left(1+t_\beta^2\right)}{2t_\beta^2} + \frac{t_\beta^2\left(\lambda_1+\lambda_2-2\lambda_{34}\right)v^2}{\left(1+t_\beta^2\right)^2}, \tag{B.22}$$

$$m_s^2 \approx \lambda_S v_S^2, \tag{B.23}$$

which are represented by **BP4** of section 3.9.

C. Theoretical Constraints

We give the derivation of the two theoretical constraints, namely the BfB and the perturbative unitarity conditions for the 2hdSMASH model, which we specify in C.1 and C.2 respectively.

C.1. Bounded from Below Conditions

We derive the BfB conditions in 2hdSMASH by imposing copositivity (conditionally positive conditions) where the biquadratic form of the quartic scalar potential is positive on non-negative vectors. This is realized by applying Sylvester's criterion. We quote the copositivity condition from Refs. [31, 50] and Sylvester's criterion from Ref. [31] in the following:

Copositivity:
"A symmetric matrix A is copositive if the quadratic form $x^T Ax \geqslant 0$ for all vectors $x \geqslant 0$ in the non-negative orthant $\mathbb{R}^n_+$. (The notation $x \geqslant 0$ means that $x_i \geqslant 0$ for each $i = 0, \ldots, n$.) A symmetric matrix A is strictly copositive if the quadratic form $x^T Ax > 0$ for all vectors $x > 0$ in the non-negative orthant $\mathbb{R}^n_+$.", cf. Refs. [31, 50].

Sylvester's criterion:
"...for a symmetric matrix A to be positive semidefinite, the principal minors of A have to be non-negative. (The principal minors are determinants of the principal submatrices. The principal submatrices of A are obtained by deleting rows and columns of A in a symmetric way, i.e. if the $i_1, \ldots, i_k$ rows are deleted, then the $i_1, \ldots, i_k$ columns are deleted as well. The largest principal submatrix of A is A itself.) Thus if the matrix A is positive, all of its submatrices, in particular the diagonal elements a_{ii} have to be non-negative.", cf. Ref. [31].

Note that Sylvester's criterion is a necessary requirement for a matrix A to be copositive and by extension $V_4 > 0$. In order to utilize copositivity and thus Sylvester's

criterion, we write the quartic part of the scalar potential V_4:

$$V_4 = \frac{1}{8}\left(\lambda_1 h_1^4 + \lambda_2 h_2^4 + \lambda_S s^4\right) + \frac{1}{4}\left(h_1^2 h_2^2(\lambda_3 + \zeta_4\lambda_4) + \lambda_{1S} h_1^2 s^2 + \lambda_{2S} h_2^2 s^2 - 2\lambda_{12S}\zeta_{12S} h_1 h_2 s^2\right) > 0\,, \tag{C.1}$$

where

$$\Phi_1^\dagger \Phi_2 = \zeta_4 h_1 h_2 \;,\; \zeta_4 = \frac{\left|\Phi_1^\dagger \Phi_2\right|^2}{|\Phi_1|^2 |\Phi_2|^2}\,, \tag{C.2}$$

$$\Phi_1^\dagger \Phi_2 S^2 = \zeta_{12S} h_1 h_2 s^2 \;,\; \zeta_{12S} = \frac{\mathrm{Re}\left(\Phi_1^\dagger \Phi_2 S^2\right)}{|S|^2 |\Phi_1| |\Phi_2|} \tag{C.3}$$

with $\zeta_4 \in [0,1]$ and $\zeta_{12S} \in [-1,1]$. As a first step, we consider the biquadratic form by imposing $\lambda_{12S} = 0$:

$$V_4' \equiv V_4|_{\lambda_{12S}=0} = \begin{pmatrix} h_1^2 & h_2^2 & s^2 \end{pmatrix} \begin{pmatrix} \lambda_1 & \lambda_3 + \zeta_4\lambda_4 & \lambda_{1S} \\ \lambda_3 + \zeta_4\lambda_4 & \lambda_2 & \lambda_{2S} \\ \lambda_{1S} & \lambda_{2S} & \lambda_S \end{pmatrix} \begin{pmatrix} h_1^2 \\ h_2^2 \\ s^2 \end{pmatrix} > 0 \tag{C.4}$$

to obtain the necessary BFB conditions by applying Sylvester's criterion:

$$\begin{aligned} &\lambda_1 > 0 \;,\; \lambda_2 > 0 \;,\; \lambda_3 + \min\{0, \lambda_4\} > -\sqrt{\lambda_1 \lambda_2}\,, \\ &\lambda_S > 0 \;,\; \sqrt{\lambda_1 \lambda_S} > \lambda_{1S} > -\sqrt{\lambda_1 \lambda_S} \;,\; \sqrt{\lambda_2 \lambda_S} > \lambda_{2S} > -\sqrt{\lambda_2 \lambda_S} \\ &, \\ &\sqrt{\lambda_1 \lambda_2 \lambda_S} + \lambda_{2S}\sqrt{\lambda_1} + \lambda_{1S}\sqrt{\lambda_2} + (\lambda_3 + \min\{0, \lambda_4\})\sqrt{\lambda_S} \\ &+ \sqrt{2\left((\lambda_3 + \min\{0, \lambda_4\}) + \sqrt{\lambda_1 \lambda_2}\right)\left(\lambda_{1S} + \sqrt{\lambda_1 \lambda_S}\right)\left(\lambda_{2S} + \sqrt{\lambda_2 \lambda_S}\right)} > 0\,, \end{aligned} \tag{C.5}$$

where the last condition is given by the combination of the following two conditions[1] [31, 50]:

$$\det A > 0\,, \tag{C.6}$$

$$\sqrt{a_{11} a_{22} a_{33}} + a_{12}\sqrt{a_{33}} + a_{13}\sqrt{a_{22}} + a_{23}\sqrt{a_{11}} > 0 \tag{C.7}$$

[1] Either of the two conditions of eqns. (C.6)-(C.7) has to hold for $V_4' > 0$

with a_{ij} as the components of $A \in \mathbb{R}^{3\times3}$ where

$$A = \begin{pmatrix} \lambda_1 & \lambda_3 + \zeta_4\lambda_4 & \lambda_{1S} \\ \lambda_3 + \zeta_4\lambda_4 & \lambda_2 & \lambda_{2S} \\ \lambda_{1S} & \lambda_{2S} & \lambda_S \end{pmatrix}.$$

By considering the s-dependent portal terms of the quartic scalar potential with $\zeta_{12S} = \pm1$ we get:

$$\begin{aligned} V_4^{\text{Portal}} &= \lambda_{1S}h_1^2s^2 + \lambda_{2S}h_2^2s^2 - 2\left(\pm\lambda_{12S}h_1h_2s^2\right) \\ &= \begin{pmatrix} h_1s & h_2s \end{pmatrix} \begin{pmatrix} \lambda_{1S} & \mp\lambda_{12S} \\ \mp\lambda_{12S} & \lambda_{2S} \end{pmatrix} \begin{pmatrix} h_1s \\ h_2s \end{pmatrix} \end{aligned} \tag{C.8}$$

to obtain the sufficient BFB conditions:

$$\lambda_{1S} > 0 \ , \ \lambda_{2S} > 0 \ , \ \lambda_{1S}\lambda_{2S} - |\lambda_{12S}|^2 > 0\,. \tag{C.9}$$

It's important to note that the sufficient BfB conditions can be overly strict and therefore exclude parameter points which are BfB but do not pass these conditions. Sufficient BfB conditions ensure that $V_4 > 0$ but they are not necessary. For that reason we chose to break these sufficient BfB conditions and checked numerically whether individual parameter points are BfB. We have used the `Mathematica` package `BFB` by Ref. [30].

C.2. Perturbative Unitarity Bounds

The full tree-level perturbative unitarity constraints are calculated by requiring that the unique eigenvalues of the $2 \to 2$ scalar scattering matrix (scalar S-matrix) $\mathcal{M}_{2\to2}$ are below the upper bound of 8π (suggested in Refs. [32] and [33]). The following calculations are done by using the perturbative unitarity `Mathematica` package included in the directory of `ScannerS` which is described in Ref. [118]. Therefore we follow the calculations on perturbative unitarity of Ref. [118].

First, we need to derive the $2 \to 2$ scalar S-matrix which is given by:

$$\mathcal{M}_{AB\to CD} = \langle AB|\,\mathcal{M}\,|CD\rangle = \frac{1}{\sqrt{(1+\delta_{AB})\,(1+\delta_{CD})}}\frac{\partial^4 V_4}{\partial A\partial B\partial C\partial D}\,, \tag{C.10}$$

where the δ_{ij}- functions are necessary symmetry factors. Here, we have used the quartic scalar potential V_4 in the gauge eigenbasis $\left(h_{1,2}, s, h^{\pm}_{1,2}, a_{1,2,S}\right)$ which is given by the following field definition:

$$\Phi_1 = \begin{pmatrix} h_1^+ \\ \frac{1}{\sqrt{2}} \cdot (h_1 + v_1 + i \cdot a_1) \end{pmatrix} , \tag{C.11}$$

$$\Phi_2 = \begin{pmatrix} h_2^+ \\ \frac{1}{\sqrt{2}} \cdot (h_2 + v_2 + i \cdot a_2) \end{pmatrix} , \tag{C.12}$$

$$S = \frac{1}{\sqrt{2}} \cdot (s + v_S + i \cdot a_S) \, . \tag{C.13}$$

The resulting $2 \to 2$ scalar S-matrix $\mathcal{M}_{2\to 2}$ is block diagonal and its eigenvalues $\mathcal{M}^i_{2\to 2}$ for $i = \{1, \ldots, n\}$ are bounded by 8π:

$$\left| \mathcal{M}^i_{2\to 2} \right| < 8\pi \, . \tag{C.14}$$

It's important to note that the eigenvalues are basis independent since unitary transformations are basis independent (see Ref.[118, 119] for details). Part of the eigenvalues reproduce the same eigenvalues for a soft $U(1)$-symmetric 2HDM in the absence of the PQ-scalar s:

$$e_{1,2,3} = \lambda_{1,2,3} \, , \tag{C.15}$$

$$e_4 = \lambda_3 - \lambda_4 \, , \tag{C.16}$$

$$e_5 = \lambda_3 + \lambda_4 \, , \tag{C.17}$$

$$e_{\pm} = \frac{1}{2} \left(\lambda_1 + \lambda_2 \pm \sqrt{(\lambda_1 - \lambda_2)^2 + 4\lambda_4^2} \right) . \tag{C.18}$$

By including the PQ-scalar s we get the following additional eigenvalues:

$$s_{1,2} = \lambda_{1S,2S} \, , \tag{C.19}$$

$$s_{3\pm} = \frac{1}{2} \left(\lambda_{1S} + \lambda_{2S} \pm \sqrt{16\lambda^2_{12S} + (\lambda_{1S} - \lambda_{2S})^2} \right) , \tag{C.20}$$

$$s_{4\pm} = \frac{1}{2} \left(\lambda_3 + 2\lambda_4 + \lambda_S \pm \sqrt{16\lambda^2_{12S} + (\lambda_3 + 2\lambda_4 - \lambda_S)^2} \right) , \tag{C.21}$$

$$\frac{1}{2} k_{1,2,3} \, , \tag{C.22}$$

where the eigenvalues $\frac{1}{2}|k_{1,2,3}|$ are the real roots of the following cubic potential:

$$\frac{1}{2}\left(48\lambda_1\lambda_{2S}^2+48\lambda_{1S}^2\lambda_2-144\lambda_1\lambda_2\lambda_S-64\lambda_{1S}\lambda_{2S}\lambda_3-32\lambda_{1S}\lambda_{2S}\lambda_4+64\lambda_3^2\lambda_S\right) \tag{C.23}$$
$$+\frac{1}{2}\left(64\lambda_3\lambda_4\lambda_S+16\lambda_4^2\lambda_S+x\left(36\lambda_1\lambda_2+24\lambda_1\lambda_S-8\lambda_{1S}^2+24\lambda_2\lambda_S-8\lambda_{2S}^2\right)\right)$$
$$-\frac{x}{2}\left(\lambda_3^2-16\lambda_3\lambda_4-4\lambda_4^2\right)+\frac{1}{2}\left(x^2(-6\lambda_1-6\lambda_2-4\lambda_S)+x^3\right).$$

Taking the absolute value of all eigenvalues, we obtain the full tree-level perturbative unitarity conditions for 2hdSMASH:

$$|\lambda_{1,2,3,1S,2S}|<8\pi\,, \tag{C.24}$$
$$|\lambda_3\pm\lambda_4|<8\pi\,, \tag{C.25}$$
$$\left|\frac{1}{2}\left(\lambda_1+\lambda_2\pm\sqrt{(\lambda_1-\lambda_2)^2+4\lambda_4^2}\right)\right|<8\pi\,, \tag{C.26}$$
$$\left|\frac{1}{2}\left(\lambda_{1S}+\lambda_{2S}\pm\sqrt{16\lambda_{12S}^2+(\lambda_{1S}-\lambda_{2S})^2}\right)\right|<8\pi\,, \tag{C.27}$$
$$\left|\frac{1}{2}\left(\lambda_3+2\lambda_4+\lambda_S\pm\sqrt{16\lambda_{12S}^2+(\lambda_3+2\lambda_4-\lambda_S)^2}\right)\right|<8\pi\,, \tag{C.28}$$
$$\frac{1}{2}\,|k_{1,2,3}|<8\pi\,. \tag{C.29}$$

D. Derived Quantities for Inflation in 2hdSMASH

All results in this appendix are expressed in terms of a mixing parameter b which distinguishes between mixed and non-mixed field space directions

$$b = \begin{cases} b_i & \text{(mixed)} \\ 1 & \text{(non-mixed)} \end{cases} \tag{D.1}$$

where b_i are the mixing parameters[1] given in sections 4.3.1-4.3.2 and correspond to the four mixed field space directions, i.e. h_{12}, sh_1, sh_2 and sh_{12}. This allows us to give the most general result w.r.t. field space directions. During our discussion we will note at appropriate passages the non-mixed results as well.

D.1. Deriving $N(\phi)$ in the potential slow-roll approximation

We can approximate N in a very simple way by starting with the first cosmological slow-roll parameter:

$$\epsilon \equiv -\frac{\dot{\mathcal{H}}}{\mathcal{H}^2} = \frac{1}{2M_p^2}\frac{\dot{\chi}^2}{\mathcal{H}^2} \tag{D.2}$$

with Hubble parameter given by:

$$\mathcal{H}^2 = \frac{1}{3M_p^2}\left(\frac{1}{2}\dot{\chi}^2 + V\right). \tag{D.3}$$

By taking the time derivative of $\mathcal{H}$ we get

$$\dot{\mathcal{H}} = -\frac{1}{2}\frac{\dot{\chi}^2}{M_p^2}, \tag{D.4}$$

[1] This concept was introduced in Ref. [7].

where we inserted the relation from the equation of motion:

$$\ddot{\chi} + 3\mathcal{H}\dot{\chi} + \frac{\partial V}{\partial \chi}\,. \tag{D.5}$$

From the relation of eq. (D.2) we get:

$$\frac{\dot{\chi}^2}{\mathcal{H}^2} = 2M_p^2\epsilon \quad \text{with} \quad \dot{\chi}^2 = \left(\frac{d\chi}{dt}\right)^2 . \tag{D.6}$$

By additionally using the relation $dN = -Hdt$ we get:

$$\chi'^2 = 2M_p^2\epsilon \quad \text{with} \quad \chi'^2 = \left(\frac{d\chi}{dN}\right)^2 , \tag{D.7}$$

which leads to:

$$\frac{d\chi}{dN} = M_p\sqrt{2\epsilon} \Longrightarrow \boxed{N = \frac{1}{M_p}\int \frac{d\chi}{\sqrt{2\epsilon}}}\,. \tag{D.8}$$

Recalling that ϵ can be approximated by the potential slow-roll parameter $\epsilon \approx \epsilon_V$ we get:

$$N \simeq \frac{1}{M_p}\int \frac{d\chi}{\sqrt{2\epsilon_V}}\,. \tag{D.9}$$

Now, we transform the expression from $\epsilon_V(\chi)$ to $\epsilon_V(\phi)$:

$$\frac{dV}{d\chi} = \frac{dV}{d\phi}\frac{d\phi}{d\chi} \Longrightarrow \epsilon_V(\phi) = \frac{M_p^2}{2}\left(\frac{V'(\phi)}{V(\phi)}\frac{d\phi}{d\chi}\right)^2 . \tag{D.10}$$

This gives us the following expression for N:

$$N \simeq \frac{1}{M_p^2}\int d\phi \frac{V(\phi)}{V'(\phi)}\left(\frac{d\chi}{d\phi}\right)^2 , \tag{D.11}$$

where we have used the fact that $d\chi = \dfrac{d\chi}{d\phi}d\phi$. This allows us to derive a general expression for N in the slow-roll approximation without making any assumptions about the non-minimal coupling ξ. Therefore the expression for the integrand of N is given by:

$$\frac{V}{V'(\phi)}\left(\frac{d\chi}{d\phi}\right)^2 = \frac{\phi}{4} + \frac{6\xi^2\phi^3}{4\left(bM_p^2 + \xi\phi^2\right)} \tag{D.12}$$

and thus leading to:

$$N = \frac{\phi^2}{8M_p^2} + \frac{1}{M_p^2}\int \frac{6\xi^2\phi^3}{4\left(b\,M_p^2 + \xi\phi^2\right)}d\phi \tag{D.13}$$
$$= \frac{\phi^2}{8M_p^2} + \frac{3\xi\phi^2}{4M_p^2}\log\left(b + \frac{\xi\phi^2}{M_p^2}\right) - \frac{3}{4}\int \log\left(b + x\right)dx\,,$$

where in the last step partial integration was performed with the substitution rule $x \equiv \frac{\xi\phi^2}{M_p^2}$. By using this substitution rule again and by using the following integral relation integral:

$$\int \log\left(b + x\right)dx = (x + b)\log\left(b + x\right) - x \tag{D.14}$$

we get:

$$\boxed{N = \frac{1 + 6\xi}{8M_p^2}\phi^2 - \frac{3\,b}{4}\log\left(b + \frac{\xi\phi^2}{M_p^2}\right)}. \tag{D.15}$$

Inserting the boundaries gives us:

$$\Delta N \simeq \frac{1}{M_p^2}\int_{\phi_E}^{\phi_I} d\phi \frac{V(\phi)}{V'(\phi)}\left(\frac{d\chi}{d\phi}\right)^2 \tag{D.16}$$

$$\Longrightarrow \boxed{\Delta N \simeq \frac{1 + 6\xi}{8M_p^2}\left(\phi_I^2 - \phi_E^2\right) - \frac{3\,b}{4}\log\left(\frac{b\,M_p^2 + \xi\phi_I^2}{b\,M_p^2 + \xi\phi_E^2}\right)}. \tag{D.17}$$

D.2. Approximating $N(\phi)$ with L'Hospital's rule

In order to acquire a simpler expression for $N(\phi)$ from eq. (D.15), we prove with L'Hospitals rule that such an approximation is justified. There are two competing terms to consider in the expression for the number of e-folds

$$N = \frac{1 + 6\xi}{8M_p^2}\phi^2 - \frac{3\,b}{4}\log\left(b + \frac{\xi\phi^2}{M_p^2}\right)\,. \tag{D.18}$$

Our hypothesis is the following approximation

$$N \simeq \frac{1 + 6\xi}{8M_p^2}\phi^2\,. \tag{D.19}$$

By applying L'Hospital's rule, we are able to determine the limit of the ratio of the two terms of eq. (D.15).

Proof. Let $f, g : I \to \mathbb{R}$ be two differentiable functions defined on an interval $I =]x_1, x_2[$, $(-\infty \leq x_1 < x_2 \leq \infty)$ with $g'(x) \neq 0$ for all $x \in I$ for which the limit

$$\lim_{x \to b} \frac{f'(x)}{g'(x)} := c \in \mathbb{R} \tag{D.20}$$

exists. Then, this leads to the following limit:

$$\lim_{x \to b} \frac{f(x)}{g(x)} = \lim_{x \to b} \frac{f'(x)}{g'(x)} := c \in \mathbb{R}\,. \tag{D.21}$$

By association the functions read

$$f(\xi) = \frac{3\,b}{4} \log\left(b + \frac{\xi \phi^2}{M_p^2}\right), \tag{D.22}$$

$$g(\xi) = \frac{(1 + 6\xi)\,\phi^2}{8 M_p^2}, \tag{D.23}$$

for which we get with L'Hospital's rule and $\alpha \in [0, \infty)$:

$$\lim_{\xi \to \alpha} \frac{\frac{3}{4} \log\left(1 + \frac{\xi \phi^2}{M_p^2}\right)}{\frac{(1 + 6\xi)\,\phi^2}{8 M_p^2}} = \lim_{\xi \to \alpha} \frac{1}{1 + \frac{\xi \phi^2}{M_p^2}} = \begin{cases} 0, & \text{if } \alpha \to \infty \\ 1, & \text{if } \alpha \to 0 \end{cases}. \tag{D.24}$$

Hence, $\exists L$ with $0 \leq L \leq 1$ defined as:

$$\lim_{\xi \to \alpha} \frac{1}{1 + \frac{\xi \phi^2}{M_p^2}} := L\,. \tag{D.25}$$

Therefore, we have an upper limit with $L \leq 1$ and we get:

$$\frac{3}{4} \log\left(1 + \frac{\xi \phi^2}{M_p^2}\right) \leq \frac{(1 + 6\xi)\,\phi^2}{8 M_p^2} \quad \forall \xi \in [0, \infty)\,. \tag{D.26}$$

□

D.3. Deriving A_s, n_s and r in the Large Non-Minimal Coupling Limit

We consider a general inflaton field ϕ and its canonically normalized field χ. The canonical transformation from ϕ to χ is given by

$$\frac{d\chi}{d\phi} = \sqrt{\frac{b\left(b + \frac{\phi^2}{M_p^2}\left(\xi + 6\xi^2\right)\right)}{\left(b + \frac{\xi\phi^2}{M_p^2}\right)^2}}. \tag{D.27}$$

In the large non-minimal coupling limit we consider $\xi \gg 1$ and obtain

$$\frac{d\chi}{d\phi} \simeq \sqrt{\frac{\frac{6\xi^2\phi^2 b}{M_p^2} + \mathcal{O}\left(\xi\right)}{\left(b + \frac{\xi\phi^2}{M_p^2}\right)^2}} \simeq \frac{\sqrt{6}\xi\phi}{M_p}\frac{b}{b + \frac{\xi\phi^2}{M_p^2}}.$$

With the help of

$$\begin{aligned} \frac{d\chi}{d\phi} &= \frac{d\chi}{d\Omega^2}\frac{d\Omega^2}{d\phi} \\ \Rightarrow \frac{d\chi}{d\Omega^2} &= \frac{d\chi}{d\phi}\frac{d\phi}{d\Omega^2} \end{aligned} \tag{D.28}$$

we get the canonically normalized field $\chi(\phi)$ by integration:

$$\begin{aligned} \frac{d\chi}{d\Omega^2} &\simeq \sqrt{\frac{3}{2}} M_p \frac{1}{\Omega^2} \\ \Rightarrow \chi(\phi) &\simeq \sqrt{\frac{3}{2}} M_p \log\left(b + \frac{\xi\phi^2}{M_p^2}\right). \end{aligned} \tag{D.29}$$

By inverting the function, we acquire $\phi(\chi)$:

$$\phi(\chi) \simeq \frac{M_p}{\sqrt{\xi}}\sqrt{\exp\left(\sqrt{\frac{2}{3}}\frac{\chi}{M_p}\right) - b} \tag{D.30}$$

which can be used to determine the scalar potential in Einstein frame[2]

$$V_E(\chi) = \frac{\lambda\phi^4(\chi)}{\Omega^4} \simeq \frac{\lambda}{8\xi^2} M_p^4 \left(1 - b\exp\left(-\sqrt{\frac{2}{3}}\frac{\chi}{M_p}\right)\right)^2 . \tag{D.31}$$

Its first and second derivates w.r.t. χ are thus given by

$$V_E'(\chi) \simeq -\frac{\lambda M_p^3 b}{2\sqrt{6}\xi^2} \exp\left(-\sqrt{\frac{2}{3}}\frac{\chi}{M_p}\right)\left(b - \exp\left(-\sqrt{\frac{2}{3}}\frac{\chi}{M_p}\right)\right) , \tag{D.32}$$

$$V_E''(\chi) \simeq -\frac{\lambda M_p^2 b}{6\xi^2} \exp\left(-\sqrt{\frac{2}{3}}\frac{\chi}{M_p}\right)\left(1 - 2b\exp\left(-\sqrt{\frac{2}{3}}\frac{\chi}{M_p}\right)\right) . \tag{D.33}$$

Hence, we can now calculate the first slow-roll parameter ϵ_V in slow-roll approximation:

$$\epsilon_V \simeq \frac{4b^2}{3}\left(\exp\left(\sqrt{\frac{2}{3}}\frac{\chi}{M_p}\right) - b\right)^{-2} , \tag{D.34}$$

and the second slow-roll parameter η_V in slow-roll approximation:

$$\eta_V \simeq \frac{4b}{3}\left(2b - \exp\left(\sqrt{\frac{2}{3}}\frac{\chi}{M_p}\right)\right)\left(\exp\left(\sqrt{\frac{2}{3}}\frac{\chi}{M_p}\right) - b\right)^{-2} . \tag{D.35}$$

The inflationary observables are calculated in slow-roll approximation to

$$A_s = \frac{1}{24\pi^2 M_{Pl}^4}\frac{V}{\epsilon_V} \ , \ n_s = 1 - 6\epsilon_V + 2\eta_V \ , \ r = 16\epsilon_V . \tag{D.36}$$

With the above slow-roll parameters in large ξ limit, we can now calculate A_s, n_s and r:

$$\boxed{A_s \simeq \frac{\lambda}{128\pi^2\xi^2\, b}\exp\left(-2\sqrt{\frac{2}{3}}\frac{\chi}{M_p}\right)\left(1 - b\ \exp\left(\sqrt{\frac{2}{3}}\frac{\chi}{M_p}\right)\right)^4} , \tag{D.37}$$

[2]We denote the Einstein frame scalar potential with subscript "E".

$$\boxed{n_s \simeq 1 - \frac{8\,b}{3}\frac{b + \exp\left(\sqrt{\frac{2}{3}}\frac{\chi}{M_p}\right)}{\left(b - \exp\left(\sqrt{\frac{2}{3}}\frac{\chi}{M_p}\right)\right)^2}}\,, \tag{D.38}$$

$$\boxed{r \simeq \frac{64\,b^2}{3\left(\exp\left(\sqrt{\frac{2}{3}}\frac{\chi}{M_p}\right) - b\right)^2}}\,. \tag{D.39}$$

D.4. Derivation of the Canonically Normalized Equation of Motion

The dynamics of the canonically normalized background field is characterized by $\chi(N)$. As a first step, we derive the Euler-Lagrange equation by varying the action

$$\frac{\delta S}{\delta \chi} = 0 \Rightarrow \frac{\partial \mathcal{L}}{\partial \chi} - \partial_\mu \left(\frac{\partial \mathcal{L}}{\partial\left(\partial_\mu \chi\right)}\right) = 0\,. \tag{D.40}$$

Now, we can write down the Klein-Gordon equation from eq. (D.40)

$$\ddot{\chi} + 3\mathcal{H}\dot{\chi} + V_\chi = 0\,, \tag{D.41}$$

where V_χ describes the derivative of the potential with respect to the field χ.

Using the relation $dN = -\mathcal{H}dt$, we can transform each time derivatives into derivatives with respect to N:

$$\dot{\chi} = \mathcal{H}\chi'\,, \tag{D.42}$$

$$\ddot{\chi} = \mathcal{H}^2\chi'' + \mathcal{H}\mathcal{H}'\chi'\,, \tag{D.43}$$

where primes denote N derivatives. With ϵ expressed in terms of N,

$$\epsilon = -\frac{\mathcal{H}'}{\mathcal{H}}\,, \tag{D.44}$$

and the Hubble rate expressed as

$$\mathcal{H}^2 = \frac{V}{M_p^2(3-\epsilon)}\,, \tag{D.45}$$

we get the following Klein-Gordon equation:

$$\chi'' + 3\chi' - \frac{1}{2M_p^2}\chi'^3 + \left(3M_p - \frac{\chi'^2}{2M_p}\right)\sqrt{2\epsilon} = 0\,. \tag{D.46}$$

D.5. Derivation of $A_s(N)$, $n_s(N)$ and $r(N)$ in Covariant Formalism

In this section we briefly discuss the covariant formalism in the effective single field inflationary model in order to derive the e-fold-dependent inflationary observables $A_s(N)$, $n_s(N)$ and $r(N)$.
We start with the general covariant formalism in a multi field model which we reduce later to an effective single field model. The first slow-roll parameter can be written as

$$\epsilon = \frac{\mathcal{G}_{ij}\phi'^i\phi'^j}{2M_p^2} \tag{D.47}$$

with $\mathcal{G}_{ij}$ as the field space metric. In slow-roll approximation, the potential first slow-roll parameter ϵ_V is thus given by:

$$\epsilon_V = \frac{M_p^2}{2}\frac{\mathcal{G}^{ij}V_{\phi^i}V_{\phi^j}}{V^2} \tag{D.48}$$

with the inverse metric $\mathcal{G}^{ij}$ for which $\mathcal{G}_{ij}\mathcal{G}^{ij} = \mathcal{G}^{ij}\mathcal{G}_{ij} = 1$ holds. This can be applied to an effective single field model where we choose a certain field direction, i.e. 2HDM-, PQ- or mixed direction, and describe for simplicity the non-canonical field by ϕ and use a general description non-minimal couplings. Then the first slow-roll parameter reads

$$\epsilon = \frac{\mathcal{G}_{\phi\phi}\phi'^2}{2M_p^2}\,, \tag{D.49}$$

$$\epsilon_V = \frac{M_p^2}{2}\frac{\mathcal{G}^{\phi\phi}V_\phi^2}{V^2(\phi)}\,, \tag{D.50}$$

with $\mathcal{G}_{\phi\phi}$ as the field space metric for ϕ in either field space direction and $\mathcal{G}^{\phi\phi}$ as its inverse. Each field space direction is therefore represented by $\mathcal{G}_{\phi\phi}$ with the appropriate non-minimal coupling ξ,

$$\mathcal{G}_{\phi\phi} = \frac{b}{\Omega^4}\left(\Omega^2 + \frac{6\xi^2\phi^2}{M_p^2}\right) \tag{D.51}$$

with frame function Ω^2 given by

$$\Omega^2 = b + \frac{\xi\phi^2}{M_p^2}\,. \tag{D.52}$$

If we were to transform from ϕ to χ, we would just have to use the following relation

$$G_{\chi\chi} = G_{\rho\rho}\left(\frac{d\rho}{d\chi}\right)^2 = G_{\rho\rho}G^{\rho\rho} = 1 \tag{D.53}$$

which results to $G_{\chi\chi} = 1$ as expected.

The Klein-Gordon equation in covariant formalism for the non-canonical field ϕ is expressed in terms of covariant time derivates given as

$$\mathcal{D}_t\dot{\phi}^i + 3\mathcal{H}\dot{\phi}^i + \mathcal{G}^{ij}V_\phi = 0 \tag{D.54}$$

with

$$\mathcal{D}_t\dot{\phi}^i \equiv \frac{d\dot{\phi}^i}{dt} + \Gamma^i_{ab}\dot{\phi}^a\dot{\phi}^b \tag{D.55}$$

as the covariant time derivative and Γ^i_{ab} as the Christoffel symbol given by

$$\Gamma^i_{ab} = \Gamma^i_{ab} = \frac{1}{2}\mathcal{G}^{ic}\left(\partial_b\mathcal{G}_{ca} + \partial_a\mathcal{G}_{cb} - \partial_c\mathcal{G}_{ab}\right)\,. \tag{D.56}$$

By using the relation $dN = -Hdt$ and by implementing eq. (D.47) in eq. (D.55) we get the general Klein-Gordon equation for the inflaton ϕ w.r.t. to derivates of N,

$$\phi''^i + \Gamma^i_{ab}\phi'^a\phi'^b + \phi'^i\left(3-\epsilon\right) + \frac{\mathcal{G}^{ij}V_j}{\mathcal{H}^2} = 0\,, \tag{D.57}$$

where $\mathcal{H}$ is the Hubble rate defined as

$$\mathcal{H}^2 = \frac{V}{M_p^2\left(3-\epsilon\right)} \tag{D.58}$$

and ϵ is the slow-roll parameter defined in eq. (D.47).

Since we are solely interested in effective single field inflation, the Klein-Gordon equation for ϕ w.r.t. derivatives of N reduces to

$$\phi''^i + \Gamma^{\phi}_{\phi\phi}\phi'^2 + \phi'\,(3-\epsilon) + \frac{\mathcal{G}^{\phi\phi}V_\phi}{\mathcal{H}^2} = 0 \tag{D.59}$$

with Christoffel symbol for the inflaton in either field space direction given by

$$\Gamma^{\phi}_{\phi\phi} = -\frac{\xi\phi\left(bM_p^2(1-6\xi)+\xi\phi^2(6\xi+1)\right)}{\left(bM_p^2+\xi\phi^2\right)\left(bM_p^2+\xi\phi^2(6\xi+1)\right)}\,. \tag{D.60}$$

The Klein-Gordon equation given in eq. (D.59) can only be solved numerically. However, we can use the slow-roll approximation to simplify the expressions in (D.59) and thus find an analytic solution. As a first step, we determine the inflaton's field value at the end of inflation[3], i.e. ϕ_E, which can be obtained by setting $\epsilon_V \simeq 1$. ϵ_V is given by

$$\epsilon_V = \frac{M_p^2}{2}\frac{\mathcal{G}^{\phi\phi}V_\phi^2}{V^2(\phi)} = \frac{8M_p^4\,b}{\phi^2\left(b\,M_p^2+\xi\,(1+6\xi)\,\phi^2\right)} \tag{D.61}$$

which gives us

$$\begin{aligned}\phi_E^2 &\simeq \frac{b\,M_p^2\left(\sqrt{\frac{32\xi(6\xi+1)}{b}+1}-1\right)}{2\xi(6\xi+1)} \\ &= \frac{16M_p^2\,b\left(\sqrt{\frac{(8\xi+1)(24\xi+1)-1}{b}+1}-1\right)}{\left(\sqrt{(8\xi+1)(24\xi+1)}-1\right)\left(\sqrt{(8\xi+1)\,(24\xi+1)}+1\right)}\end{aligned} \tag{D.62}$$

where we used in the last step of the equation the following relations

$$32\xi(6\xi+1) = (8\xi+1)(24\xi+1)-1\,, \tag{D.63}$$

$$2\xi(6\xi+1) = \frac{16}{\left(\sqrt{(8\xi+1)(24\xi+1)}-1\right)\left(\sqrt{(8\xi+1)\,(24\xi+1)}+1\right)}\,. \tag{D.64}$$

[3]We denote subscript "E" as the field value at the end of Inflation and subscript "I" as the field value at the beginning of Inflation.

This simplifies for the non-mixed field space directions to

$$\phi_E^2 \simeq \frac{16M_p^2}{\sqrt{(8\xi+1)\,(24\xi+1)}+1}\,. \tag{D.65}$$

In a second step, we want to relate the inflaton field ϕ with the number of e-folds N. In appendix D.1 we have derived an approximate expression for N which is given by eq. (D.17)

$$\Delta N \simeq \frac{1+6\xi}{8M_p^2}\left(\phi_I^2-\phi_E^2\right)-\frac{3\,b}{4}\log\left(\frac{b\;M_p^2+\xi\phi_I^2}{b\;M_p^2+\xi\phi_E^2}\right)\,. \tag{D.66}$$

This expression can be further simplified by applying L'Hospitals rule where the log-term can be neglected[4]. Thus, we can approximate the number of e-folds as follows

$$\Delta N \simeq \frac{1+6\xi}{8M_p^2}\left(\phi_I^2-\phi_E^2\right)\,. \tag{D.67}$$

With ΔN from eq. (D.67), we acquire an expression for $\phi(\Delta N)$

$$\phi^2(\Delta N) \simeq \frac{8M_p^2}{1+6\xi}\Delta N+\frac{M_p^2\;b\left(\sqrt{\frac{32\xi(6\xi+1)}{b}+1}-1\right)}{2\xi(6\xi+1)} \tag{D.68}$$

which reduces to

$$\phi^2(\Delta N) \simeq \frac{8M_p^2}{1+6\xi}\Delta N+\frac{16M_p^2}{\sqrt{1+32\xi\,(1+6\xi)}+1} \tag{D.69}$$

for non-mixed directions. In order to determine the A_s, n_s and r w.r.t. ΔN we need to determine $\epsilon_V(\Delta N)$

$$\epsilon_V(\Delta N) = \frac{b(1+6\xi)}{\Delta N\,(b+8\Delta N\xi)}\,, \tag{D.70}$$

where we used the approximation given by:

$$\phi^2\,(\Delta N) \approx \frac{8M_p^2\Delta N}{1+6\xi}+\mathcal{O}\left(\phi_E^2\right) \approx \frac{8M_p^2\Delta N}{b(1+6\xi)} \tag{D.71}$$

[4]We give a proof in appendix D.2.

since $\phi_E^2 < \phi_I^2$ at horizon crossing. This approximation will be used for the following computations as well. The second slow-roll parameter η is given by

$$\eta = \epsilon + \frac{1}{2\epsilon}\epsilon' , \tag{D.72}$$

where we insert $\epsilon_V(\Delta N)$ of eq. (D.70) into η to acquire $\eta(\Delta N)$:

$$\eta\left(\Delta N\right) \simeq \frac{b(1+12\xi) - 16\Delta N\xi}{2\Delta N\left(b + 8\Delta N\xi\right)} . \tag{D.73}$$

With this at hand, we can now compute the scalar perturbation amplitude $A_s(\Delta N)$, the spectral index $n_s(\Delta N)$ and the tensor-to-scalar ratio $r(\Delta N)$

$$n_s\left(\Delta N\right) = 1 - 4\epsilon_V\left(\Delta N\right) + 2\eta\left(\Delta N\right) , \tag{D.74}$$

$$r = 16\epsilon_V(\Delta N) , \tag{D.75}$$

$$A_s = \frac{1}{24\pi^2}\frac{V(\phi(\Delta N))}{\epsilon_V(\Delta N)M_p^4} , \tag{D.76}$$

for which we get:

$$\boxed{n_s\left(\Delta N\right) \simeq 1 - \frac{b(3+12\xi) + 16\Delta N\xi}{\Delta N\left(b + 8\Delta N\xi\right)}} , \tag{D.77}$$

$$\boxed{A_s(\Delta N) \simeq \frac{\lambda\Delta N^3\left(b + 8\Delta N\xi\right)}{3\pi^2 b(1+6\xi)\left(1 + (6 + 8\Delta N)\xi\right)^2}} , \tag{D.78}$$

$$\boxed{r \simeq 16\frac{b(1+6\xi)}{\Delta N\left(b + 8\Delta N\xi\right)}} . \tag{D.79}$$

This reduces to

$$\boxed{n_s\left(\Delta N\right) \simeq 1 - \frac{3 + 12\xi + 16\Delta N\xi}{\Delta N\left(1 + 8\Delta N\xi\right)}} , \tag{D.80}$$

$$\boxed{A_s(\Delta N) \simeq \frac{\lambda\Delta N^3\left(1 + 8\Delta N\xi\right)}{3\pi^2(6\xi+1)\left((6\xi+1) + 8\Delta N\xi\right)^2}} , \tag{D.81}$$

$$\boxed{r \simeq 16\frac{(1+6\xi)}{\Delta N\left(1 + 8\Delta N\xi\right)}} , \tag{D.82}$$

for the non-mixed directions.

E. Renormalisation Group Equations

In the following is the full list of one-loop RGEs in the 2hdSMASH model[1]:

$$\mathcal{D}M_{11}^2 = M_{11}^2\left(6\lambda_1 - \frac{3}{2}g_1^2 - \frac{9}{2}g_2^2 + 6Y_t^2\right) + M_{22}^2\left(4\lambda_3 + 2\lambda_4\right) + M_{SS}^2 2\lambda_{1S}, \tag{E.1}$$

$$\begin{aligned}\mathcal{D}M_{22}^2 = {} & M_{22}^2\left(6\lambda_2 - \frac{3}{2}g_1^2 - \frac{9}{2}g_2^2 + 6Y_b^2 + 2Y_\tau^2 + 2\mathrm{Tr}\left(Y_\nu^\dagger Y_\nu\right)\right) \\ & + M_{11}^2\left(4\lambda_3 + 2\lambda_4\right) + M_{SS}^2 2\lambda_{2S},\end{aligned} \tag{E.2}$$

$$\mathcal{D}M_{SS}^2 = M_{SS}^2\left(4\lambda_S + \mathrm{Tr}\left(Y_N^\dagger Y_N\right)\right) + M_{11}^2 4\lambda_{1S} + M_{22}^2 4\lambda_{2S}, \tag{E.3}$$

$$\mathcal{D}\langle S\rangle^2 = -\mathrm{Tr}\left(Y_N^\dagger Y_N\right)\langle S\rangle^2 \quad \text{[i.e. the wave function renormalisation]}, \tag{E.4}$$

$$\mathcal{D}g_{\{1,2,3\}} = \{7,-3,-7\}g_{\{1,2,3\}}^3, \tag{E.5}$$

$$\mathcal{D}\lambda_1 = \frac{3}{4}g_1^4 + \frac{3}{2}g_1^2 g_2^2 + \frac{9}{4}g_2^4 - \lambda_1\left(3g_1^2 + 9g_2^2\right) + 12\lambda_1^2 \tag{E.6}$$

$$\begin{aligned}& + 4\lambda_3\lambda_4 + 4\lambda_3^2 + 2\lambda_4^2 + 2\lambda_{1S}^2 + 12\lambda_1 Y_b^2 - 12Y_b^4 \\ & + 4\lambda_1 Y_\tau^2 - 4Y_\tau^4 + 4\lambda_2\mathrm{Tr}\left(Y_\nu^\dagger Y_\nu\right) - 4\mathrm{Tr}\left(Y_\nu^\dagger Y_\nu Y_\nu^\dagger Y_\nu\right),\end{aligned} \tag{E.7}$$

$$\begin{aligned}\mathcal{D}\lambda_2 = {} & \frac{3}{4}g_1^4 + \frac{3}{2}g_1^2 g_2^2 + \frac{9}{4}g_2^4 - \lambda_2\left(3g_1^2 + 9g_2^2\right) + 12\lambda_2^2 \\ & + 4\lambda_3\lambda_4 + 4\lambda_3^2 + 2\lambda_4^2 + 2\lambda_{2S}^2 + 12\lambda_2 Y_t^2 - 12Y_t^4,\end{aligned} \tag{E.8}$$

$$\begin{aligned}\mathcal{D}\lambda_3 = {} & \frac{3}{4}g_1^4 - \frac{3}{2}g_1^2 g_2^2 + \frac{9}{4}g_2^4 - \lambda_3\left(3g_1^2 + 9g_2^2\right) + \left(6\lambda_3 + 2\lambda_4\right)\left(\lambda_1 + \lambda_2\right) \\ & + 4\lambda_3^2 + 2\lambda_4^2 + 2\lambda_{1S}\lambda_{2S} + \lambda_3\left(6Y_t^2 + 6Y_b^2 + 2Y_\tau^2 + 2\mathrm{Tr}\left(Y_\nu^\dagger Y_\nu\right)\right) - 12Y_t^2 Y_b^2,\end{aligned} \tag{E.9}$$

$$\begin{aligned}\mathcal{D}\lambda_4 = {} & 3g_1^2 g_2^2 - \lambda_4\left(3g_1^2 + 9g_2^2\right) + 2\lambda_4\left(\lambda_1 + \lambda_2\right) + 8\lambda_4\lambda_3 + 4\lambda_4^2 + 4\lambda_{12S}^2 \\ & + \lambda_4\left(6Y_t^2 + 6Y_b^2 + 2Y_\tau^2 + 2\mathrm{Tr}\left(Y_\nu^\dagger Y_\nu\right)\right) + 12Y_t^2 Y_b^2,\end{aligned} \tag{E.10}$$

$$\mathcal{D}\lambda_S = 10\lambda_S^2 + 2\lambda_S\mathrm{Tr}\left(Y_N^\dagger Y_N\right) + 4\lambda_{1S}^2 + 4\lambda_{2S}^2 + 8\lambda_{12S}^2 - 2\mathrm{Tr}\left(Y_N^\dagger Y_N Y_N^\dagger Y_N\right), \tag{E.11}$$

$$\begin{aligned}\mathcal{D}\lambda_{1S} = {} & \lambda_{1S}\left(-\frac{3}{2}g_1^2 - \frac{9}{2}g_2^2 + 4\lambda_{1S} + 4\lambda_S + 6\lambda_2\right) + \lambda_{2S}\left(4\lambda_3 + 2\lambda_4\right) + 8\lambda_{12S}^2 \\ & + \lambda_{1S}\left(6Y_b^2 + 2Y_\tau^2 + 2\mathrm{Tr}\left(Y_\nu^\dagger Y_\nu\right) + \mathrm{Tr}\left(Y_N^\dagger Y_N\right)\right) - 4\mathrm{Tr}\left(Y_\nu^\dagger Y_\nu Y_N^\dagger Y_N\right),\end{aligned} \tag{E.12}$$

$$\begin{aligned}\mathcal{D}\lambda_{2S} = {} & \lambda_{2S}\left(-\frac{3}{2}g_1^2 - \frac{9}{2}g_2^2 + 4\lambda_{2S} + 4\lambda_S + 6\lambda_2\right) + \lambda_{1S}\left(4\lambda_3 + 2\lambda_4\right) + 8\lambda_{12S}^2 \\ & + \lambda_{2S}\left(6Y_t^2 + \mathrm{Tr}\left(Y_N^\dagger Y_N\right)\right)\end{aligned} \tag{E.13}$$

[1] Ref. [25] has also given the one-loop RGEs of 2hdSMASH, but neglected terms quadratic in λ_{12S} systematically. We have restored them here using `SARAH` and `PYR@TE`.

$$\mathcal{D}\lambda_{12S} = \lambda_{12S}\left(-\frac{3}{2}g_1^2 - \frac{9}{2}g_2^2 + 2\lambda_3 + 4\lambda_4 + 2\lambda_S + 4\lambda_{1S} + 4\lambda_{2S} + 3Y_t^2 + 3Y_b^2 + Y_\tau^2\right) + \lambda_{12S}\left(\mathrm{Tr}\left(Y_\nu^\dagger Y_\nu\right) + \mathrm{Tr}\left(Y_N^\dagger Y_N\right)\right), \tag{E.14}$$

$$\mathcal{D}Y_t = Y_t\left(-\frac{17}{12}g_1^2 - \frac{9}{4}g_2^2 - 8g_3^2 + \frac{9}{2}Y_t^2 + \frac{1}{2}Y_b^2\right), \tag{E.15}$$

$$\mathcal{D}Y_b = Y_b\left(-\frac{5}{12}g_1^2 - \frac{9}{4}g_2^2 - 8g_3^2 + \frac{9}{2}Y_b^2 + \frac{1}{2}Y_t^2 + Y_\tau^2\right), \tag{E.16}$$

$$\mathcal{D}Y_\tau = Y_\tau\left(-\frac{15}{4}g_1^2 - \frac{9}{4}g_2^2 + \frac{5}{2}Y_\tau^2 + 3Y_b^2\right), \tag{E.17}$$

$$\mathcal{D}Y_\nu = Y_\nu\left(-\frac{3}{4}g_1^2 - \frac{9}{4}g_2^2 + 3Y_b^2 + \mathrm{Tr}\left(Y_\nu^\dagger Y_\nu\right)\right) + Y_\nu Y_\tau^2 - \frac{3}{2}\mathrm{Diag}\left(0, 0, Y_\tau^2\right) Y_\nu + \frac{3}{2}Y_\nu Y_\nu^\dagger Y_\nu + \frac{1}{2}Y_\nu Y_N^\dagger Y_N, \tag{E.18}$$

$$\mathcal{D}Y_N = \frac{1}{2}\mathrm{Tr}\left(Y_N^\dagger Y_N\right) Y_N + Y_N Y_N^\dagger Y_N + Y_N Y_\nu^\dagger Y_\nu + Y_\nu^T Y_\nu^* Y_N, \tag{E.19}$$

where $\mathcal{D} \equiv (4\pi)^2 \frac{d}{d\ln\mu_R}$.

F. Coleman-Weinberg Potential

The Coleman-Weinberg potential is an RG-improved potential which is given by, cf. Ref. [92],

$$V_{\rm CW}(\phi_i) = \frac{1}{64\pi^2} \times \left(\sum_b g_b m_b^4(\phi_i) \left[\log\left(\frac{m_b^2(\phi_i)}{\Lambda^2} \right) - \frac{3}{2} \right] - \sum_f g_f m_f^4(\phi_i) \left[\log\left(\frac{m_f^2(\phi_i)}{\Lambda^2} \right) - \frac{5}{2} \right] \right) \tag{F.1}$$

where $g_{f/b}$ are the degrees and $m_{f/b}$ are the masses of fermions/bosons. The sum is performed over all scalars $S = \{h_1, h_2, s, h_1^+, h_2^+, a_1, a_2, a_S\}$, Fermions[1] $F = \{t, N_i\}$ and transverse (longitudinal) vectors $V_{T,L} = \left\{ Z_{T,L}, W_{T,L}^\pm \right\}$ with the following degrees of freedom:

$$\begin{aligned} &g_{Z_T} = 2 \ , \ g_{Z_L} = 1 \ , \ g_{W_T^\pm} = 4 \ , \ g_{W_L^\pm} = 2 \ , \ g_t = 12 \ , \ g_{h_1} = g_{h_2} = g_s = 1 \\ &g_{h_1^+} = g_{h_2^+} = 2 \ , \ g_{a_1} = g_{a_2} = g_{a_S} = 1 \ , \ g_N = 6 \, . \end{aligned} \tag{F.2}$$

The masses of S, F and V are given by:

$$\begin{aligned} &m_Z^2 = \frac{1}{4}\left(h_1^2 + h_2^2\right)\left(g_1^2 + g_2^2\right) \quad , \quad m_{W^\pm}^2 = \frac{1}{4}\left(h_1^2 + h_2^2\right) g_1^2 \quad , \quad m_t^2 = \frac{Y_t}{2} h_2^2 \\ &m_{h_{1,2}}^2 = \frac{3h_{1,2}^2\lambda_{1,2} + h_{2,1}^2\lambda_{34} + s^2\lambda_{1S,2S}}{2} \quad , \quad m_s^2 = \frac{h_1^2\lambda_{1S} - 2h_1h_2\lambda_{12S} + h_2^2\lambda_{2S} + 3s^2\lambda_S}{2} \\ &m_{a_{1,2}}^2 = \frac{1}{2}\left(h_{1,2}^2\lambda_{1,2} + h_{2,1}^2(\lambda_3 + \lambda_4) + h_3^2\lambda_{1S}\right) \quad , \quad m_{h_{1,2}^+}^2 = \frac{1}{2}\left(h_{1,2}^2\lambda_{1,2} + h_{2,1}^2\lambda_3 + h_3^2\lambda_{1S}\right) , \\ &m_{a_s}^2 = \frac{1}{2}\left(h_1^2\lambda_{1S} + 2h_1h_2\lambda_{12S} + h_2^2\lambda_{2S} + s^2\lambda_S\right) . \end{aligned} \tag{F.3}$$

[1] We only consider the top quark and Majorana neutrino contributions since their masses are the largest amongst the fermions. However, we note that one has to include all fermions in order to give a complete description, which is beyond the scope of what we are considering.

References

[1] Georges Aad et al. Observation of a new particle in the search for the Standard Model Higgs boson with the ATLAS detector at the LHC. *Phys. Lett. B*, 716:1–29, 2012.

[2] Serguei Chatrchyan et al. Observation of a New Boson at a Mass of 125 GeV with the CMS Experiment at the LHC. *Phys. Lett. B*, 716:30–61, 2012.

[3] Peter W. Higgs. Broken Symmetries and the Masses of Gauge Bosons. *Phys. Rev. Lett.*, 13:508–509, 1964.

[4] F. Englert and R. Brout. Broken Symmetry and the Mass of Gauge Vector Mesons. *Phys. Rev. Lett.*, 13:321–323, 1964.

[5] G. S. Guralnik, C. R. Hagen, and T. W. B. Kibble. Global Conservation Laws and Massless Particles. *Phys. Rev. Lett.*, 13:585–587, 1964.

[6] Guillermo Ballesteros, Javier Redondo, Andreas Ringwald, and Carlos Tamarit. Unifying inflation with the axion, dark matter, baryogenesis and the seesaw mechanism. *Phys. Rev. Lett.*, 118(7):071802, 2017.

[7] Guillermo Ballesteros, Javier Redondo, Andreas Ringwald, and Carlos Tamarit. Standard Model—axion—seesaw—Higgs portal inflation. Five problems of particle physics and cosmology solved in one stroke. *JCAP*, 08:001, 2017.

[8] Jihn E. Kim. Weak Interaction Singlet and Strong CP Invariance. *Phys. Rev. Lett.*, 43:103, 1979.

[9] Mikhail A. Shifman, A. I. Vainshtein, and Valentin I. Zakharov. Can Confinement Ensure Natural CP Invariance of Strong Interactions? *Nucl. Phys. B*, 166:493–506, 1980.

[10] R. D. Peccei and Helen R. Quinn. CP Conservation in the Presence of Instantons. *Phys. Rev. Lett.*, 38:1440–1443, 1977.

[11] John Preskill, Mark B. Wise, and Frank Wilczek. Cosmology of the Invisible Axion. *Phys. Lett. B*, 120:127–132, 1983.

[12] L. F. Abbott and P. Sikivie. A Cosmological Bound on the Invisible Axion. *Phys. Lett. B*, 120:133–136, 1983.

[13] Michael Dine and Willy Fischler. The Not So Harmless Axion. *Phys. Lett. B*, 120:137–141, 1983.

[14] Peter Minkowski. $\mu \to e\gamma$ at a Rate of One Out of 10^9 Muon Decays? *Phys. Lett. B*, 67:421–428, 1977.

[15] Murray Gell-Mann, Pierre Ramond, and Richard Slansky. Complex Spinors and Unified Theories. *Conf. Proc. C*, 790927:315–321, 1979.

[16] Tsutomu Yanagida. Horizontal gauge symmetry and masses of neutrinos. *Conf. Proc. C*, 7902131:95–99, 1979.

[17] Rabindra N. Mohapatra and Goran Senjanovic. Neutrino Mass and Spontaneous Parity Nonconservation. *Phys. Rev. Lett.*, 44:912, 1980.

[18] M. Fukugita and T. Yanagida. Baryogenesis Without Grand Unification. *Phys. Lett. B*, 174:45–47, 1986.

[19] Fedor L. Bezrukov and Mikhail Shaposhnikov. The Standard Model Higgs boson as the inflaton. *Phys. Lett. B*, 659:703–706, 2008.

[20] Oleg Lebedev and Hyun Min Lee. Higgs Portal Inflation. *Eur. Phys. J. C*, 71:1821, 2011.

[21] Guillermo Ballesteros, Javier Redondo, Andreas Ringwald, and Carlos Tamarit. Several Problems in Particle Physics and Cosmology Solved in One SMASH. *Front. Astron. Space Sci.*, 6:55, 2019.

[22] A. R. Zhitnitsky. On Possible Suppression of the Axion Hadron Interactions. (In Russian). *Sov. J. Nucl. Phys.*, 31:260, 1980.

[23] Michael Dine, Willy Fischler, and Mark Srednicki. A Simple Solution to the Strong CP Problem with a Harmless Axion. *Phys. Lett. B*, 104:199–202, 1981.

[24] R. R. Volkas, A. J. Davies, and Girish C. Joshi. NATURALNESS OF THE INVISIBLE AXION MODEL. *Phys. Lett. B*, 215:133–138, 1988.

[25] Jackson D. Clarke and Raymond R. Volkas. Technically natural nonsupersymmetric model of neutrino masses, baryogenesis, the strong CP problem, and dark matter. *Phys. Rev. D*, 93(3):035001, 2016.

[26] Domenec Espriu, Federico Mescia, and Albert Renau. Axion-Higgs interplay in the two Higgs-doublet model. *Phys. Rev. D*, 92(9):095013, 2015.

[27] Daniele Lombardi. The DFSZ axion: analysis and generalization. Laurea thesis, U. Bologna, DIFA, 2018.

[28] Tsutomu Yanagida. Horizontal Symmetry and Masses of Neutrinos. *Prog. Theor. Phys.*, 64:1103, 1980.

[29] D. Jurčiukonis and L. Lavoura. The three- and four-Higgs couplings in the general two-Higgs-doublet model. *JHEP*, 12:004, 2018.

[30] Igor P. Ivanov, Marcel Köpke, and Margarete Mühlleitner. Algorithmic Boundedness-From-Below Conditions for Generic Scalar Potentials. *Eur. Phys. J. C*, 78(5):413, 2018.

[31] Kristjan Kannike. Vacuum Stability Conditions From Copositivity Criteria. *Eur. Phys. J. C*, 72:2093, 2012.

[32] Margarete Muhlleitner, Marco O. P. Sampaio, Rui Santos, and Jonas Wittbrodt. The N2HDM under Theoretical and Experimental Scrutiny. *JHEP*, 03:094, 2017.

[33] J. Horejsi and M. Kladiva. Tree-unitarity bounds for THDM Higgs masses revisited. *Eur. Phys. J. C*, 46:81–91, 2006.

[34] Satsuki Oda, Yutaro Shoji, and Dai-Suke Takahashi. High Scale Validity of the DFSZ Axion Model with Precision. *JHEP*, 03:011, 2020.

[35] Robert Foot, Archil Kobakhidze, Kristian L. McDonald, and Raymond R. Volkas. Poincaré protection for a natural electroweak scale. *Phys. Rev. D*, 89(11):115018, 2014.

[36] Jackson D. Clarke, Robert Foot, and Raymond R. Volkas. Natural leptogenesis and neutrino masses with two Higgs doublets. *Phys. Rev. D*, 92(3):033006, 2015.

[37] P.A. Zyla et al. Review of Particle Physics. *PTEP*, 2020(8):083C01, 2020.

[38] Daniel Baumann. TASI Lectures on Inflation. *arXiv e-prints*, page arXiv:0907.5424, July 2009.

[39] Daniel Baumann. Primordial Cosmology. *PoS*, TASI2017:009, 2018.

[40] Daniel Baumann and Liam McAllister. *Inflation and String Theory*. Cambridge Monographs on Mathematical Physics. Cambridge University Press, 5 2015.

[41] Jinn-Ouk Gong, Hyun Min Lee, and Sin Kyu Kang. Inflation and dark matter in two Higgs doublet models. *JHEP*, 04:128, 2012.

[42] Tanmoy Modak and Kin-ya Oda. Echoes of 2HDM inflation at the collider experiments. *Eur. Phys. J. C*, 80(9):863, 2020. [Erratum: Eur.Phys.J.C 81, 518 (2021)].

[43] Kazunori Nakayama and Masahiro Takimoto. Higgs inflation and suppression of axion isocurvature perturbation. *Phys. Lett. B*, 748:108–112, 2015.

[44] Gian F. Giudice and Hyun Min Lee. Unitarizing Higgs Inflation. *Phys. Lett. B*, 694:294–300, 2011.

[45] Andreas Ringwald and Carlos Tamarit. Revealing the Cosmic History with Gravitational Waves. *arXiv e-prints*, page arXiv:2203.00621, March 2022.

[46] Steven Weinberg. A New Light Boson? *Phys. Rev. Lett.*, 40:223–226, 1978.

[47] Frank Wilczek. Problem of Strong P and T Invariance in the Presence of Instantons. *Phys. Rev. Lett.*, 40:279–282, 1978.

[48] Georg G. Raffelt. Astrophysical axion bounds. *Lect. Notes Phys.*, 741:51–71, 2008.

[49] P. A. Zyla et al. Review of Particle Physics. *PTEP*, 2020(8):083C01, 2020.

[50] Kristjan Kannike. Vacuum Stability of a General Scalar Potential of a Few Fields. *Eur. Phys. J. C*, 76(6):324, 2016. [Erratum: Eur.Phys.J.C 78, 355 (2018)].

[51] Luca Di Luzio, Maurizio Giannotti, Enrico Nardi, and Luca Visinelli. The landscape of QCD axion models. *Phys. Rept.*, 870:1–117, 2020.

[52] J. L. F. Barbon, J. A. Casas, J. Elias-Miro, and J. R. Espinosa. Higgs Inflation as a Mirage. *JHEP*, 09:027, 2015.

[53] Alan H. Guth. Inflationary universe: A possible solution to the horizon and flatness problems. *Phys. Rev. D*, 23:347–356, Jan 1981.

[54] G. Gamow. Expanding universe and the origin of elements. *Phys. Rev.*, 70:572–573, Oct 1946.

[55] R. A. Alpher, H. Bethe, and G. Gamow. The origin of chemical elements. *Phys. Rev.*, 73(7):803–804, April 1948.

[56] Ralph A. Alpher and Robert C. Herman. On the relative abundance of the elements. *Phys. Rev.*, 74:1737–1742, Dec 1948.

[57] Ralph A. Alpher and Robert C. Herman. Remarks on the evolution of the expanding universe. *Phys. Rev.*, 75:1089–1095, Apr 1949.

[58] A. A. Penzias and R. W. Wilson. A Measurement of Excess Antenna Temperature at 4080 Mc/s. *The Astrophysical Journal*, 142:419–421, July 1965.

[59] Alexei A. Starobinsky. A New Type of Isotropic Cosmological Models Without Singularity. *Phys. Lett. B*, 91:99–102, 1980.

[60] Y. Akrami et al. Planck 2018 results. X. Constraints on inflation. *Astron. Astrophys.*, 641:A10, 2020.

[61] N. Aghanim et al. Planck 2018 results. VI. Cosmological parameters. *Astron. Astrophys.*, 641:A6, 2020. [Erratum: Astron.Astrophys. 652, C4 (2021)].

[62] Albert Einstein. The Foundation of the General Theory of Relativity. *Annalen Phys.*, 49(7):769–822, 1916.

[63] Richard L. Arnowitt, Stanley Deser, and Charles W. Misner. The Dynamics of general relativity. *Gen. Rel. Grav.*, 40:1997–2027, 2008.

[64] Juan Martin Maldacena. Non-Gaussian features of primordial fluctuations in single field inflationary models. *JHEP*, 05:013, 2003.

[65] Jinn-Ouk Gong. Multi-field inflation and cosmological perturbations. *Int. J. Mod. Phys. D*, 26(01):1740003, 2016.

[66] A.D. Linde. Eternally existing self-reproducing chaotic inflanationary universe. *Physics Letters B*, 175(4):395–400, 1986.

[67] B. L. Spokoiny. INFLATION AND GENERATION OF PERTURBATIONS IN BROKEN SYMMETRIC THEORY OF GRAVITY. *Phys. Lett. B*, 147:39–43, 1984.

[68] T. Futamase and Kei-ichi Maeda. Chaotic Inflationary Scenario in Models Having Nonminimal Coupling With Curvature. *Phys. Rev. D*, 39:399–404, 1989.

[69] D. S. Salopek, J. R. Bond, and James M. Bardeen. Designing Density Fluctuation Spectra in Inflation. *Phys. Rev. D*, 40:1753, 1989.

[70] R. Fakir and W. G. Unruh. Improvement on cosmological chaotic inflation through nonminimal coupling. *Phys. Rev. D*, 41:1783–1791, 1990.

[71] Sandhya Choubey and Abhass Kumar. Inflation and Dark Matter in the Inert Doublet Model. *JHEP*, 11:080, 2017.

[72] P. A. R. Ade et al. Improved Constraints on Primordial Gravitational Waves using Planck, WMAP, and BICEP/Keck Observations through the 2018 Observing Season. *Phys. Rev. Lett.*, 127(15):151301, 2021.

[73] Viatcheslav F. Mukhanov and G. V. Chibisov. Quantum Fluctuations and a Nonsingular Universe. *JETP Lett.*, 33:532–535, 1981.

[74] Alexei A. Starobinsky. Dynamics of Phase Transition in the New Inflationary Universe Scenario and Generation of Perturbations. *Phys. Lett. B*, 117:175–178, 1982.

[75] Dmitry Gorbunov and Anna Tokareva. R^2-inflation with conformal SM Higgs field. *JCAP*, 12:021, 2013.

[76] J. L. F. Barbon and J. R. Espinosa. On the Naturalness of Higgs Inflation. *Phys. Rev. D*, 79:081302, 2009.

[77] C. P. Burgess, Hyun Min Lee, and Michael Trott. Comment on Higgs Inflation and Naturalness. *JHEP*, 07:007, 2010.

[78] Georgios K. Karananas, Mikhail Shaposhnikov, and Sebastian Zell. Field redefinitions, perturbative unitarity and Higgs inflation. *Journal of High Energy Physics*, 2022(6):132, June 2022.

[79] Marc Kamionkowski and Ely D. Kovetz. The Quest for B Modes from Inflationary Gravitational Waves. *Ann. Rev. Astron. Astrophys.*, 54:227–269, 2016.

[80] Andrew R Liddle and Samuel M Leach. How long before the end of inflation were observable perturbations produced? *Phys. Rev. D*, 68:103503, 2003.

[81] Daniel G. Figueroa and Francisco Torrenti. Gravitational wave production from preheating: parameter dependence. *JCAP*, 10:057, 2017.

[82] Andreas Ringwald, Ken'ichi Saikawa, and Carlos Tamarit. Primordial gravitational waves in a minimal model of particle physics and cosmology. *JCAP*, 02:046, 2021.

[83] Andrew R. Liddle and David H. Lyth. The Cold dark matter density perturbation. *Phys. Rept.*, 231:1–105, 1993.

[84] Wilfried Buchmuller and Michael Plumacher. Matter antimatter asymmetry and neutrino properties. *Phys. Rept.*, 320:329–339, 1999.

[85] W. Buchmuller, P. Di Bari, and M. Plumacher. Leptogenesis for pedestrians. *Annals Phys.*, 315:305–351, 2005.

[86] Laura Covi, Esteban Roulet, and Francesco Vissani. CP violating decays in leptogenesis scenarios. *Phys. Lett. B*, 384:169–174, 1996.

[87] Sacha Davidson and Alejandro Ibarra. A Lower bound on the right-handed neutrino mass from leptogenesis. *Phys. Lett. B*, 535:25–32, 2002.

[88] J. A. Casas and A. Ibarra. Oscillating neutrinos and $\mu \to e, \gamma$. *Nucl. Phys. B*, 618:171–204, 2001.

[89] P. F. de Salas, D. V. Forero, S. Gariazzo, P. Martínez-Miravé, O. Mena, C. A. Ternes, M. Tórtola, and J. W. F. Valle. 2020 global reassessment of the neutrino oscillation picture. *JHEP*, 02:071, 2021.

[90] Nabarun Chakrabarty, Ujjal Kumar Dey, and Biswarup Mukhopadhyaya. High-scale validity of a two-Higgs doublet scenario: a study including LHC data. *JHEP*, 12:166, 2014.

[91] Joel Oredsson and Johan Rathsman. $\mathbb{Z}_2$ breaking effects in 2-loop RG evolution of 2HDM. *JHEP*, 02:152, 2019.

[92] Erick J. Weinberg. *Radiative corrections as the origin of spontaneous symmetry breaking*. PhD thesis, Harvard U., 1973.

[93] Florian Staub. SARAH 4 : A tool for (not only SUSY) model builders. *Comput. Phys. Commun.*, 185:1773–1790, 2014.

[94] Werner Porod. SPheno, a program for calculating supersymmetric spectra, SUSY particle decays and SUSY particle production at e+ e- colliders. *Comput. Phys. Commun.*, 153:275–315, 2003.

[95] Philip Bechtle, Sven Heinemeyer, Oscar Stål, Tim Stefaniak, and Georg Weiglein. *HiggsSignals*: Confronting arbitrary Higgs sectors with measurements at the Tevatron and the LHC. *Eur. Phys. J. C*, 74(2):2711, 2014.

[96] Philip Bechtle, Daniel Dercks, Sven Heinemeyer, Tobias Klingl, Tim Stefaniak, Georg Weiglein, and Jonas Wittbrodt. HiggsBounds-5: Testing Higgs Sectors in the LHC 13 TeV Era. *Eur. Phys. J. C*, 80(12):1211, 2020.

[97] J. P. Lees et al. Precision Measurement of the $B \to X_s\gamma$ Photon Energy Spectrum, Branching Fraction, and Direct CP Asymmetry $A_{CP}(B \to X_{s+d}\gamma)$. *Phys. Rev. Lett.*, 109:191801, 2012.

[98] M. Misiak, Abdur Rehman, and Matthias Steinhauser. Towards $\overline{B} \to X_s\gamma$ at the NNLO in QCD without interpolation in m_c. *JHEP*, 06:175, 2020.

[99] Pierluca Carenza, Tobias Fischer, Maurizio Giannotti, Gang Guo, Gabriel Martínez-Pinedo, and Alessandro Mirizzi. Improved axion emissivity from a supernova via nucleon-nucleon bremsstrahlung. *JCAP*, 10(10):016, 2019. [Erratum: JCAP 05, E01 (2020)].

[100] Pierluca Carenza, Bryce Fore, Maurizio Giannotti, Alessandro Mirizzi, and Sanjay Reddy. Enhanced Supernova Axion Emission and its Implications. *Phys. Rev. Lett.*, 126(7):071102, 2021.

[101] Richard Lynn Davis. Cosmic Axions from Cosmic Strings. *Phys. Lett. B*, 180:225–230, 1986.

[102] David H. Lyth. Estimates of the cosmological axion density. *Phys. Lett. B*, 275:279–283, 1992.

[103] Ya. B. Zeldovich, I. Yu. Kobzarev, and L. B. Okun. Cosmological Consequences of the Spontaneous Breakdown of Discrete Symmetry. *Zh. Eksp. Teor. Fiz.*, 67:3–11, 1974.

[104] P. Sikivie. Of Axions, Domain Walls and the Early Universe. *Phys. Rev. Lett.*, 48:1156–1159, 1982.

[105] Richard Holman, Stephen D. H. Hsu, Thomas W. Kephart, Edward W. Kolb, Richard Watkins, and Lawrence M. Widrow. Solutions to the strong CP problem in a world with gravity. *Phys. Lett. B*, 282:132–136, 1992.

[106] Marc Kamionkowski and John March-Russell. Planck scale physics and the Peccei-Quinn mechanism. *Phys. Lett. B*, 282:137–141, 1992.

[107] Stephen M. Barr and D. Seckel. Planck scale corrections to axion models. *Phys. Rev. D*, 46:539–549, 1992.

[108] S. Ghigna, Maurizio Lusignoli, and M. Roncadelli. Instability of the invisible axion. *Phys. Lett. B*, 283:278–281, 1992.

[109] Howard M. Georgi, Lawrence J. Hall, and Mark B. Wise. Grand Unified Models With an Automatic Peccei-Quinn Symmetry. *Nucl. Phys. B*, 192:409–416, 1981.

[110] Alex G. Dias, V. Pleitez, and M. D. Tonasse. Naturally light invisible axion and local Z(13) x Z(3) symmetries. *Phys. Rev. D*, 69:015007, 2004.

[111] Alex G. Dias, V. Pleitez, and M. D. Tonasse. Naturally light invisible axion in models with large local discrete symmetries. *Phys. Rev. D*, 67:095008, 2003.

[112] Alex G. Dias and V. Pleitez. Stabilizing the invisible axion in 3-3-1 models. *Phys. Rev. D*, 69:077702, 2004.

[113] Linda M. Carpenter, Michael Dine, and Guido Festuccia. Dynamics of the Peccei Quinn Scale. *Phys. Rev. D*, 80:125017, 2009.

[114] Keisuke Harigaya, Masahiro Ibe, Kai Schmitz, and Tsutomu T. Yanagida. Peccei-Quinn symmetry from a gauged discrete R symmetry. *Phys. Rev. D*, 88(7):075022, 2013.

[115] A. G. Dias, A. C. B. Machado, C. C. Nishi, A. Ringwald, and P. Vaudrevange. The Quest for an Intermediate-Scale Accidental Axion and Further ALPs. *JHEP*, 06:037, 2014.

[116] Andreas Ringwald and Ken'ichi Saikawa. Axion dark matter in the post-inflationary Peccei-Quinn symmetry breaking scenario. *Phys. Rev. D*, 93(8):085031, 2016. [Addendum: Phys.Rev.D 94, 049908 (2016)].

[117] E. Armengaud et al. Physics potential of the International Axion Observatory (IAXO). *JCAP*, 06:047, 2019.

[118] Margarete Mühlleitner, Marco O. P. Sampaio, Rui Santos, and Jonas Wittbrodt. ScannerS: Parameter Scans in Extended Scalar Sectors. *arXiv e-prints*, page arXiv:2007.02985, July 2020.

[119] Shinya Kanemura, Takahiro Kubota, and Eiichi Takasugi. Lee-Quigg-Thacker bounds for Higgs boson masses in a two doublet model. *Phys. Lett. B*, 313:155–160, 1993.

Eidesstattliche Versicherung

Hiermit versichere ich an Eides statt, dass ich die vorliegende Arbeit selbstständig und ohne fremde Hilfe angefertigt und mich anderer als der im beigefügten Verzeichnis angegebenen Hilfsmittel nicht bedient habe. Alle Stellen, die wörtlich oder sinngemäß aus Veröffentlichungen entnommen wurden, sind als solche kenntlich gemacht. Ich versichere weiterhin, dass ich die Arbeit vorher nicht in einem anderen Prüfungsverfahren eingereicht habe und die eingereichte schriftliche Fassung der auf dem elektronischen Speichermedium entspricht.
Ich bin mit einer Einstellung in den Bestand der Bibliothek des Fachbereiches einverstanden.

Hamburg, den 27.07.2022 Unterschrift:_____